Chapter 9
Nanotube and Graphene Polymer Composites for Photonics and Optoelectronics

T. Hasan, V. Scardaci, P.H. Tan, F. Bonaccorso, A.G. Rozhin, Z. Sun, and A.C. Ferrari

Abstract Polymer composites are an attractive near-term means to exploit the unique properties of single wall carbon nanotubes and graphene. This is particularly true for composites aimed at photonic and optoelectronic applications, where a number of devices have already been demonstrated. These include transparent conductors, saturable absorbers, electroluminescent and photovoltaic devices. Here, we present an overview of such composites, from solution processing of the raw materials, their sorting, characterization, to their incorporation into polymers, device fabrication and testing.

9.1 Introduction

Incorporation of carbon nanotubes (CNTs) into polymer matrices was first reported in Ref. [5]. Since then, polymer composites of nanostructured carbon materials have developed into a vast research area, mostly focusing on their mechanical applications [72, 82, 88, 237, 281, 382, 486]. A notable difference between CNT/graphene-polymer composites for mechanical applications and optics/photonics is the method by which CNTs/graphene flakes are incorporated into the host matrix. Strong interaction between these carbon nanomaterials and the host polymer is the key for mechanical strength. This is typically attained by functionalization [20, 23, 75, 105–107, 172, 486] and/or in-situ polymerization [117, 237, 281, 327, 349, 449, 475]. These incorporation methods and the mechanical characterizations of the resultant materials will not be covered here. An overview of current progress can be found, e.g., in Refs. [81, 82, 156, 307].

The fabrication and characterization processes of CNT and graphene based composites for photonics and optoelectronics differ from those aimed at mechanical applications. For optical grade composites, fine dispersion, without covalent functionalization, and control of CNT-bundle size are of key importance [96, 125, 220, 358–360, 363, 370, 371, 376, 380, 396, 478]. Different strategies have been developed to produce/grow graphene and transfer it onto flexible substrates [18, 40]. Liquid phase exfoliation (LPE) of graphite [161, 166, 271] is an economic,

A.C. Ferrari (✉)
Department of Engineering, University of Cambridge, Cambridge, CB3 0FA, UK
e-mail: acf26@eng.cam.ac.uk

O. Hayden, K. Nielsch (eds.), *Molecular- and Nano-Tubes*,
DOI 10.1007/978-1-4419-9443-1_9,

up-scalable and promising approach for photonic and optoelectronic applications. A significant effort is ongoing to achieve graphene mono-layer enriched dispersions [160, 161, 166, 271, 284, 411]. For both CNTs and graphene, once the initial dispersion is produced, the fabrication, characterization and integration into devices of the resulting composites follows a similar protocol. We will therefore focus mostly on CNTs, adding additional information on graphene, where necessary.

This chapter is organized as follows. Section 9.3 reviews CNT-dispersion via solution processing, which is essential to overcome the insolubility or near insolubility of unfunctionalized CNTs into various solvents compatible with host polymer matrices. The dispersion of Single Wall Carbon Nanotubes (SWNTs) in aqueous, non-aqueous solvents and liquid crystals are separately discussed in Sections 9.3.1, 9.3.2 and 9.3.3, respectively. Dispersion of graphene in aqueous and non-aqueous media follows a similar principle, though the choice of surfactants is limited due to the two dimensional nature of graphene. This is discussed in Section 9.4. Recent progress in density gradient based sorting of SWNTs, which can be used to fine-tune the optoelectronic device performances is covered in Section 9.5. Section 9.6 discusses inkjet printing of SWNTs. Optical characterization of the SWNT dispersions, with particular focus on the estimation of loading and investigation of the bundle size, is discussed in Sections 9.7.1. and 9.7.2. Section 9.8 covers the preparation of SWNT/graphene-polymer composites for optical applications (Section 9.8.1) and the alignment of SWNTs (Section 9.8.1.1). The desirable characteristics of host polymer matrices with a list of available commercial polymers are presented in Section 9.8.2. The key optical characterizations for such composites, such as Z-scan, photoluminescence, Raman and pump-probe spectroscopies, are summarized in Section 9.9. Particular emphasis is given to Raman spectroscopy, which is one of the most powerful, yet non-destructive characterization techniques available for carbon nanomaterials. Section 9.10 briefly discusses some optical/photonic applications of SWNT-polymer composites. Section 9.11 reviews the application of SWNT-polymer composites as mode-locker in ultra fast lasers. Finally, Section 9.12 discusses graphene based saturable absorbers for ultrafast pulse generation.

9.2 Nanotubes and Graphene for Photonics

SWNTs exhibit strong optical absorption, covering a broad spectral range from UV to near IR [134, 151, 185, 193, 201, 207, 265, 319, 462]. To a first approximation, their band gap varies inversely with the diameter. This can, in principle, be fine-tuned by modifying the growth parameters [191, 200, 249]. Isolated semiconducting SWNTs (s-SWNTs) and small SWNT bundles exhibit photoluminescence (PL) [17, 63, 175, 187, 255–258, 302–304, 319, 324, 342, 421, 433, 463]. PL is quenched for increasing bundle size and the presence of metallic SWNTs (m-SWNTs) [64, 138, 158, 296, 316, 319, 421, 433]. The PL properties of SWNTs have been extensively investigated over the past few years [17, 63, 175, 187, 255–258, 302–304, 319, 324, 330, 342, 353, 421, 433, 439, 463], and the excitonic nature of electronic

transitions in SWNTs has been theoretically predicted [10, 66, 197, 335, 402, 492] and experimentally proven [293, 456]. Sub-picosecond carrier relaxation time was also observed in SWNTs [76, 152, 168–170, 178, 230, 246, 283, 329, 351, 427]. In addition, they show significant third-order optical nonlinearities, as theoretically predicted [78, 184, 286, 287] and experimentally confirmed [44, 93, 195, 268, 278, 427] by several groups.

This fast nonlinear optical response is of great technological importance. SWNTs can be used to fabricate ultrafast optoelectronic devices, such as ultrafast sources, optical switches. These are crucial for various applications, for example, high bit rate optical fiber transmission, signal regeneration, dispersion compensator, etc. However, the heterogeneity, impurity and bundling of as-grown SWNTs make it difficult to precisely control the device parameters. Also, it is still difficult to use SWNTs directly grown on substrates [477] to fabricate efficient devices, due to scattering losses [39]. In this context, a more effective solution for the fabrication of SWNT based photonic and optoelectronic devices is to incorporate the processed SWNTs into polymer matrices [96, 125, 220, 358–360, 363, 370, 371, 376, 380, 396, 478]. Wet chemistry processes developed over the past few years can now be readily used. Indeed, it is now possible to untangle [15, 19, 100, 138, 158, 183, 245, 308, 319, 320, 405, 495] and sort SWNTs [12, 13, 41, 86]. A combination of wet chemistry with compatible non-aqueous solvents and polymers of appropriate properties is therefore a viable route for the fabrication of optoelectronic devices. Furthermore, this holds great promise for the mass production of inexpensive photonic devices and their simplified integration into various lightwave systems.

A single layer graphene absorbs 2.3% of incident light [311]. This remains constant from the visible to the near infrared (NIR), due to the linear dispersion of Dirac electrons in graphene [40, 160, 311, 411]. As we discuss later in Section 9.12, such broad absorption band, coupled with ultrafast relaxation dynamics, make graphene one of the most promising candidates for next generation photonic and optoelectronic applications. A viable route for mass fabrication of such graphene based devices also follows a wet chemistry based strategy, similar to SWNTs [160, 411].

9.3 Nanotube Dispersion in Liquid Media

As produced SWNTs usually form entangled networks of bundles or ropes [4, 77, 87, 192, 229, 261, 273, 364, 430, 431, 448] due to strong van der Waals interactions [140, 171, 229, 270, 364, 430]. In such entangled networks, SWNTs do not possess the optimum mechanical, thermal and optoelectronic properties [31, 69, 72, 82, 88, 239, 262, 382]. It is thus important to produce isolated/individual SWNTs from the bundles. Strong ultrasonic treatments in presence of water or non-aqueous solvents and ‘dispersants’ (e.g. surfactants, polymers etc., aiding the dispersion process) are commonly used to exfoliate highly aggregated SWNT networks into small bundles [100, 138, 157, 158, 183, 279, 299, 308, 319–331, 420, 495]. In the following sections, we present an overview of the methods to achieve

dispersions with high concentration of individual SWNTs and small bundles without covalent functionalization. The SWNT dispersions thus obtained are mainly characterized by absorption and photoluminescence spectroscopy, covered in the subsequent sections.

9.3.1 Nanotube Dispersion in Water

The non-polar nature of unfunctionalized (i.e. pristine) SWNTs makes it hard to directly disperse them in a highly polar solvent like water without any functionalization [107, 267, 317, 426]. Therefore, much effort has been devoted to find suitable molecules to interface the non-polar sidewalls of nanotubes with water. To date, stable dispersions of pristine SWNTs in water have been achieved with the aid of ionic and non-ionic surfactants [183, 308, 319, 348, 423, 466], polymers [22, 308, 320], DNA [13, 64, 495], polypeptides [100, 474, 498] and cellulose derivatives [299, 420]. Covalent functionalization of SWNTs disrupts the extended π-network, hence changes their optoelectronic properties [20, 23, 24, 57, 254].

Micelles are aggregated surfactant molecules. The critical micelle concentration (CMC) is the concentration of surfactants in a liquid above which micelles are spontaneously formed [54]. At the CMC, the surface-area between two liquids (e.g., air-water interface) becomes loaded with surfactant molecules. Addition of any more surfactant molecules leads to the formation of micelles [54]. In aqueous solutions, a typical surfactant (e.g. SDBS) micelle arranges its hydrophillic heads in contact with water and the hydrophobic tails in the micelle center [54]. Surfactants, in concentration above the CMC, form micelles around individual SWNTs and small bundles, interfacing their non-polar tail with the tube sidewalls and their polar or ionic end with water, making SWNTs compatible with the aqueous medium [183, 296, 308, 319]. This creates a density difference between individualized and bundled SWNTs. For example, an individual SWNT encapsulated in an SDS micelle is less dense than a 7-tube bundle encapsulated by the same micelles [319]. After centrifugation, heavier bundles precipitate due to higher sedimentation coefficient [46], while the supernatant becomes enriched with individually suspended SWNTs. Several types of surfactants, both ionic and non-ionic, have been reported to stably suspend SWNTs in water [183, 308]. These include SDS, SDBS, SC, SDC, TDC, DTAB, CTAB on the ionic side, and the Triton-X and Brij series on the non-ionic side [183, 308], though the border between surfactant and polymer for the latter is arbitrary. Bile salt surfactants have recently been demonstrated to be very effective in individualizing SWNTs in aqueous dispersions [41]. Bile salts (e.g. SDC, TDC, SC) have a rigid molecular structure, consisting of a cholesterol group with dissimilar sides with a steroid skeleton with a carboxylic acid side-chain and one to three hydroxyl (–OH) groups on the steroid backbone [295, 391]. They are amphiphilic, having both hydrophobic and hydrophilic sides [391], enabling them to individualize SWNTs much more effectively than linear chain surfactants [41]. Figure 9.1 shows some surfactants and polymers commonly used to disperse SWNTs in different solvents.

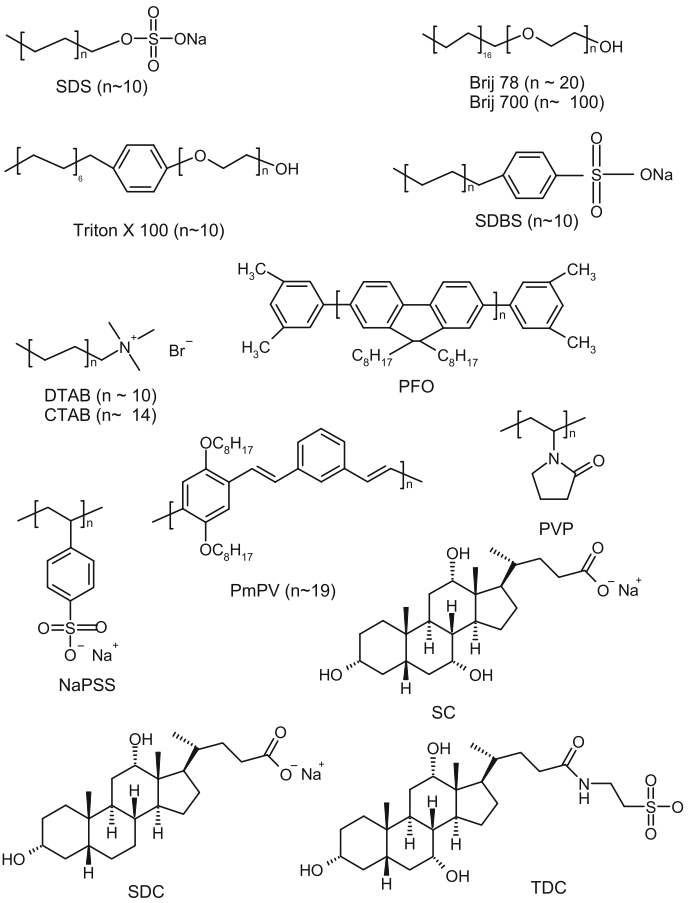

Fig. 9.1 Chemical structures of common surfactants and polymers used to disperse SWNTs in aqueous and organic solvents. SDS: sodium dodecyl sulfate; SDBS: sodium dodecylbenzene-sulphonate; DTAB: dodecyltrimethylammonium bromide; CTAB: cetyltrimethylammonium bromide; PFO: poly(9,9-dioctylfluorenyl-2,7-diyl; PmPV: poly(p-phenlyenevinyleneco-2,5-dioctoxy-m-phenylenevinylene); PVP: polyvinylpyrrolidone; NaPSS: sodium polystyrene sulphonate; SC: sodium cholate; SDC: sodium deoxycholate; TDC: sodium taurodeoxycholate

Water-soluble polymers are reported to wrap around SWNTs [22, 320], thus facilitating their de-bundling and dispersion. In particular, polyvinylpyrrolidone (PVP) and its copolymers with vinyl acetate, acrylic acid, dimethylaminoethyl methacrylate, polystyrene sulphonate, polyvinylsulphate can stably disperse SWNTs in water [320]. The wrapping by water-soluble polymers is thermodynamically favored by the removal of the hydrophobic interface between the nanotube sidewall and the aqueous medium [22, 320]. Cellulose derivatives, e.g. sodium carboxymethylcellulose (Na-CMC) [299, 420] and hydroxyethylcellulose [299] can also disperse a high amount of SWNTs without forming visible aggregations.

DNA is also an excellent dispersant of SWNTs in water [64, 441, 495]. Reference [495] proposed that single-stranded DNA forms a helical wrapping around the tube sidewalls by π-stacking. They also showed that the binding free-energy of single stranded DNA to SWNTs is higher than that between two tubes, facilitating dispersion [495]. Other biomolecules, such as polypeptides, efficiently disperse SWNTs in water [100, 474, 498]. Reference [100] designed a peptide, called nano-1, which folds into an α-helix, whose hydrophobic side interacts with the tube sidewall, whereas the hydrophilic side interacts with water molecules. Increasing the aromatic residues within the peptides improves dispersion [498]. This can be further improved by cross-linking the peptides on the external side of the α-helixes [474].

9.3.2 Nanotube Dispersion in Non-aqueous Solvents

Although the highest concentrations (>1.5 gL^{-1}) of pristine, individualized SWNTs or small bundles have so far been achieved in water, the presence of dispersant molecules is not the best option in view of their integration in devices when preservation of the pristine electronic structure is necessary. Also, the aqueous medium is not suitable for SWNT integration into water-insoluble polymer composites. Therefore, much effort has been devoted to the dispersion of SWNTs in pure non-aqueous solvents, such as N,N-dimethylformamide (DMF), N,N-dimethylacetamide (DMA) and N-methyl-2-pyrrolidone (NMP) [15, 19, 32, 33, 138, 158, 222, 236, 245]. A range of surfactants and polymers has also been investigated as dispersing agents in such solvents to improve the loading of unfunctionalized SWNTs [157–160, 198, 279, 403–405].

Ref. [15] proposed that important criteria for solvents to get good dispersion of SWNTs include high electron-pair donicity, β (hydrogen bond acceptance ability [242, 354]), low hydrogen bond donation parameter, α and high solvatochromic parameter [15], π^*. The latter describes the polarity and polarizability of solvents [285, 354]. Therefore, the Lewis basicity (i.e. electron pair acceptance ability [242, 285, 354]) without hydrogen donors is key to good dispersion of SWNTs [15]. However, this does not cover all the requirements. For example, Ref. [15] showed that, even though DMSO meets all the above criteria, it is only a mediocre solvent for SWNTs. In addition, highly polar alkyl amide solvents with "optimal geometries" are reported to be vital for good SWNT dispersion ability [245]. Amongst the amide solvents, NMP has been described as one of the most effective for dispersing pristine SWNTs [15, 19, 138, 158]. Pure NMP is able to disperse SWNTs with the highest fraction ($\sim$70%) of individual tubes at a very low concentration ($\sim$0.004 gL^{-1}), with growing average bundle size as the SWNT concentration increases [138]. Individual tubes remain stable in NMP for at least 3 weeks [158].

Dispersion and stabilization of nanoparticles, e.g. nanotubes in pure solvents, can be explained by considering the relative solvent-solvent, solvent-particle and

particle-particle interaction strengths [166]. Stable nanoparticle dispersions require the Gibbs free energy of mixing, ΔG_{mix}, to be zero or negative [155]:

$$\Delta G_{mix} = \Delta H_{mix} - T\Delta S_{mix} \tag{9.1}$$

where, T is the absolute temperature, ΔH_{mix} is the enthalpy of mixing and ΔS_{mix} is the entropy change in the mixing process [166]. For large solute particles like graphene and nanotubes, ΔS_{mix} is small [32, 166]. Therefore, for dispersion and stabilization of SWNTs in solvents, ΔH_{mix} needs to be very small. This can be achieved by choosing a solvent whose surface energy is very close to that of SWNTs. This supports the experimental evidence of NMP being the best solvent in dispersing pristine SWNTs [32, 138, 158].

We also investigated non-ionic surfactants such as Triton-X 100, Pluronic F98, Igepal DM-970 in NMP as dispersing agents [158, 159]. Though they are able to disperse a higher amount of SWNTs than pure NMP, they do not help in individualizing nor stabilizing them [158, 159]. Interestingly, if polyvinylpyrrolidone (PVP) is added to SWNTs dispersed in pure NMP, spontaneous de-bundling occurs [158], even after re-aggregation of SWNTs [159]. This process depends on diameter and chirality [158]. In addition, reduction of PVP concentration initiates re-aggregation of dispersed SWNTs, thereby proving PVP to be essential to stabilize the dispersions [157]. Figure 9.2 illustrates the stabilizing effect of PVP concentration on SWNT dispersions in NMP [157].

Amphiphilic block copolymers may also be used to efficiently individualize SWNTs in DMF [198]. Indeed, they act as surfactants, having a hydrophobic block and a hydrophilic one. Polystyrene-block-polyacrilic acid (PS-b-PAA) forms micelles around individual SWNTs by gradual addition of water. The external hydrophilic blocks are finally cross-linked giving stable micelles, see Fig. 9.3 [198].

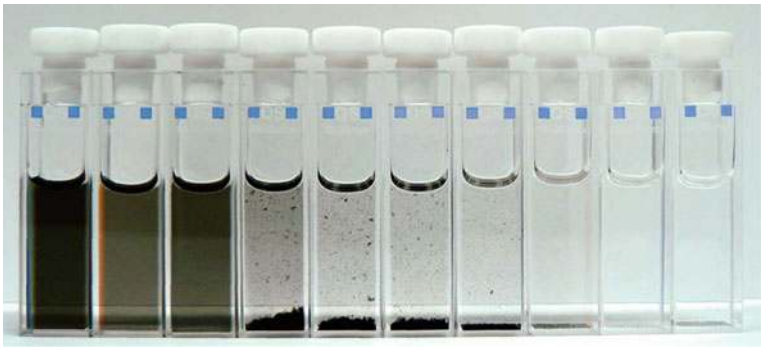

Fig. 9.2 Photograph of SWNT dispersion sets prepared with gradually lower PVP concentration (from *left* to *right*; 8.75, 6.56, 4.38, 2.63, 1.75, 1.31, 0.88, 0.44, 0.22, 0 gL^{-1}) with SWNT concentration (0.02 to ~0.0002 gL^{-1}). Previously dispersed SWNTs (~0.013 gL^{-1}) re-aggregate below ~3 gL^{-1} of PVP concentration [157]

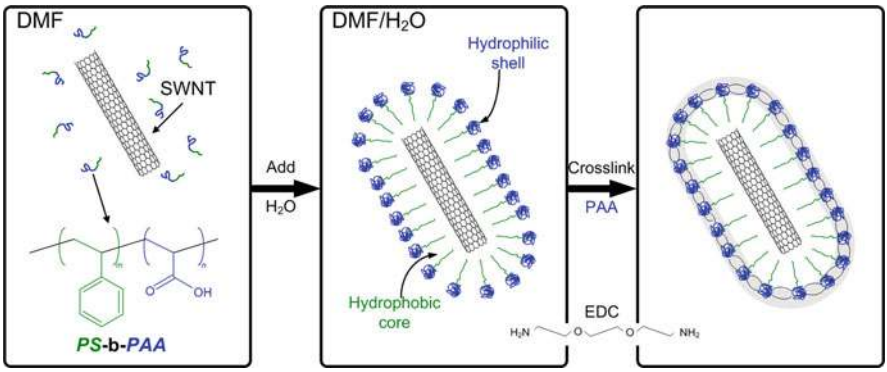

Fig. 9.3 Scheme of the individualization process of a SWNT by the PS-b-PAA block copolymer by creating micelle-like structures by cross-linking. Adapted from [198]

Conjugated polymers can also disperse high amounts of SWNTs in non-aqueous solvents [403–406]. Poly-[(m-phenylenevinylene)-co-(2,5-dioctyloxy-p-phenylenevinylene)] (PmPV) and its derivatives preferentially wrap around bundles rather than individual tubes, when chloroform is used as solvent [405, 406]. PmPV derivatives containing ionic side-groups can also disperse SWNT bundles in protic solvents like ethanol [403]. The dispersion mechanism is proposed to be π-π stacking and van der Waals interaction between PmPV and tube sidewalls [403]. On the other hand, if a hyper-branched variant of PmPV is used, SWNTs can be individually dispersed in chloroform [404]. In this case, the branched structure of the polymer forms cavities that are suitable to host individual SWNTs [404]. Individual SWNTs can also be separated in THF if poly(p-phenylene-1,2-vinylene) (PPV) is co-polymerized with units of p-phenylene-1,1-vinylidene [443]. The resulting copolymer (coPPV) has structural defects (the 1,1-vinylidene units) that allow the polymer backbone to fit the curvature of the nanotube sidewalls better than the homopolymer, thus wrapping around the SWNT by π-stacking [443].

9.3.3 Nanotube Dispersion in Liquid Crystals

The unique structure of Liquid Crystal (LC) molecules enables them to be aligned by surface treatment or by an applied field. The highly anisotropic interaction of SWNTs with light [6, 266, 387] dictates the need of their alignment parallel to the light polarization, so to maximize their absorption with minimal loading [179, 309, 357]. Dispersion of SWNTs in LC is therefore an attractive proposition for SWNT alignment, due to interaction with LCs, for photonic/optical applications [102, 243, 244, 276, 369, 438]. In fact, alignment of multiwall nanotube (MWNT) bundles was reported using E7 LCs and applying an electric field, even higher than the orientational ordering of E7 itself [101, 102]. In addition, even with very small CNT concentrations (e.g. <0.01∼0.05 wt%) [251], enhancement of the nonlinear

[218, 251, 369, 437], electrooptical [74, 176, 252, 253] and dielectric properties [73, 369] of pristine LCs was observed [73, 176, 218, 252, 253, 369]. The resulting high optical intensity of ~100 μWcm^{-2} [218], lower driving voltage [252, 253], suppression of field-screening [73] and faster reorientation of LCs, could improve the stability and response time of LC displays [176, 369]. SWNTs can be dispersed in LCs [369] directly, or using the LC molecules as dispersants [243, 244, 437]. Lyotropic LCs are amphiphillic compounds dissolved in solvents whose LC state or mesophase formation depends on their concentration and on the solvent itself [114]. Lyotropic LCs, in their solvents, have a hydrophobic and hydrophillic part in their structure, much like surfactants, and can be effectively used as dispersants for SWNTs. Reference [243] reported that lyotropic LC molecules arrange in micellar structures around CNTs, similar to the encapsulation of SWNTs by ionic surfactant micelles in aqueous suspensions [17]. Compared to CNT dispersions with thermotropic LCs (whose LC state or mesophase formation depends on temperature [114, 244]) [102, 276, 437, 438], lyotropic LC molecules in solvents allow higher loading (up to 0.15 wt%) [464] and better stability of the resultant dispersion [243, 244, 464]. Even higher loading of SWNTs results in phase separation and consequent decrease in viscosity [464]. It is important to note that for display applications, low loading of SWNTs in LC is desirable to minimize conductive contributions from m-SWNTs [369]. Therefore, lyotropic LCs might be used for CNT alignment only [244, 464]. Nevertheless, in both types of LCs, irrespective of CNT loading, CNTs can be aligned using the LC molecules by applying electric or magnetic fields [101, 102, 244, 464]. Thus, SWNT-LC dispersions are very attractive for large scale CNT alignment [102, 244].

9.4 Graphene Dispersion in Aqueous and Non-Aqueous Solvents

Exfoliation of graphene from graphite is a promising route for up-scalable, graphene based applications. Like SWNTs, graphene/graphite is hydrophobic and requires surfactants to form stable aqueous dispersions. Bile salts are excellent in exfoliating graphite flakes to produce aqueous dispersions of graphene [83, 161, 271, 284, 411]. This is due to the flat molecular structure of bile salts, which readily adsorb on graphitic surfaces [391, 409]. SDC, in particular, forms a large contact area (~1.8–3 nm^2) per surfactant molecule [368] with its β side compared to linear chain surfactants (e.g. sodium dodecylbenzene sulfonate (SDBS) [94, 271]), which adsorbs on graphitic surfaces through its alkyl chains [183]. The hydrophobicity of bile salts dictates how strongly their molecules are adsorbed on the graphitic surfaces. This is measured by the Hydrophobic Index (HI), defined as [301]:

$$HI = HI_\alpha + HI_\beta \tag{9.2}$$

where,

$$HI_{\alpha(\beta)} = \frac{Hydrophobic\ surface\ area_{\alpha(\beta)}}{Hydrophilic\ surface\ area_{\alpha(\beta)}} \times anomer\% \tag{9.3}$$

The *HI* of deoxycholic acid is 7.27, higher than that of its tri-hydroxy counterpart, cholic acid (6.91) [301]. This is also reflected in the higher effective contact area of SDC molecules with per gram of graphite (6.96 nm^2g^{-1}) compared to that of SC (5.72 nm^2g^{-1}) [368]. This also implies a denser and more regular graphene surface coverage with SC [161]. Di-hydroxy bile salts, e.g. SDC or sodium taurodeoxycholate (TDC), are thus more effective than the trihydroxy ones, e.g. SC or sodium taurocholate (TC), and significantly better than linear chain surfactants, such as SDBS. Thermodynamic parameters of bile salts adsorbing on graphite at 25–30°C show that ΔG_{mix} for SDC adsorbed on graphite (~ -28 kJ mol^{-1} [409]) is more negative than for SC ($\Delta G_{mix} \sim -26$ kJ mol^{-1} [409]). Since Eq. (1) dictates the thermodynamic stability of dispersions, graphene flakes dispersed by SDC in water are expected to be more stable compared to those dispersed by SC-water [409].

For a given graphene volume fraction and flake thickness in non-aqueous solvents, it was shown that [166]:

$$\Delta H_{mix} \propto (\delta_1 - \delta_2)^2 \tag{9.4}$$

where, δ_i is the square root of surface energy of graphene and solvent. This requires the surface energies of graphene and solvent to be very close for a stabilized dispersion, similar to what is empirically observed for pristine SWNTs, as discussed in Section 9.3.2. The surface tensions (γ) of NMP and *ortho*-dichlorobenzene (*o*-DCB) are 35.71 and 44.56 mJ m^{-2} [484]. When converted to solvent surface energy (E_{Sur}) with a generalized surface entropy (S_{Sur}) of 0.1 mJ K^{-1} m^{-2} [137, 275] using the relation $\gamma = (E_{Sur} - TS_{Sur})$ [275], we get ~65–75 mJ m^{-2} [161]. This is within the range of estimated surface energies (~70 mJ m^{-2}) of nanotubes and graphite

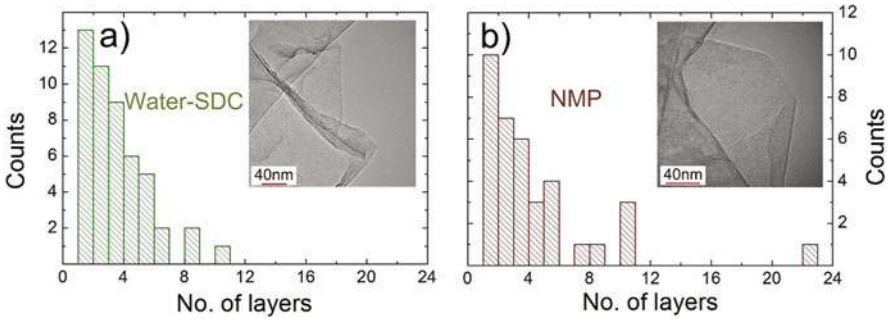

Fig. 9.4 TEM statistics for (**a**) water-SDC graphene dispersions showing ~50% SLG and BLG (**b**) anhydrous NMP dispersions showing ~50% SLG and BLG. Inset:folded SLG. Adapted from Ref. [161]

[32, 141, 166, 374, 436, 488] and explains efficient exfoliation of graphite in certain solvents, e.g. NMP and *o*-DCB. The concentrations of flakes in aqueous and non-aqueous dispersions can be >100 mg L^{-1} [161], with >50% SLG and BLG [161, 166, 271, 284]. Figure 9.4 shows TEM statistics and images of typical exfoliated flakes obtained by LPE.

9.5 Sorting Nanotubes by Chirality and Electronic Type Using Density Gradient Differentiation

The separation of SWNTs by different chiralities from as-grown, heterogeneous mixture of SWNTs would be the ideal way to exploit their full potential in any applications, since one could mix the different chiralities according to the needs. This is particularly important for optoelectronic applications, when SWNTs with defined electronic properties, diameter or chirality are most preferable. To date, different approaches for post-growth selection have been proposed, such as chromatography [496], electrophoresis [104, 235, 259], and conventional [461] or density gradient ultracentrifugation(DGU) [12, 13, 41, 86, 482]. Amongst these techniques, DGU has emerged as the most promising and versatile strategy. Indeed, separation of nanotubes by length [113], number of walls [147], diameter [13], metallic vs semiconducting (m/s) character [12] and chirality [41] has been reported. Here we will use "sorting" to indicate a generic process of postgrowth nanotube selection; "separation" to indicate a process resulting in a sample with diameter in a certain range or to indicate separation of m/s nanotubes; "enrichment" to indicate a process resulting in an increase of the percentage of nanotubes with certain chirality with respect to the pristine material.

Analytical ultracentrifugation is a well established and versatile technique for a wide range of applications [418]. It is, for example, useful to determine molecular weight [85], thermodynamic [361] and hydrodynamic [162] properties of molecules. Preparative ultracentrifugation was historically used in separation and manipulation of biological molecules such as DNA, RNA and different proteins [46, 84, 129, 144, 163, 228, 313]. When a uniform medium is used, this is referred to as differential ultracentrifugation [418]. If density gradient is introduced, this is knows as DGU [30, 337]. Differential ultracentrifugation separates particles based on their sedimentation rate [418], which determines how quickly they sediment out of the fluid in which they are dispersed, in response to a centrifugal force acting on them. In DGU, particles are ultracentrifuged in a preformed density gradient medium (DGM) [30, 337, 467]. During the process, they move along an ultracentrifuge cell, dragged by the centrifugal force, until they reach the corresponding isopycnic point, *i.e.*, the point where their buoyant density equals that of the surrounding DGM [467]. The buoyant density is defined as the density of the medium at the corresponding isopycnic point (measured in g/cm^3), which depends on the dispersion, on the type of surfactant and may also be different in diverse gradient media [180]. Such process depends only on the particles buoyant density, and is

also known as isopycnic separation. If the ultracentrifugation is stopped before the particles achieve their isopycnic points, a zonal separation (ZS) is attained [46]. The latter also depends on the particle sedimentation rates [46].

Isopycnic separation thus allows sorting and separation of SWNTs based on their density differences [12, 13, 86]. The DGM choice is largely driven by the material one needs to separate. Salts (such as cesium chloride, lithium chloride, sodium chloride, etc.), sucrose, and Optiprep, i.e. 60% w/v iodixanol (a non-ionic iso-osmotic derivative of tri-iodobenzoic acid [126]) solution in water [12, 41, 86] (ρ ~1.32 g cm^{-3}), are usually exploited in isopycnic separations. Due to the low viscosity of the DGM, density gradients produced by salts are less stable compared to those produced with Sucrose and Optiprep [41]. Moreover, salts induce strong aggregation on the hydrophobic solutes [55, 70] that sometimes affect the separation process itself [41]. Also, the percentage of sucrose used as DGM can have a significant impact on the separation [41]. Sucrose has high viscosity, increasing at high concentrations, and is mainly used in DGU for ZS rather than for isopycnic separation [41]. On the other hand, Optiprep is better suited for isopycnic separation due to its higher viscosity than salts, and better density tunability than sucrose [41]. Moreover, it has an almost constant viscosity as function of the gradient density [489], low osmolarity [109], is dialyzable and its gradients are self-forming [126]. There are different approaches (linear, non-linear or step gradient [12, 80, 133, 390, 447]) to prepare the density gradient. These are related to how the density of the liquid medium is varied across the length of a centrifuge cell. Step gradients are created by a series of steps increasing in density in order to separate the particles of interest from their undesirable neighbors [390, 447]. Non-linear gradients are formed so that the particles sediment at the same rate over the entire length of the cell [80]. Linear gradients are used to separate materials with very small differences in their buoyant density [46, 133] e.g. in SWNT sorting, as the difference in densities of SWNT is very small. Linear gradients are created directly in centrifuge cells either by using a linear gradient maker or making discrete layers of gradually increasing densities. In the latter case, the discrete layers diffuse into each other and form a linear density gradient [12, 86].

For sorting, a dispersion containing the SWNTs, after sonication and pre-ultracentrifugation, is inserted in the density gradient at the top or at a point where the density of the prepared gradient closely matches that of the solution. This can be determined by measuring the density of the SWNT dispersions and comparing it to that of different layers before their diffusion. The dispersion is then ultracentrifuged until equilibrium is reached. Because of the different densities of the gradient medium along the centrifuge cell, SWNTs are redistributed at their respective isopycnic points [12, 167]. A schematic of the process is presented in Fig. 9.5a. The appearance of different color bands is an indication of SWNTs sorting [12, 86]. The colors depend on the peak optical absorption. Thus, e.g., the purple color (non spectral red-blue combination) of the top band in Fig. 9.5b is due to (6,5) tubes that absorb at ~570 nm (eh_{22}) (yellow).

After ultracentrifugation, the sorted SWNTs are removed from the ultracentrifuge cells, layer by layer, using a fractionation technique. This is a widely used

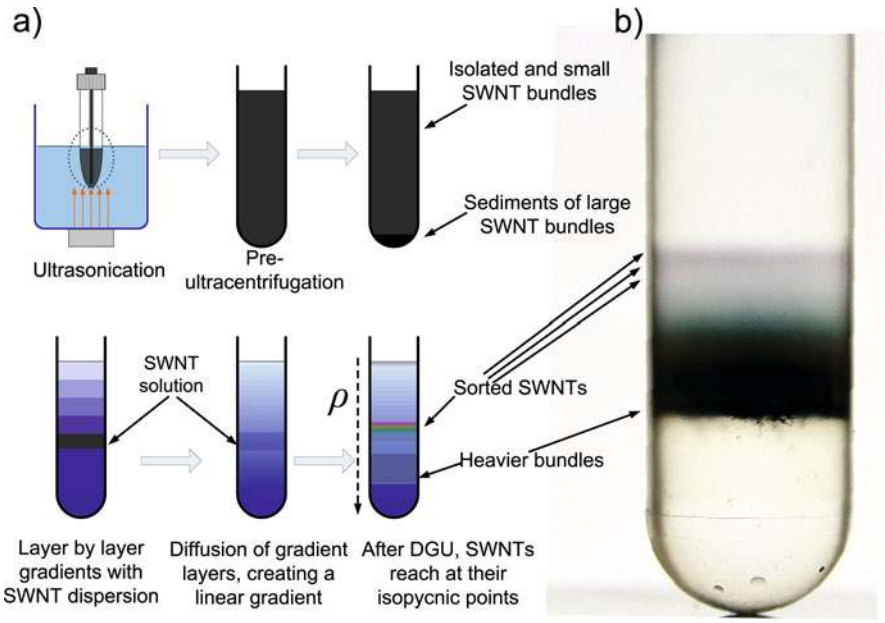

Fig. 9.5 Sorting of SWNTs using isopycnic separation: (**a**) Schematic of the process. (**b**) Sorted SWNTs at their isopycnic points. Adapted from Ref. [12]

process in life sciences by which certain quantities of a mixture are separately extracted to a large number of aliquots, whose composition varies according to the density gradient of the original mixture [407]. Fractionation methods are classified into three main categories: piston [47], down [48] and upward [47] displacement. For SWNT separation, upward displacement fractionation can be used to extract small aliquots [41, 86]. A dense solution, Fluorinert FC-40, is inserted with a needle at the bottom, pushing the gradient up into an inverted collection needle [7]. Because the density of the tubes changes with their diameter, considering a uniform surfactant coverage, this immediately links buoyant density to tube diameter, thus enabling an effective diameter sorting by isopycnic separation [12, 13, 41, 86].

Natural bile salts [356], such as SC, SDC or TDC are the most suitable surfactants for isopycnic separation, due to their steroid skeleton polar tail. These, in aqueous environments, expose their hydrophilic sides to the water and the hydrophobic sides to the SWNTs [465]. This is a key requirement in the adsorption of flat molecules onto the hydrophobic graphitic surface whose structure is composed of carbon atoms [301]. This also allows the exfoliation [161, 271, 284, 411] and separation of graphitic flakes by number of layers [148]. In contrast, linear chain surfactants, such as SDBS, have a flexible cylindrical body and inefficiently form micelles around SWNTs [295]. We demonstrated that the poor performance of linear chain surfactants in diameter separation, with respect to bile salts, is related, other than to inefficient de-bundling, to their surface coverage of SWNTs [41].

Linear chain surfactants form micelles around SWNTs with a random number of molecules, similar to their behavior with hydrophobic particles in aqueous solutions [295]. Since DGU is sensitive to the buoyant density of the SWNT-surfactant assembly, a uniform surface coverage of the sidewalls is critical. This is why linear chain surfactants are less effective.

Isopycnic separation allows m/s separation [12] with minimal modification of the protocol used for diameter separation [13]. This is achieved in a co-surfactant mixture, based on the principle that surfactants with different chemical structure adsorb in a different way on m/s-SWNTs sidewalls, due to their different polarizability [289], resulting in different buoyant densities. Mixtures of linear chain surfactants and bile salts are ideal due to their competitive absorption on SWNT sidewalls depending on the m/s nature of the tubes [272]. This creates subtle differences in the density of the micelle encapsulated SWNTs, enough to separate m- and s-SWNTs [12, 167].

Combining m/s and diameter separation, it is possible to enrich a single chirality [41]. For example, a (7,4) tube, with diameter 0.75 nm and chiral angle $\theta = 21°$ is geometrically close to a (6,5) (d = 0.75 nm and $\theta = 27°$). However, (7,4) is metallic and (6,5) is semiconducting. Hence, they can be separated due to their different electronic properties [12]. In order to reduce the (n,m) combinations and obtain the highest percentage of a single chirality, a two step procedure can be used: m/s separation exploiting a co-surfactant mixture (TDC-SDS) followed by diameter separation (SC). This allows, e.g., to selectively enrich (6,5) with respect to (7,4) and (6,6). Figures 9.6a, b demonstrate the enhancement of (6,5) [41]. Note that for an absolute population measurement, the PL cross section of individual species of SWNTs must be taken into account [323, 330, 353].

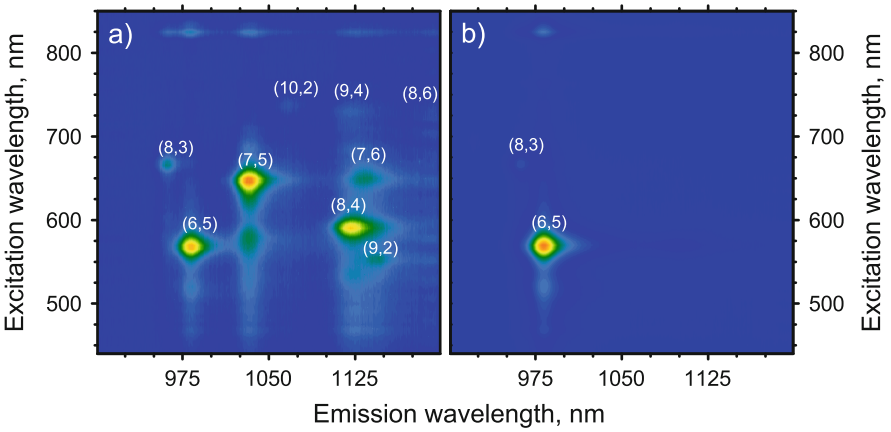

Fig. 9.6 Photoluminescence excitation map of (**a**) initial CoMoCAT dispersion showing the exciton-exciton resonances from different SWNTs; (**b**) After isopycnic separation. The enrichment of (6,5) is shown by the strong (eh_{22}, eh_{11}) resonance at ca. (982, 569) nm

9.6 Inkjet Printing of Nanotube and Graphene Dispersions

Deposition of fluidic droplets to form patterns directly on substrates using inkjet printing offers a mask-less, inexpensive and scalable low-temperature process for large area fabrication [34, 132, 204, 336, 388, 389, 408]. The core technology is very similar to that of consumer-level inkjet printers. Solution processable conjugated polymers are ideal to fully exploit such an inexpensive and flexible printing technique to realize all-polymer devices on a variety of substrates [34, 204, 389, 408]. In fact, a variety of devices for different applications, ranging from all-plastic electronics [204, 389, 408] to organic light emitting displays [386] has so far been demonstrated using this technology. The resolution of inkjet printing can be enhanced by pre-patterning the substrates, so that the functionalized patterns can act as barriers for the deposited droplets [203, 458]. Device channel lengths as small as 500 nm can be obtained [458]. Even higher resolution of 100–400 nm was recently demonstrated by a self-aligned inkjet printing method [318]. Using inkjet printing in conjunction with micro-embossing, self-aligned, vertical channel all-polymer thin film transistors were also reported [408].

Several inkjet printed devices on various un-patterned and pre-patterned substrates have thus far been demonstrated, using conjugated polymers, nanomaterials (e.g. pigments [231], microemulsions [196], magnetic nanoparticle-based inks [65], diamond [128] or metallic nanoparticles [315, 494]), CNTs [28, 174, 392], and graphene dispersed in carrier solvents. To minimize sedimentation, the particle sizes must have dimensions $< 1\ \mu m$ [56]. This limits the maximum nanoparticle volume fraction due to increased viscosity [56]. Direct inkjet printing of soluble organic precursors for making metal contacts in organic field effect transistors was recently reported [131, 471]. However, inkjet printing of silver-copper nanoparticle-based solutions yielded lower contact resistance compared to the organic precursor-based approach [131]. The advantages of inkjet printing of nanoparticles suspended in carrier solvents include greater ease of selective deposition and high concentration of materials for partially soluble compounds [56].

Printing nanotubes, graphene and nanotube-polymer composites directly on a range of substrates is thus an attractive technological proposition, due to its flexibility and selective deposition on a small target area [28, 40, 174, 233, 388, 392, 419]. This is even more attractive as it could result in improved mobility, environmental stability and lifetime compared to organic electronic devices [14, 28, 38]. Figure 9.7a, b show a printing head and a high speed close-up of a fluidic droplet being expelled from the 50 μm nozzle. Figure 9.7c is an optical micrograph of an array of inkjet printed SWNT-TFT devices [28] without any boundary patterns to restrict the spreading of the deposited droplets. Nevertheless, this demonstrates the effectiveness of selective deposition. As for nanoparticle-based solutions, it is vital to obtain an effective dispersion of SWNTs for inkjet printing. This is because aggregation of SWNTs, frequently encountered in organic solvents, easily clogs the print nozzles. Dispersions of pristine SWNTs in pure NMP are not stable. The aggregation is triggered by the tendency of NMP to absorb moisture. That is why using even a week-old SWNT dispersion for inkjet printing results in lumps

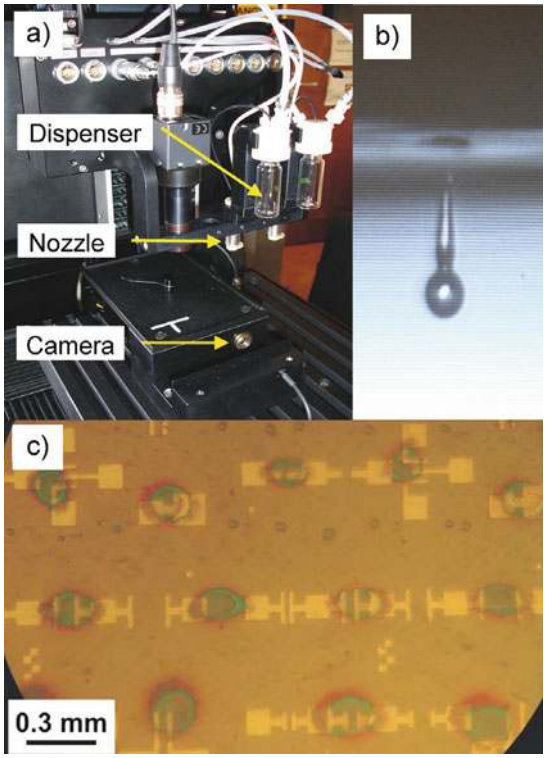

Fig. 9.7 (**a**) Inkjet printing head (**b**) High speed photographic close-up of the nozzle showing a droplet being expelled (**c**) Optical micrograph TFT-SWNT devices printed using inkjet [28]

on the substrate [28]. Printing percolated networks of SWNTs as transparent conductors replacements is also being investigated [98] (see Section 9.10.1). Though mostly unfunctionalized SWNTs have been used in literature, using different sidewall functionalizations, it was shown that the general characteristics of SWNT based inkjet printed transistors may be modified [142]. SWNTs stabilized by a water-soluble conducting polymer, namely poly(2-methoxyaniline-5-sulfonic acid) (PMAS), were also ink-jet printed on plastic substrates to yield transparent, conducting films [392]. Also, exclusively inkjet-printed SWNT thin film transistors with low-voltage operation were recently demonstrated using high-capacitance ionic-liquid dielectrics [326]. We also prepared a graphene-ink suitable for inkjet printing, achieving graphene TFTs with up to 95 $cm^2V^{-1}s^{-1}$ mobility and 80% optical transmittance, paving the way to high mobility all-inkjet printed graphene-based optoelectronics.

9.7 Optical Characterizations of Nanotube and Graphene in Dispersions

Significant efforts have been devoted to understanding the electronic and optical properties of nanotubes [17, 201, 293, 319, 335, 456]. Their quasi-one dimensionality gives rise to sharp spikes (van Hove singularities) in their electronic density

of states. The nature of the electronic transitions responsible for the optical properties in SWNTs has been the subject of intense debate. Many authors have discussed their experimental observations in terms of band-band transitions [201] involving free electron-hole pairs, Fig. 9.8a. The ensemble of transition energies E_{ii} between i-th van Hove peaks on opposite sides of the Fermi level vs tube diameter form the so-called *Kataura plot* [201]. This is widely used to understand absorption spectroscopy and resonant Raman spectroscopy of SWNTs. However, the electron-hole interaction in nanotubes is very strong [335]. The exciton binding energies of SWNTs are very large, ranging from tens of meV to 1 eV, depending on diameter, chirality, and dielectric screening [293, 335, 456]. Therefore, an incoming photon creates an exciton formed by bound electron(e)-hole(h) pairs in the i-th sub-band, Fig. 9.8b.

SWNT dispersions are usually characterized by UV-Vis absorption and photoluminescence excitation (PLE) spectroscopy, in order to assess the concentration and presence of individual tubes or bundles [16, 17, 175, 187, 226, 255, 293, 303, 304, 319, 321, 342, 355, 421, 456, 463]. As an example, Fig. 9.9 plots absorption spectra of SWNTs in different solvent-surfactant systems. The peaks in these spectra represent excitonic transitions, while their sharpness is an indication of the presence of isolated SWNTs [151, 308, 319]. For example, the features from 400 to 550 nm, 550 to 900 nm and 1,100 to 1,430 nm in the spectra represent eh_{11} of m-SWNTs, eh_{22} of s-SWNTs and eh_{11} of s-SWNTs, respectively [116, 187, 293, 319, 421, 456]. Bundling results in broadening of the absorption peaks [116, 321, 352, 421, 422, 457] and reduction of the transition energies. This causes a red-shift in the absorption spectra [116, 257, 321, 352, 422, 457]. However, changes in excitonic transition energies can also be caused by increase in the dielectric constant (ε) of the surrounding environment, the so-called "dielectric screening effect" [60, 116, 124, 335, 452, 457]. Due to this, the absorption spectra of SWNTs dispersed in aqueous solvents exhibit small shifts in transition energies depending on the dispersants used [299,

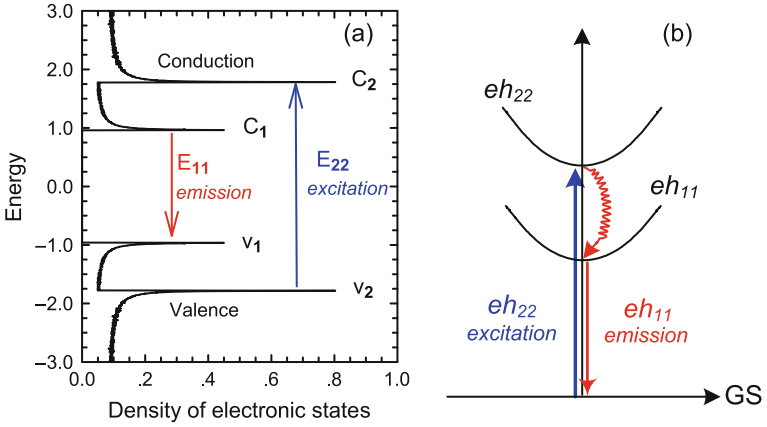

Fig. 9.8 Schemes of the optical excitation and emission of s-SWNTs based on the (**a**) band-to-band model and (**b**) exciton picture. GS represents ground state

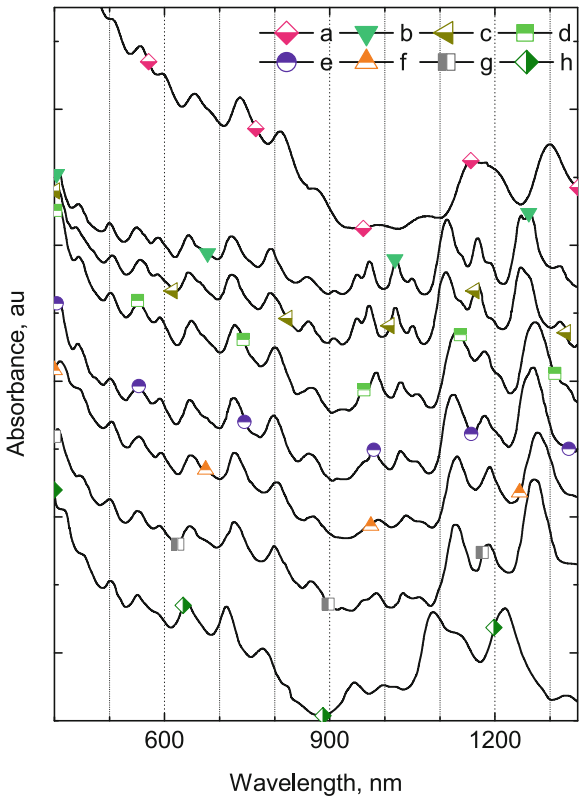

Fig. 9.9 Absorption spectra of SWNTs in different solvent-surfactant systems, (**a**) Pure NMP [158]; (**b**) Water/SDBS [308]; (**c**) Water/SDS [308]; (**d**) Water/CTAB [308]; (**e**) Water/Brij [308]; (**f**) Water/Na-CMC [299]; (**g**) Water/DNA [495]; (**h**) Water/Nano-1 [498]. These spectra illustrate the shift in absorption peaks due to the different dielectric environments surrounding the SWNTs

308, 495, 498]. In the case of organic solvents, a larger red-shift of 30–50 meV is usually observed, and attributed to large increase in dielectric screening [138, 158, 279, 384].

9.7.1 Estimation of Nanotube Loading

When preparing SWNT-polymer composites for optical applications, estimation of the SWNT aggregation in the dispersions (i.e. bundle size) is usually carried out by comparing SWNT dispersions prepared using the same dispersant/solvent combination, to eliminate the effects caused by different dielectric environments [60, 79, 124, 227, 305, 335, 352, 452, 457]. However, more specific information on SWNT bundling can be obtained using PLE spectroscopy, as discussed in Section 9.7.2. The SWNT concentration in a dispersion can be determined by the Beer-Lambert law $A_\lambda = \alpha_\lambda\, lc$, where A_λ is the absorbance of the material at the wavelength λ, α_λ is the corresponding absorption coefficient, l is optical path length and c is the concentration of the material. In case of very high SWNT concentration, the dispersion

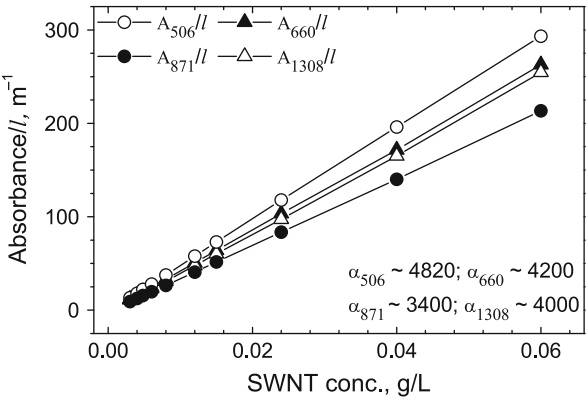

Fig. 9.10 Absorption coefficients of HiPco SWNTs in NMP at four wavelengths. Adapted from Ref. [158]

needs to be diluted to avoid scattering losses [39, 158, 159, 299]. In order to get a reliable result, it is necessary to determine α_λ at several wavelengths from a set of solutions with known SWNT concentration [138, 158, 245]. These wavelengths are chosen to match well-defined peaks in the absorption spectra of SWNTs in dispersions, e.g. eh_{11} of m-SWNTs (at 506 nm), eh_{22} of s-SWNTs (at 660 and 871 nm), and eh_{11} of s-SWNTs (at 1,308 nm) for SWNTs dispersed in NMP. Figure 9.10 shows an example used to estimate α_λ of HiPco SWNTs dispersed in pure NMP at four different wavelengths [158]. The values of α_λ thus obtained can then be used to assess the SWNT concentrations in unknown samples [138, 158, 245].

9.7.2 Detection of Nanotube Bundles

Bundling can decrease the gap in s-SWNTs even if the surrounding dielectric environment remains unchanged [321, 421, 422, 457]. Indeed, red-shift and broadening of excitonic transitions as a consequence of bundling was observed by resonant Raman profiles of radial breathing modes [321], Rayleigh scattering [457], absorption and PL spectroscopy [421, 422]. This is attributed to the modification of Coulomb interactions by dielectric screening induced by the adjacent nanotubes [452, 457]. In comparison to Raman scattering and Rayleigh scattering, absorption and PL spectroscopy are faster techniques to probe the red-shift of excitonic transitions in SWNT ensembles [321, 421, 422, 457]. However, because the optical transitions of SWNTs are strongly modulated by the dielectric environment [60, 79, 124, 227, 305, 335, 352, 452, 457], the comparison between different SWNT dispersions only works between dispersions prepared with the same combination of dispersant and solvent. It is not known how sensitively absorption or PLE spectroscopy can probe the bundle size in dispersions and composite films, because the optical transitions of SWNTs are usually very broad due to bundling inhomogeneity, packing efficiency and wide distribution of bundle sizes in the ensemble samples

[421, 422]. Therefore, it is necessary to explore a direct, simple and independent way to identify the presence of bundles in SWNT dispersions and films.

We observed exciton energy transfer (EET) between nanotubes in bundles [371, 421, 422]. EET is very common and widely studied in biological systems, conjugated polymers, quantum wires, dots, and other low-dimensional systems [1, 27, 36, 127, 194]. A thorough investigation of PL and PLE spectra of SWNT dispersions shows that the apparently complex absorption and emission features can be explained by EET between adjacent s-SWNTs within a bundle [421]. Detection of EET does not require any reference sample; hence, is an independent method to monitor bundles. For example, Ref. [421] showed that 2 months after preparation, CoMoCAT dispersions in water with 1 wt% SDBS form small bundles. This was hinted by a red-shift in eh_{11} emission wavelengths [321, 422, 457]. However, a number of new resonance spots were also detected, not corresponding to any exciton-exciton resonances of SWNTs in the emission range from 1,150 to 1,350 nm [16, 17]. We attributed these spots to EET from large-gap s-SWNTs (donors) to small-gap s-SWNTs (acceptors). Because of the large exciton binding energies [293, 335, 456], energy transfer between s-SWNTs occurs via excitons [421], not via inter-tube electron or hole migration as suggested by Ref. [433]. Note that these optical features are distinct from the deep excitonic states (DE) reported in Ref. [248]. The intensity of the DE features is very weak and their positions are dependent on the associated excitonic transition energies, while the EET features can be very strong and are exclusively dependent on the excitonic transition energies of the donor and acceptor s-SWNTs [421]. Figure 9.11 schematically describes EET from a donor nanotube to an acceptor. The emission-absorption overlap between donor and acceptor SWNTs depends on the specific donor-acceptor couple. We proposed Förster resonance energy transfer (FRET) [127] as the EET mechanism [421] because of the high degree of orientation and small wall to wall distance between tubes in bundles, the latter also favoring multipolar contributions [127, 194]. The EET features, marked in circles and ellipses in the PLE map shown in Fig. 9.12, are summarized in Table 9.1. These can thus be used to detect the presence of bundles in SWNT dispersions.

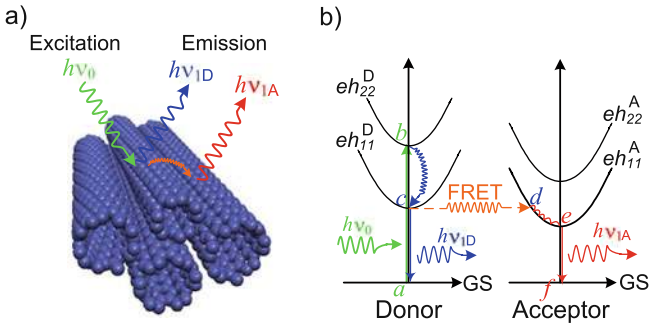

Fig. 9.11 Schematic illustration of EET from a large gap s-SWNT to a smaller gap s-SWNT [421]

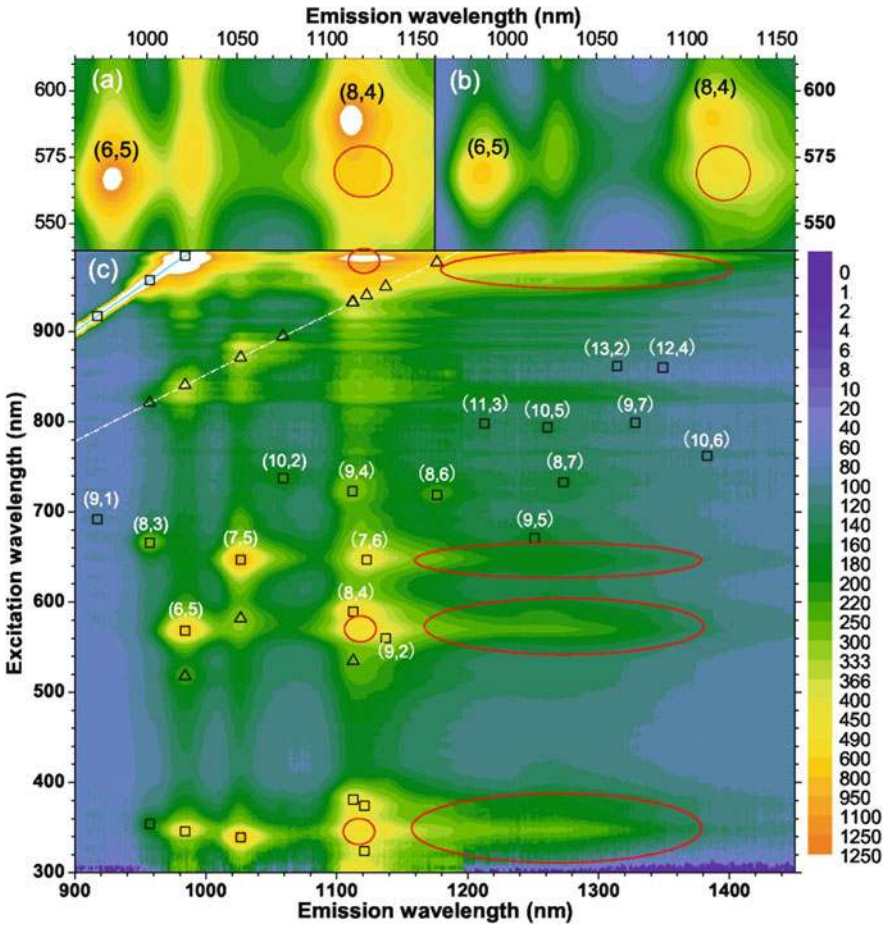

Fig. 9.12 PLE map for (**a**) as-prepared dispersions and (**b**, **c**) after 2 months of incubation, where the PLE maps in (**a**) and (**b**) are within the eh_{11} emission and the eh_{22} excitation of (6,5) and (8,4) tubes. *Solid lines* at upper left corners represent resonances with same excitation and recombination energies. The *dashed-dotted lines* are associated with the *D* sideband of eh_{11} excitons. *Open squares* represent eh_{11} emission of SWNTs for which excitation matches their eh_{11}, eh_{22}, eh_{33} and eh_{44} transitions. Each (eh_{22}, eh_{11}) resonance is labeled with the chiral index of the corresponding SWNT. *Open up-triangles* are phonon sidebands of eh_{11} and eh_{22} excitons. *Open circles* mark emission from (8, 4), (7, 6) and (9,4) SWNTs, with excitation matching eh_{11}, eh_{22} and eh_{33} of (6,5). Broad spectral features marked by *ellipses* are assigned to EET between s-SWNTs [421]

9.7.3 Optical Characterizations of Graphene in Dispersions

The linear dispersion of Dirac electrons in graphene [40, 160, 311, 411] results in flat absorption spectra from the visible to the near IR region. A UV peak is also observed which is a signature of the van Hove singularity in the graphene density of states [234]. As for SWNTs, the loading of graphene in aqueous or non-aqueous

Table 9.1 Assignment of exciton-exciton bands and corresponding EET features in the PLE map of as-prepared CoMoCAT SWNT dispersions in D_2O/SDBS. λ_{ex} and λ_{em} are excitation and emission wavelengths in nm, E_{ex} and E_{em} the excitation and emission energy in eV. (n, m) is the chirality. eh_{ii}^{D} (i = 1,2,3,4) and eh_{11}^{A} are excitonic transitions of donors (D) and excitonic emission of acceptors (A), respectively. Here, eh_{ii} (i=1,2,3,4) correspond to the excitonic states associated with the i-th electronic inter band transition E_{ii} (i=1,2,3,4) in the single-particle picture

		EET features		
(λ_{ex},λ_{em})	(E_{ex}, E_{em})	Donor	Assign.	Acceptor
(980,1025)	(1.265,1.210)	(6,5)	$(eh_{11}^{D}, eh_{11}^{A})$	(7,5)
(980,∼1116)	(1.265,1.111)	(6,5)	$(eh_{11}^{D}, eh_{11}^{A})$	(8,4),(9,4),(7,6)
(980,1139)	(1.265,1.088)	(6,5)	$(eh_{11}^{D}, eh_{11}^{A})$	(9,2)
(980,1180)	(1.265,1.051)	(6,5)	$(eh_{11}^{D}, eh_{11}^{A})$	(8,6)
(980,∼1260)	(1.265,0.984)	(6,5)	$(eh_{11}^{D}, eh_{11}^{A})$	(9,5),(10,5),(8,7)
(980,∼1330)	(1.265,0.932)	(6,5)	$(eh_{11}^{D}, eh_{11}^{A})$	(13,2),(9,7),(12,4)
(914,∼1116)	(1.357,1.111)	(9,1)	$(eh_{11}^{D}, eh_{11}^{A})$	(8,4),(9,4),(7,6)
(879,∼1116)	(1.411,1.111)	(6,4)	$(eh_{11}^{D}, eh_{11}^{A})$	(8,4),(9,4),(7,6)
(828,980)	(1.498,1.265)	(5,4)	$(eh_{11}^{D}, eh_{11}^{A})$	(6,5)
(828,1025)	(1.498,1.210)	(5,4)	$(eh_{11}^{D}, eh_{11}^{A})$	(7,5)
(828,∼1116)	(1.498,1.111)	(5,4)	$(eh_{11}^{D}, eh_{11}^{A})$	(8,4),(9,4),(7,6)
(828,1139)	(1.498,1.088)	(5,4)	$(eh_{11}^{D}, eh_{11}^{A})$	(9,2)
(828,1180)	(1.498,1.051)	(5,4)	$(eh_{11}^{D}, eh_{11}^{A})$	(8,6)
(828,∼1260)	(1.498,0.984)	(5,4)	$(eh_{11}^{D}, eh_{11}^{A})$	(9,5),(10,5),(8,7)
(828,∼1330)	(1.498,0.932)	(5,4)	$(eh_{11}^{D}, eh_{11}^{A})$	(13,2),(9,7),(12,4)
(645,1060)	(1.922,1.170)	(7,5)	$(eh_{22}^{D}, eh_{11}^{A})$	(10,2)
(646,1139)	(1.919,1.089)	(7,5)(7,6)	$(eh_{22}^{D}, eh_{11}^{A})$	(9,2)
(646,1180)	(1.919,1.051)	(7,5)(7,6)	$(eh_{22}^{D}, eh_{11}^{A})$	(8,6)
(646,∼1260)	(1.919,0.984)	(7,5)(7,6)	$(eh_{22}^{D}, eh_{11}^{A})$	(9,5)(10,5)(8,7)
(646,∼1330)	(1.919,0.932)	(7,5)(7,6)	$(eh_{22}^{D}, eh_{11}^{A})$	(13,2),(9,7),(12,4)
(589,1139)	(2.105,1.089)	(8,4)	$(eh_{22}^{D}, eh_{11}^{A})$	(9,2)
(589,1180)	(2.105,1.051)	(8,4)	$(eh_{22}^{D}, eh_{11}^{A})$	(8,6)
(589,∼1260)	(2.105,0.984)	(8,4)	$(eh_{22}^{D}, eh_{11}^{A})$	(9,5)(10,5)(8,7)
(566,1025)	(2.191,1.209)	(6,5)	$(eh_{22}^{D}, eh_{11}^{A})$	(7,5)
(566,∼1116)	(2.191,1.111)	(6,5)	$(eh_{22}^{D}, eh_{11}^{A})$	(8,4)(9,4)(7,6)
(566,1139)	(2.191,1.089)	(6,5)	$(eh_{22}^{D}, eh_{11}^{A})$	(9,2)
(566,1180)	(2.191,1.051)	(6,5)	$(eh_{22}^{D}, eh_{11}^{A})$	(8,6)
(566,∼1260)	(2.191,0.984)	(6,5)	$(eh_{22}^{D}, eh_{11}^{A})$	(9,5)(10,5)(8,7)
(566,∼1330)	(2.191,0.932)	(6,5)	$(eh_{22}^{D}, eh_{11}^{A})$	(13,2),(9,7),(12,4)
(371,1139)	(3.342,1.089)	(7,6)	$(eh_{33}^{D}, eh_{11}^{A})$	(9,2)

Table 9.1 (continued)

		EET features		
(λ_{ex},λ_{em})	(E_{ex}, E_{em})	Donor	Assign.	Acceptor
(371,1180)	(3.342,1.051)	(7,6)	(eh^D_{33}, eh^A_{11})	(8,6)
(371,∼1260)	(3.342,0.984)	(7,6)	(eh^D_{33}, eh^A_{11})	(9,5)(10,5)(8,7)
(321,1139)	(3.863,1.089)	(7,6)	(eh^D_{44}, eh^A_{11})	(9,2)
(321,1180)	(3.863,1.051)	(7,6)	(eh^D_{44}, eh^A_{11})	(8,6)
(346,1060)	(3.584,1.170)	(6,5)	(eh^D_{33}, eh^A_{11})	(10,2)
(346,∼1116)	(3.584,1.111)	(6,5)	(eh^D_{33}, eh^A_{11})	(8,4)(9,4)(7,6)
(346,1139)	(3.584,1.089)	(6,5)	(eh^D_{33}, eh^A_{11})	(9,2)
(346,1180)	(3.584,1.051)	(6,5)	(eh^D_{33}, eh^A_{11})	(8,6)
(346,∼1260)	(3.584,0.984)	(6,5)	(eh^D_{33}, eh^A_{11})	(9,5)(10,5)(8,7)
(346,∼1330)	(3.584,0.932)	(6,5)	(eh^D_{33}, eh^A_{11})	(13,2),(9,7),(12,4)
(337,1060)	(3.679,1.170)	(7,5)	(eh^D_{33}, eh^A_{11})	(10,2)
(337,∼1116)	(3.679,1.111)	(7,5)	(eh^D_{33}, eh^A_{11})	(8,4)(9,4)(7,6)
(337,1139)	(3.679,1.089)	(7,5)	(eh^D_{33}, eh^A_{11})	(9,2)
(337,1180)	(3.679,1.051)	(7,5)	(eh^D_{33}, eh^A_{11})	(8,6)
(337,∼1260)	(3.679,0.984)	(7,5)	(eh^D_{33}, eh^A_{11})	(9,5)(10,5)(8,7)
(337,∼1330)	(3.679,0.932)	(7,5)	(eh^D_{33}, eh^A_{11})	(13,2),(9,7),(12,4)

dispersions can be estimated by UV-Vis absorption spectroscopy in conjunction with Beer-Lambert law, using experimentally determined absorption co-efficient of graphene at the desired wavelength [161, 166, 271].

9.8 Nanotube/Graphene Polymer Composites

The following subsections review generalized procedures used to prepare SWNT or graphene polymer composites and the desirable characteristics of host matrices for some selected applications, such as saturable absorbers (SAs).

9.8.1 Incorporation of Nanotube/Graphene in Host Polymer Matrices

SWNTs or graphene are dispersed in appropriate solvents, generally by ultrasonic treatment. The dispersions may initially contain aggregates or bundles, which can then be removed by centrifugation or filtration. There is a trade-off between the desired SWNT bundle sizes/unexfoliated graphene flakes and their concentration.

In case of water, high loading of both SWNTs and graphene may be achieved using surfactants, making it easier to control the optical density in the resultant composites. Organic solvents, on the other hand, cannot generally disperse a high amount of SWNTs/graphene. If allowed by the final application, nanotubes can be oxidized [2, 476] or functionalized [260, 347] to improve dispersion and loading. This also holds true for graphene, where functionalization dramatically improves the amount of material that can be dispersed [332]. For SWNTs, when covalent functionalization is not an option, different polymers are employed as dispersants, which can also act as the host in the final composite [206, 362, 476]. Commonly used organic solvents are *o*-DCB [476], chloroform [240, 338, 476], NMP [158, 159, 362] and toluene [206]. For graphene, NMP and *o*-DCB are usually the common non-aqueous solvents. After removal of aggregates or un-exfoliated material, the dispersions are mixed with the host polymer. The same protocol is followed in organic solvents if a different polymer is used as the dispersant. The mixtures are then drop-cast or spin coated, depending on the final application. Free standing or substrate-bound composites with homogeneous, submicrometer distribution of SWNTs/graphene are then obtained by evaporating the solvent [241, 357, 359, 360, 363, 370, 371].

For SWNTs, composites with individually dispersed nanotubes may also be fabricated using cellulose derivatives [299, 428]. In this instance, the dispersions are drop-cast [299, 428]. Cellulose-based composites eliminate the need for surfactants, as they are used both as the dispersant and host matrix [299, 428]. Individually dispersed SWNTs can also be prepared in gelatine films [224]. SWNT-SDS dispersions, mixed with a gelatine aqueous solution, are sonicated at 40°C and cast on a substrate to dry at room temperature to obtain such composites. Gelatine undergoes gelation at 37°C while cooling down, thus preventing re-aggregation [224].

9.8.1.1 Alignment of Nanotubes in Composites

Alignment of SWNTs is important, due to the high anisotropic interaction of SWNTs with light [6, 266, 387]. In aligned SWNTs, absorption is maximum when polarization is parallel to the alignment direction [177, 179, 182, 263, 309, 357]. Various methods, in particular mechanical stretching and Langmuir-Blodgett (LB), have been used to achieve alignment of SWNTs.

High degree of alignment within the polymer matrix can be achieved by laterally stretching the composite [179, 224, 299, 357]. A SWNT-polytstyrene-toluene dispersion cast on a teflon sheet was reported to be stretchable 10 times, yielding 56% of SWNTs aligned within ∼15° of the stretching axis [179]. PVA can be stretched up to 6 times by heating at 60°C in a humid environment [357], whereas gelatine films may be stretched up to three times under swelling in a water-ethanol mixture, and dried under constant elongation [224]. Hydroxyethylcellulose composites can be stretched up to three times at 100°C by adding glycerine as plasticizer [299]. Figure 9.16 shows the change of absorption of a mechanically stretched SWNT-PVA composite for incident light with varying polarization [179, 357].

LB may also be used to fabricate self-aligned SWNTs [150, 225, 385]. A graphical illustration of the LB technique used with a SWNT aqueous dispersion is shown

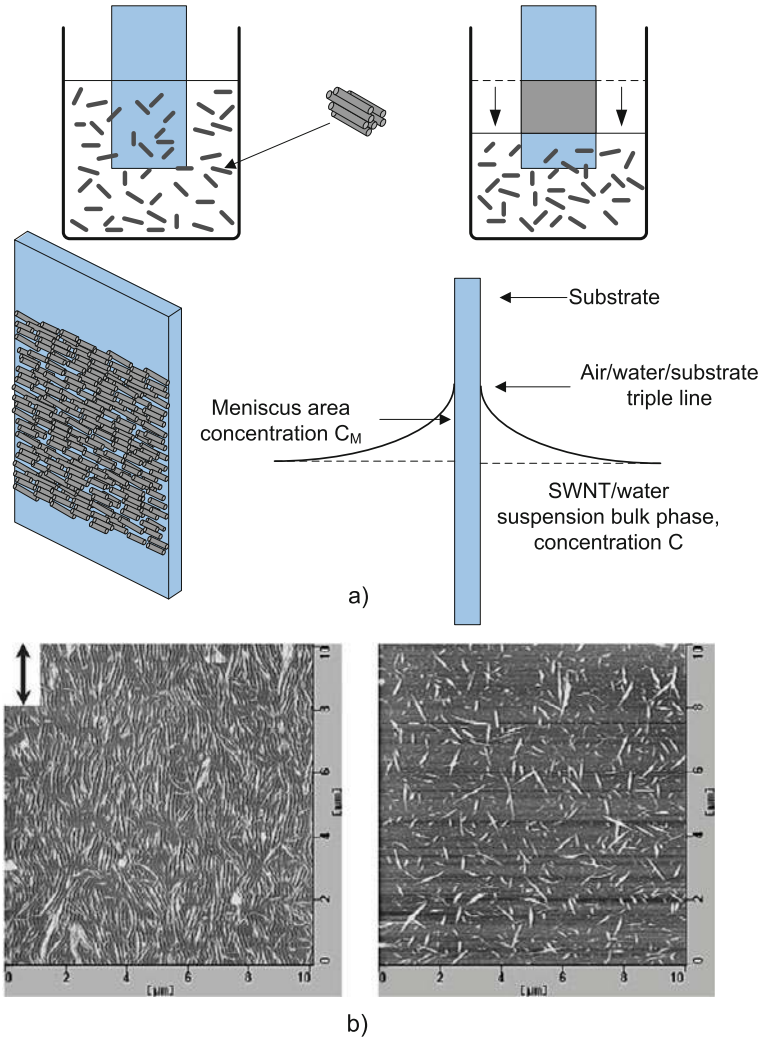

Fig. 9.13 (**a**) Schematic illustration of the SWNT self-assembly process. A hydrophilic glass slide is vertically immersed in a stable dispersion of short SWNTs. With gradual evaporation of the water, the SWNT bundles self-assemble on the glass substrate around the air/dispersion/substrate triple line. As the triple line progress downwards, a continuous SWNT film forms on the substrate. Figure adapted from [385]. (**b**) AFM images of an s-SWNT single layer on mica prepared by vertical dipping (*left*) and a drop-and-dry film prepared from the same dispersion (*right*). The *arrow* indicates the dipping direction. Adapted from Ref. [225]

in Fig. 9.13a [385]. A comparison between the AFM images of randomly oriented and aligned SWNTs can be seen in Fig. 9.13b [225]. The nanotube self-alignment process occurs at the air-substrate-solution triple line as the solvent gradually evaporates [385]. Also, in-plane compression can be used to further align the tubes

[225]. Composites with poly(N-dodecylacrylamide) (PDDA) polymer have been reported using the LB method, but no specific information on the degree of alignment was available [150]. As discussed in Section 9.3.3, LCs can also be used to align SWNTs.

LB may also be used to fabricate graphite oxide [71] or graphene [264, 425] composites with in-plane flake orientation or stacking.

9.8.2 Desirable Characteristics of Host Polymers

Important requirements for high efficiency photovoltaic cells include effective hole-transport, suitable bandgap and high stability against humidity [205]. Nanotube and graphene composites with conjugated polymers are generally used for electroluminescent and photovoltaic devices [2, 205, 206, 240, 260, 333, 347, 476]. For the case of SWNTs, the use of conjugated polymers has the added advantage of improved dispersion during the solution processing step. However, these are sensitive to moisture and light [405, 406].

Thus, desirable characteristics of polymers for telecommunication applications also include stability of the optical properties against humidity [277]. The host polymer must not have high absorption losses at the device operation wavelength. These usually arise from vibration overtones, see Table 9.2. The bonds giving higher overtone absorption intensities are C–H and O–H, while C–F overtones give the least absorption [277]. As shown in Table 9.3, fluorinated polymers are the most transparent polymers commercially available for telecommunication applications [277].

Polymers commonly used for optical applications are, e.g., polymethylmethacrylate (PMMA), polystyrene (PS), polycarbonate (PC) and epoxy resins [277]. Over the years, several new polymers have been developed, which comply with the requirement of low optical loss and environmental stability, such as deuterated or halogenated polyacrylates and fluorinated polyimides [277]. These have low losses

Table 9.2 Wavelengths and intensities of some important vibration overtones (Adapted from [66])

	Overtone order	Wavelength [nm]	Intensity (relative)
C–H	1	3,390	1
C–H	2	1,729	7.2×10^{-2}
C–H	3	1,176	6.8×10^{-3}
C–D	3	1,541	1.6×10^{-3}
C–D	4	1,174	1.3×10^{-4}
C–F	5	1,626	6.4×10^{-6}
C–F	6	1,361	1.9×10^{-7}
C–F	7	1,171	6.4×10^{-9}
C=O	3	1,836	1.2×10^{-2}
C=O	4	1,382	4.3×10^{-4}
C=O	5	1,113	1.8×10^{-5}
O–H	2	1,438	7.2×10^{-2}

Table 9.3 Characteristics of commercially available polymers for optical applications (from [277])

Company	Polymer type	Patterning techniques	Propagation loss, single-mode waveguide [db/cm] (wavelength, [nm])	Other properties (wavelength, [nm])
Optical crosslinks (formerly Dupont and Polymer photonics)	Acrylate (Polyguide)	Diffusion	0.18 (800) 0.2 (1,300) 0.6 (1,550)	Laminated sheets excimer-laser machinable
Corning (formerly AlliedSignal)	Acrylate	Photoexposure/wet etch, RIE, laser ablation	0.02 (840) 0.3 (1,300) 0.8 (1,550)	Birefringence: 0.0002 (1,550) crosslinked, Tg: 25°C Environmentally stable
	Halogenated acrylate	Photoexposure/wet etch, RIE, laser ablation	0.01 (840) 0.06 (1,300) 0.2 (1,550)	Birefringence: 0.000001 (1,550) Crosslinked, Tg: −50°C Environmentally stable
NTT	Halogenated acrylate	RIE	0.02 (830) 0.07 (1,310) 1.7 (1,550)	Birefringence: 0.000006 (1,310) Tg: 110°C
	Deuterated polysiloxane	RIE	0.17 (1,310) 0.43 (1,550)	Environmentally stable
	Fluorinated polyimide	RIE	TE:0.3, TM:0.7 (1,310) PDL: 0.4 dB/cm (1,310)	Environmentally stable
Amoco	Fluorinated polyimide (Ultradel)	Photoexposure/wet etch	0.4 (1,300) 1.0 (1,550)	Birefringence: 0.025, crosslinked, thermally stable
General electric	Polyetherimide (Ultem)	RIE, laser ablation	0.24 (830)	Thermally stable
Hitachi	Fluorinated polyimide	Photoexposure/wet etch	TE:0.5, TM:0.6 (1,300)	Birefringence: 0.009 (1,300), PDL: 0.1 dB/cm (1,300), Tg: 310°C, thermally stable
Dow chemical	Perfluorocyclobutane (XU 35121)	Photoexposure/wet etch	0.25 (1,300) 0.25 (1,550)	Tg: 400°C
	Benzocyclobutene (Cyclotene)	RIE	0.8 (1,300) 1.5 (1,550)	Tg: > 350°C
Asahi glass	Perfluorovinyl ether cyclopolymer (CYTOP)			n = 1.34 Tg = 108°C

Table 9.3 (continued)

Company	Polymer type	Patterning techniques	Propagation loss, single-mode waveguide [db/cm] (wavelength, [nm])	Other properties (wavelength, [nm])
Dupont	Tetrafluoroethylene and perfluorovinyl ether copolymer (Teflon AF)			n = 1.31 (AF 1,600) n = 1.29 (AF 2,400)
JDS uniphase (formerly Akzo Nobel) telephotonics	Polycarbonate (BEAMBOX)	RIE	0.6 (1,550)	Thermally stable
	(OASIC)	Photoexposure/wet etch, RIE, laser ablation	<0.01 (840) 0.03 (1,300) 0.1 (1,550)	Environmentally stable
Gemfire	(Gemfire)	Photoexposure, wet etch	1.0 (1,550)	Birefringence: 0.0002 (1,550) crosslinked
K-JIST	Fluorinated poly(arylene ether sulfide) (FPAESI)	RIE	TE:0.42, TM:0.4 (1,550)	Birefringence: 0.0003 (1,550) PDL: 0.02 dB/cm (1,550), crosslinked, thermally stable
Redfern	Inorganic polymer glass (IPG)	RIE		Environmentally stable
Hoechst celanese	PMMA copolymer (P2ANS)	Photobleaching	1.0 (1,330)	NLO polymer
PacificWave	Polycarbonate with CLD-1 chromophore (PC-CLD-1)	RIE	1.8 (1,550)	NLO polymer, r_{33} = 70 pm/V (1,310), pigtail loss = 1.5 dB/facet
Lumera	Polyurethane with FTC chromophore (PU-FTC)	RIE	2.0 (1,330)	NLO polymer, r_{33} = 25 pm/V (1,310), pigtail loss = 5 dB/facet
Ipitek	Poly (methylmethacrylate) with CLD-1 chromophore (PMMA-CLD-1)	RIE	5.0 (1,330)	NLO polymer, r_{33} = 60 pm/V (1,300), pigtail loss = 3.5 dB/facet

at the telecommunication wavelengths. However, their thermal stability is poor [277]. Fluorinated polyimides have high thermal stability and low optical losses and are, therefore, an ideal choice for telecommunication applications [277]. Polymers should also be resistant to laser-induced damage.

Nevertheless, water-soluble polymers, such as polyvinylalcohol (PVA) and cellulose derivatives, have predominantly been used for SAs due to their compatibility with high concentration SWNT/graphene aqueous solutions [160, 344, 345, 357, 359, 360, 363, 370, 371, 411, 414, 428]. High SWNT/graphene concentration allows to obtain the desired level of optical density, while minimizing unwanted non-saturable absorption losses [96, 160, 358, 363, 370]. PVA has been employed for the fabrication of freestanding films embedding both bundles and individualized SWNTs for fundamental studies of saturable absorption [357, 359], and for SWNT/graphene devices [96, 160, 344, 345, 358, 360, 363, 370, 411, 414]. Polyimides [362] and Polycarbonates (PC) [372] have been considered as alternative to PVA. In particular, PC has higher transparency and environmental stability compared to PVA and cellulose derivatives. High SWNT loading can be obtained in DCB using regioregular poly(3-hexylthiophene-2,5-diyl) (P3HT) as dispersant polymer [372].

Thermal stability is an important issue for all photonic and optical applications, as polymers lose their transparency over time due to oxidation [206, 277]. This process depends on the chemical structure, as it is induced by the formation of double bonds resulting mainly from the expulsion of H-halogen molecules [277]. Totally halogenated materials are thus the most stable due to the absence of hydrogen [277].

9.9 Characterization of Composites

9.9.1 Optical Microscopy

Composites prepared for optical applications can be characterized using different methods. Examination of the presence of voids, cracks, bubbles, particles, SWNT/graphene aggregations or other physical defects is generally carried out by optical or scanning electron microscopy. Figure 9.14 shows a set of optical microscope images of SWNT composites to be used as a SA at the telecommunication wavelength ($\sim$1.5 μm) [359]. No significant aggregation can be resolved, indicating homogeneous dispersion. Composites of similar optical quality may also be prepared from liquid phase exfoliated graphene [160, 411, 414].

9.9.2 UV-Vis-IR Spectrophotometry

The optical density of SWNTs/graphene in SA composites at the device operation wavelength is an important indicator of the expected performance [358]. UV-Vis-IR spectrophotometry can be used to determine the optical density. Figure 9.15 shows

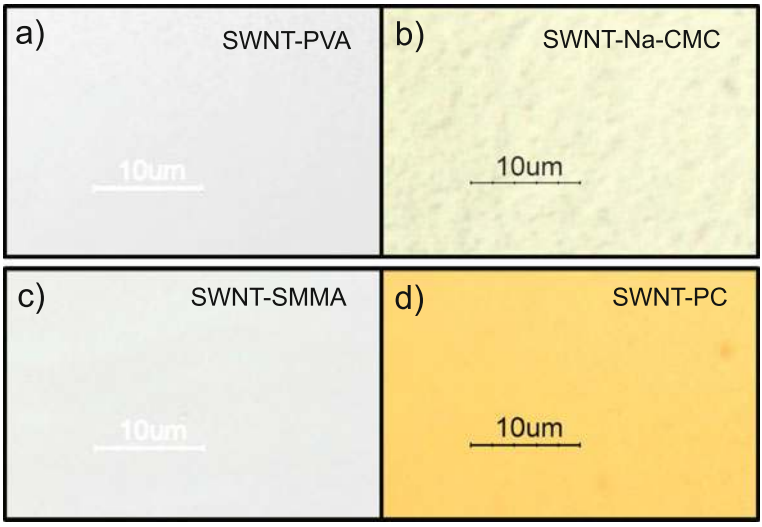

Fig. 9.14 Representative optical micrographs of SWNT-polymer composites from: aqueous dispersion (**a**) PVA, (**b**) Na-CMC and non-aqueous dispersion (**c**) SMMA and (**d**) PC [160]

the absorption spectra of a SWNT-PVA film (thickness ~80 μm), a pure PVA film and the SWNT dispersion from which the SWNT-PVA film is prepared [371]. The SA made from this composite is intended to operated at ~1.5 μm, where the SWNTs in the composite exhibit strong absorption [371]. Note the shift in absorbance for the SWNTs embedded in the host polymer compared to the dispersion. This can be attributed to change in dielectric environment [60, 116, 452, 457] as well as mechanical stress experienced by the SWNTs embedded in the host matrix [468].

Alignment of SWNTs in samples with same loading and thickness can be studied using UV-Vis-IR absorption. For example, in Figure 9.16, the three major SWNT

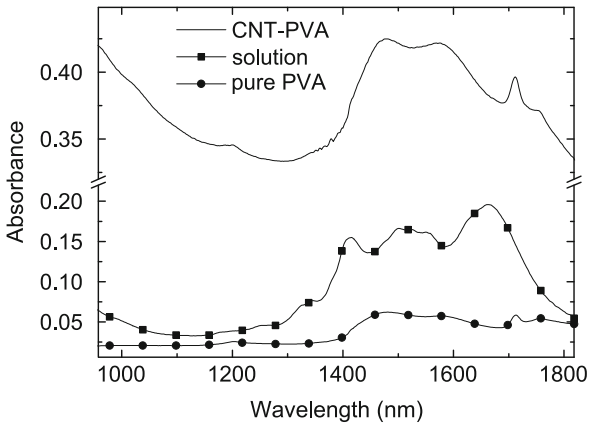

Fig. 9.15 Absorption spectra of SWNTs in a PVA-LA-SWNT composite (*top*) exhibits red-shift compared to that in the dispersion due to change in dielectric environment and mechanical stress

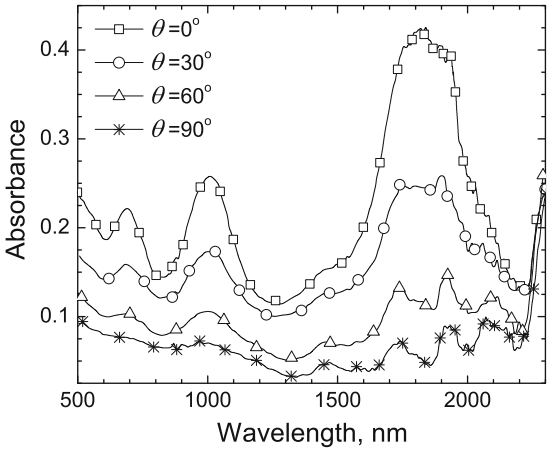

Fig. 9.16 Change in the absorption of aligned SWNTs with the polarization of incident light. Adapted from Ref. [357]

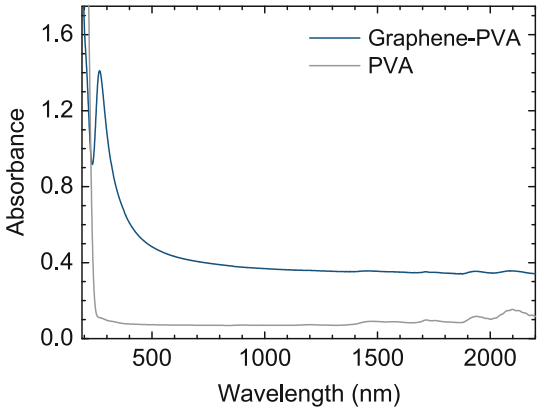

Fig. 9.17 Absorption spectra of a graphene-PVA composite and a reference PVA film. Adapted from Ref. [411]

absorption bands at 700, 1,000 and 1,800 nm decrease in intensity with increasing polarization angle, even though the SWNT loading remains unchanged [357].

Similar observations on optical density may also be made from graphene polymer composites. Figure 9.17 shows absorption spectrum of a graphene-PVA composite. The flat absorption band, due to the linear dispersion of Dirac electrons in graphene [40, 160, 311, 411], underscores the potential of graphene for wideband applications [414].

9.9.3 Raman Spectroscopy

Raman spectroscopy is a fast, powerful and non-destructive method for characterization of carbon materials [119]. A number of important information, such as

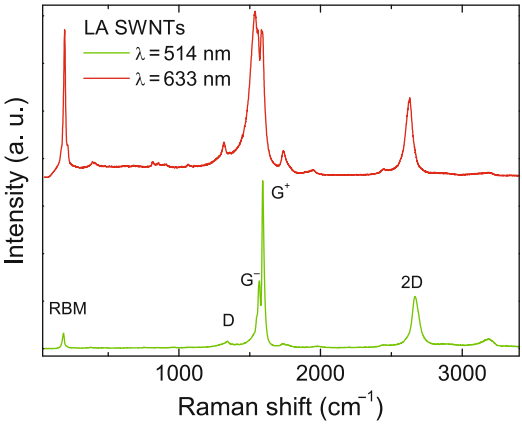

Fig. 9.18 Typical features in the Raman spectrum of SWNTs, measured at 514 and 633 nm excitation on Laser Ablation SWNTs

diameter, orientation, metallic or semiconducting character and chirality can be obtained from the Raman spectra of SWNTs [116, 189, 190, 247, 291, 340, 341, 350, 429]. Typical features in the Raman spectra of SWNTs are shown in Fig. 9.18. The spectra are taken from Laser Ablation (LA) SWNTs [249] in the form of powder.

Raman spectroscopy also allows monitoring of doping, defects, strain, disorder, chemical modifications, edges, and relative orientation of the graphene layers [26, 61, 62, 89, 90, 110, 118, 120, 122, 143, 306, 339, 340, 375, 480].

9.9.3.1 Optical Phonons in Graphene and Carbon Nanotubes

Phonons can be regarded as a perturbation of a crystal [43, 53, 111, 487]. In general, given their dynamic nature, they should be described by the time-dependent perturbation theory (TDPT) [42, 43, 53, 111, 487]. Within the adiabatic Born-Oppenheimer Approximation (BOA), they are seen as static perturbations and treated by the time-independent perturbation theory (TIPT) [42, 43, 53, 111, 487].

In materials without an electronic band-gap, like graphene, graphite and m-SWNTs, the interaction between phonons and electrons must be taken into account to calculate phonon energies [42, 43, 53, 111, 341]. In a metal, for certain phonons with a wave vector connecting two points of the Fermi surface, it is possible to have an abrupt change of the electronic screening of the atomic vibrations. This results in a sudden softening of the phonon frequencies, which is called the Kohn Anomaly (KA), and appears as a singularity in the dymamical matrix [217]. In graphene, the Fermi surface consists of the two inequivalent points **K** and **K**'. Thus, KA can occur only for phonons with $\mathbf{q} = 0$ or $\mathbf{q}$ connecting the two Fermi points (i. e. $\mathbf{q} = \mathbf{K}$). In graphene, a necessary condition for KA is a significant nonzero electron-phonon coupling (EPC) between electrons near the Fermi energy for phonons at $\mathbf{q} = 0$ or $\mathbf{q} = \mathbf{K}$ [340]. Due to their reduced dimensionality, m-SWNTs are expected to have stronger KA than graphite and graphene for the corresponding phonons [340, 341].

In graphene, KAs can be observed as sharp kinks for modes E_{2g} at Γ and A'_1 at **K** [292, 340]. The E_{2g} mode involves the in-plane bond-stretching of pairs of C

sp^2 atoms, while the A'_1 corresponds to the breathing mode of carbon rings. These two phonons are of major relevance to Raman spectroscopy of sp^2 carbon materials [120, 121, 312, 440], as the *G* peak originates from the E_{2g} phonon at Γ, while the *D* peak originates from modes around **K** [120, 340, 432].

In SWNTs, the E_{2g} mode splits in two components: the longitudinal optical (LO, polarized along the tube axis) and the transverse optical (TO, polarized along the tube circumference) modes. In s-SWNTs, the LO-TO splitting is usually explained in terms of curvature. Indeed, the σ-π mixing along the circumference results in a softening of the TO mode, which accounts for both the splitting and the diameter dependence [51, 189, 190, 338, 341]. In m-SWNTs, however, the reason for this splitting is different: the LO mode is modified by a KA, which causes a strong downshift of the LO frequency [247, 341].

Another important, low-frequency, optical mode of SWNTs is the so-called Radial Breathing Mode (RBM), which arises from the radial, in phase, vibration of all the carbon atoms in the SWNT unit cell [186, 350].

In materials without an electronic gap, the BOA is not easily justifiable, although experience proves that in most cases this accurately reproduces the phonon dispersion of metals. While this approximation still holds in intrinsic graphene, it fails in doped graphene and SWNTs [339, 341]. In these cases, phonons must be considered as time-dependent perturbations. It can be shown that KAs occur, within the static approach of the BOA, at $q = 0$ and $q = 2\,k_F$. The description of KAs is modified by the time-dependent approach, for which KAs occur at $q = \pm\hbar\omega_q/\beta$ and $q = k_F \pm \hbar\omega_q/\beta$ resulting in a shift of the position of the KAs [341].

9.9.3.2 Radial Breathing Mode

RBMs are important Raman fingerprints of SWNTs. A diameter dependence of this mode is expected [103, 165, 186, 188, 238, 280, 346, 365], with its frequency increasing as the diameter decreases [186]:

$$\omega_{RBM} = \frac{C_1}{d} + C_2 \tag{9.5}$$

Several groups have derived a variety of C_1 and C_2, as summarized in Table 9.4. More recently, the literature has converged to the values of $C_1 = 214.4\ \text{cm}^{-1}$ nm, $C_2 = 18.7\ \text{cm}^{-1}$ [11, 116, 297, 429]. References [11, 116, 297, 429] report tables where for each (*n*,*m*) the corresponding RBM frequency and transition energies are assigned. However, if we are just interested in an estimation of the band gap, any parameter can be used, as the difference in the calculated diameter is negligible. For example, let us consider two well-separated RBM frequencies (100 and 350 cm^{-1}) and calculate the diameter using the two most different values for C_1 (218 and 261) from Table 9.4. For the higher RBM frequency (i. e. lower diameters) the calculated diameters (0.62 and 0.75 nm) differ from their average by ∼10%; an average bandgap of ∼1.3 eV can be inferred from [200], from which the two extremes deviate by ∼ 8%. For the lower RBM frequency (higher diameters) the

Table 9.4 Values of C_1 and C_2 proposed in the literature

Authors	C1	C2
Jishi et al. [186]	218	
Rao et al. [350]	221	
Bandow et al. [21]	223	
Kürti et al. [238]	236 (armchair)	
	232 (zig-zag)	
Jorio et al. [188]	248	
Alvarez et al. [8]	238	
Sánchez-Portal et al. [365]	233	
Popov et al. [346]	230	
Henrard et al. [165]	261 (armchair)	
	256 (zig-zag)	
	258 (averaged)	
Mahan et al. [280]	227	
Dobardžić et al. [103]	224.3	
Bachilo et al. [17]	223.5	12.5
Milnera et al. [298]	234	10
Telg et al. [429]	214.4	18.7
Meyer et al. [297]	204	27
Araujo et al. [11]	217.8	15.7

calculated diameters (2.18 and 2.61 nm) differ from their average by ∼10%; an average bandgap of ∼ 0.35 eV can be inferred, from which the two extremes deviate by ∼ 9%. Thus the evaluation of optical absorption through the Kataura plot [200] is not deeply affected.

Matching the diameter given by RBM with excitation wavelength in the Kataura plot gives information on the semiconducting or metallic character. For example, in the spectra shown in Fig. 9.18 at 514 nm the RBM is at 185 cm^{-1}, from which a diameter of 1.29 nm is derived. From Ref. [200] we deduce that s-SWNTs are excited. At 633 nm, the RBM is at 193 cm^{-1}, from which a diameter of 1.23 nm is derived, and from Ref. [200] we deduce that m-SWNTs are excited.

If we want to probe the overall diameter distribution of a SWNT sample and whether they are metallic or semiconducting, Raman spectra have to be taken at as many wavelengths as possible, as a single excitation may probe only a limited range of diameters or only semiconducting or m-SWNTs. Usually, three well separated wavelengths, such as 514, 633 and 785 nm, can probe a wide range of tubes within a material and are enough to get significant, albeit not fully comprehensive, information on the diameter distribution.

9.9.3.3 D and 2D Peaks

The D peak is due to the breathing modes of sp^2 rings and requires a defect for its activation [120, 121, 340, 343, 432, 440, 446]. It comes from TO phonons around the **K** point of the Brillouin zone [120, 440], is active by double resonance (DR) [25, 432] and is strongly dispersive with excitation energy due the Kohn Anomaly at

K [340]. The activation process for the D peak is an inter-valley process as follows: (i) a laser induced excitation of an electron/hole pair; (ii) electron-phonon scattering with an exchanged momentum $\mathbf{q} \sim \mathbf{K}$; (iii) defect scattering; (iv) electron/hole recombination. The D peak intensity is not related to the number of graphene layers, but only to the amount of disorder [120, 440]. Indeed, when moving from graphite to nanocrystalline graphite, the ratio between the intensity of D and G peak, I(D)/I(G), varies inversely with the size of the crystalline grain or inter-defect distance [58, 120, 440]. DR can also happen as intra-valley process i.e. connecting two points belonging to the same cone around **K** (or **K**′). This gives rise to the so-called D′ peak, which can be seen around 1,620 cm^{-1} in defected graphite [312]. The 2D peak is the second order of the D peak. This is a single peak in monolayer graphene, whereas it splits in four bands in bilayer graphene, reflecting the evolution of the band structure [122]. The 2D′ peak is the second order of the D′ peak. Since 2D and 2D′ originate from a Raman scattering process where momentum conservation is obtained by the participation of two phonons with opposite wavevectors (**q** and $-\mathbf{q}$), they do not require the presence of defects for their activation, and are thus always present.

Figure 9.19 plots the evolution of the 2D band as a function of the number of layers for 514.5 and 633 nm excitations [122]. Bi-layer graphene has a much broader and up-shifted 2D band with respect to single layer. This is also quite different from that of bulk graphite, which consists of two components $2D_1$ and $2D_2$ [312, 446] roughly 1/4 and 1/2 the height of the G peak, respectively. Indeed, the 2D peak in bi-layer graphene has 4 components, $2D_{1B}$, $2D_{1A}$, $2D_{2A}$, $2D_{2B}$, 2 of which, $2D_{1A}$ and $2D_{2A}$, have higher relative intensities than the other 2. A further increase of the number of layers leads to a significant decrease of the relative intensity of the lower frequency $2D_1$ peaks. For more than 5 layers the Raman spectrum becomes hardly distinguishable from that of bulk graphite [440]. On the other hand the shape of the G peak does not change with the number of layers.

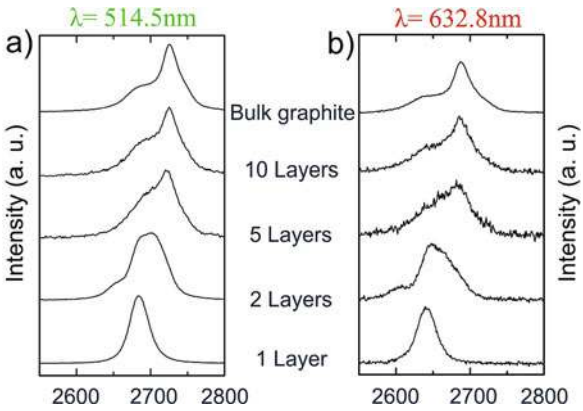

Fig. 9.19 Evolution of the 2D band in Raman spectra of graphene and few layer graphene at (**a**) 514.5 and (**b**) 632.8 nm with the number of layers. Adapted from Ref. [122]

9.9.3.4 G Peak

The G peak corresponds to the E_{2g} phonon at the Brillouin zone centre of graphene [120, 440]. The Raman spectrum of SWNTs is characterized by the presence of two distinct features around 1,550 cm^{-1}: the G^+ and G^- peaks. These arise from the splitting of the doubly degenerate, Raman-active $E_{2\,g}$ mode of graphene [120, 440]. The G^- peak position decreases with diameter, while the G^+ is almost diameter independent [190]. While in s-SWNT both peaks appear as sharp Lorentzians, the G^- peak of metallic SWNTs is very broad and its position is strongly downshifted with respect to that in s-SWNTs of the same diameter (Fig. 9.18) [51, 189, 190, 291, 338, 429].

The G^+ and G^- peaks originate from the LO and TO modes, which are polarized along the tube axis and along the tube circumference, respectively (Fig. 9.20) [341]. In s-SWNTs, the G^+ peak is assigned to the LO mode, while the G^- is assigned to the TO [51, 189, 190, 338, 341]. In m-SWNTs, however, the assignment is the opposite: the LO mode is affected by KA, which causes a strong downshift of its frequency [247, 341]. Thus the G^+ peak is due to the TO mode, while the G^- arises from the LO (Fig. 9.20) [247, 341].

9.9.4 PL Spectroscopy

PL spectroscopy can be used to determine the presence of isolated SWNTs or small bundles in the composites [224, 299]. Figure 9.21 shows the polarized PL signal from a mechanically stretched SWNT-SDS-gelatine film excited by depolarized 662 nm light, indicating isolated (8,3), (7,5), (7,6), (9,5) tubes or small bundles [224].

9.9.5 Z-Scan

Z-scan experiments probe the optical nonlinearities associated with the change in refraction and absorption coefficient induced by intense laser power. The sample is moved along the waist of a Gaussian beam as shown in Fig. 9.22a. This results in a variation of the laser power density on the sample, reaching its maximum at the focal point. An analysis of the transmitted beam through the sample as a function of sample position, Z, is done in either the open and close aperture scheme [383, 444]. Open aperture Z-scan is used for the investigation of processes associated with nonlinear absorption, while close aperture Z-scan is used to investigate nonlinear refraction [444].

Samples containing SWNTs can be investigated by Z-scan in order to understand the mechanisms of optical limiting [322, 450] and saturable absorption [278, 357, 359, 363, 427]. A typical Z-scan trace for a SWNT-polymer composite, taken in near

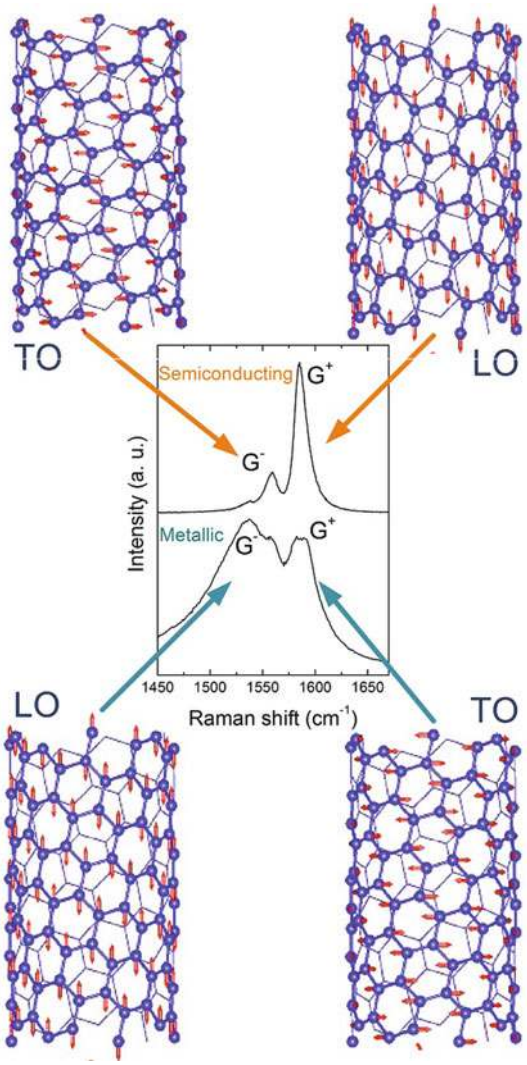

Fig. 9.20 Schematic representation of the G mode for m- and s-SWNTs. Adapted from Ref. [341]

resonant conditions, is shown in Fig. 9.22b. Here, SWNTs show strong saturable absorption, with about 30% increase in transmission when the sample passes the focal point.

9.9.6 Pump-Probe Spectroscopy

Pump-probe spectroscopy is widely in use to characterize response time of SAs [212]. The material is irradiated by a pump pulse, yielding a carrier excitation. Then,

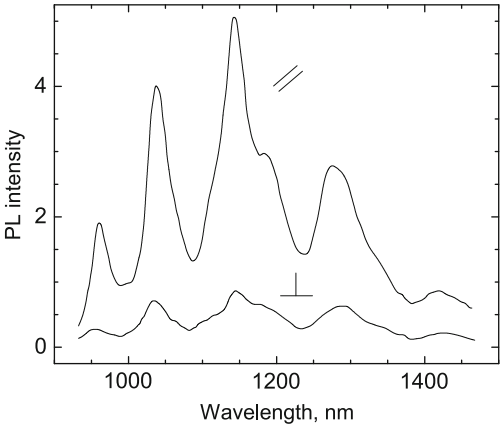

Fig. 9.21 Polarized photoluminescence from a stretch-aligned SWNT/SDS/gelatin dried film (draw ratio=3) excited by depolarized 662 nm light. Adapted from [224]

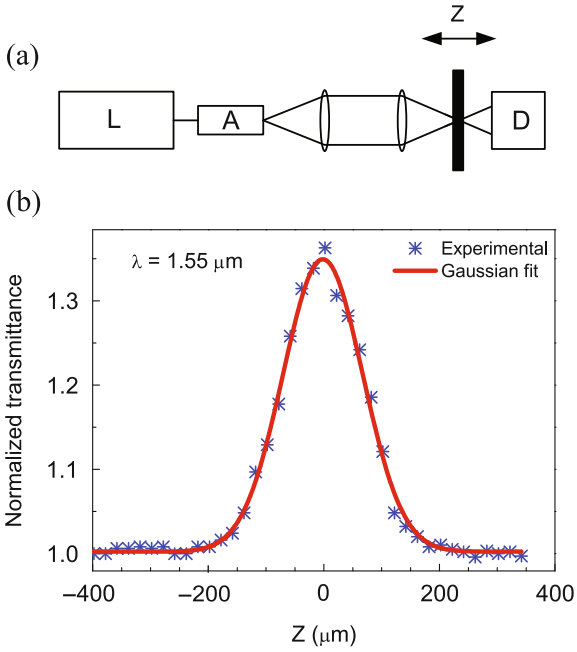

Fig. 9.22 (**a**) Z-scan setup. L: laser, A: attenuator, D: photodetector. (**b**) Z-scan measurement of a SWNT-PVA composite

after a short time, controlled by an optical delay line, the sample is irradiated by a probe pulse. By studying the transmittance or reflectance of the probe pulse it is possible to obtain information on the excitation decay (SA recovery time) caused by the pump pulse. SWNTs have an intrinsic bitemporal response, including a fast component and a slow component, which are due to different time-scale relaxation processes (interband and intraband, respectively) [215, 329]. Graphene also exhibit an ultrafast bitemporal relaxation process. This is further discussed in Section 9.12.

9.10 Nanotube/Graphene-Composites for Photonics and Optoelectronics

The desirable characteristics of the host polymer matrix for optical applications vary depending on the type of applications. The most important requirement is the compatibility with SWNTs/graphene and solvents so that a homogeneous dispersion of SWNTs/graphene in the composite can be achieved. It is also essential to reduce scattering losses in such applications, which generally arise from aggregates or particles, cracks, bubbles or voids inside the composite [277]. The optical applications so far demonstrated using SWNT/graphene-polymer composites are SA for optical signal regeneration and passive mode-locking [29, 96, 130, 160, 161, 209, 210, 220, 344, 345, 358, 360, 363, 370, 372, 380, 411, 413, 415, 416, 453–455, 479] electroluminescence [206, 476], and photovoltaic applications [2, 205, 206, 240, 241, 260, 347, 469, 476]. Significant progresses have also been made in using percolating SWNT and graphene networks and their composites as transparent, flexible conductors [40, 99, 123, 149, 221, 331, 469, 470, 472]. In addition, such composites could be used as optical modulators under strong electric field [216, 334, 493].

9.10.1 Graphene/Nanotube Networks as Transparent Conductors

Optoelectronic devices such as displays, touch-screens, light emitting diodes and solar cells require materials with low sheet resistance R_s and high transparency (T). The majority of flexible transparent optoelectronic devices utilizes Indium Thin Oxide (ITO) as transparent conductive (TC) material. ITO suffers from severe limitations: an ever-increasing cost due to indium scarcity [153], brittleness [154], difficulties in patterning [145, 153] and a sensitivity to both acidic and basic environments [154]. This demands new TC materials with improved performance. Metal grids [250], metallic nanowires [95], or other metal oxides [145] have been explored as alternative. SWNTs [136, 149, 373, 472, 497] and graphene [18, 40] also show great promise.

R_s and T need to be considered linked to analyze data for TC films. Both are determined by the response of electrons to either dynamic (light) or static (voltage) electric fields. R_s is ultimately controlled by the "dc" conductivity, σ_{dc}, via

$$R_s = (\sigma_{dc} t)^{-1} \tag{9.6}$$

where t is the film thickness.

T depends on the optical conductivity G_0,

$$T = \left(1 + \frac{G_0}{2\epsilon_0 c} t\right)^{-2}, \tag{9.7}$$

Combining Eqs. (9.6, 9.7), eliminating t, gives:

$$T = \left[1 + \frac{Z_0}{2R_s}\frac{G_0}{\sigma_{dc}}\right]^{-2} \tag{9.8}$$

where, $Z_0 = \frac{1}{\varepsilon_0 c} = 377\Omega$ is the free space impedance.

For instance, in graphene [135] we can take $\sigma_{dc} = n\mu e$, where n is the number of charge carriers. Note that for n∼0, σ_{dc} does not go to zero, but assumes a constant value [135] $\sigma_{dc,min} \sim 4e^2/h$, resulting in $R_s \sim 6$ kΩ for an ideal intrinsic SLG with $T \sim 97.7\%$. Thus, ideal intrinsic monolayer graphene, would beat the best ITO only in terms of T, not R_s. However, real samples deposited on substrates, or in thin films, or embedded in polymers are never intrinsic. Usual exfoliated monolayer graphene has $n \geq 10^{12}$ cm^{-2}, and much smaller R_s. The range of T and R_s that can be realistically achieved for graphene layers of varying thickness can be estimated taking $n = 10^{12}$–10^{13} cm^{-2} and $\mu = 10^3 - 2\times10^4$ cm^2/Vs, as typical for chemical vapor deposition (CVD) grown films. For instance, taking $n = 3.4 \times 10^{12}$ cm^{-2} and $\mu = 2\times10^4$ cm^2/Vs, typical for CVD grown films, it would be possible to get T = 90% and $R_s \leq 20\Omega\square^{-1}$.

Ultrathin SWNT/graphene films as transparent conductors are usually prepared on membranes by filtering SWNT/graphene dispersions and then transferring the resultant film from the membrane surface to the substrates (e.g. polymer, glass etc) [149, 472, 497] or directly spray coating the dispersions on substrates [373], or via roll-to-roll processing [18]. In such preparation methods, SWNTs are not incorporated in the polymer matrix, but are deposited on the substrate surface. Therefore, they are not truly composites. On the other hand, transparent and conducting SWNT-polymer composites, which are much easier to implement, have been prepared [99, 123, 221, 331, 490]. Inkjet printing of SWNT-polymer dispersions on flexible substrates has been demonstrated to yield conducting layers of percolating SWNTs with T up to ∼80% in the visible range [392]. Nevertheless, the conductivity and transparency of SWNT-polymer composites do not match those of SWNT only networks. It is possible to lower the resistivity of SWNT-polymer composites by functionalization [99, 123, 490]. Reference [99] reported an increase in electrical conductivity by a factor of 5 by doping the SWNTs with $SOCl_2$ while retaining good optical transparency. At 0.1 wt% loading, the authors achieved 92.4% transmittance at 500 nm with an electrical conductivity of 290 Ω.cm for a 20 μm film. By comparison, Ref. [472] reported a 50 nm thick two dimensional SWNT network with 1.5×10^{-4} Ω.cm resistivity and ca. 75% transmittance at 500 nm.

The length of SWNTs is an important factor for conductivity enhancement of SWNT networks [164]. In addition, good dispersion of SWNTs without surfactants is key to improve SWNT-polymer conducting composites, as surfactants isolate tubes from the surrounding environment, resulting in poor inter-tube connection. An approach to solve this problem is in-situ polymerization during the sonication process, as demonstrated by Ref. [331]. With 0.1% vol. SWNT loading, ca. 70% transmittance at 500 nm for 34 μm films with a conductivity of 1×10^{-8} S.cm^{-1} was achieved. Flexible, transparent and conducting thin

SWNT-poly(3,4-ethylenedioxythiophene):poly(styrenesulfonate) composites with high optical uniformity having DC conductivities of $>10^5$ S/m were demonstrated [92]. For a 80 nm SWNT-composite film, a transmittance (at 550 nm) of 75% and sheet resistance of 80 $\Omega\square^{-1}$ was achieved. Further improvement might be possible using enriched long m-SWNTs, or chemically doped graphene [18, 40]. Indeed, chemical doping is a key strategy to improve performance both for SWNTs [136] and graphene [18, 37] TCs. In the latter case, Ref. [37] prepared graphene-based TC films, starting from graphene produced by micromechanical cleavage (MC), with T∼98%, $R_s = 400\ \Omega\square^{-1}$, exploiting a layer of polyvinyl alcohol (PVA) to induce n-type doping. Ref. [18] achieved $R_s \sim 30\ \Omega\square^{-1}$, T ∼ 90% by nitric acid treatment of graphene-based TC films derived from CVD grown flakes, one order of magnitude lower in terms of R_s than previous graphene-based TC films from wet transfer of CVD films [223].

It is important to note that graphene-based TC films derived from CVD grown flakes, combined with doping, have the potential to outperform ITO and other transparent conductive materials. On the other hand, graphene-based TC films produced by other methods, such as LPE, albeit presently with higher R_s at T=90%, have already been tested in organic light emitters [290, 470] and solar cells [269, 459]. These are a cheaper and easier scalable alternative to MC or CVD films, and need be considered in applications where cost reduction is the key factor.

9.10.2 Electroluminescent and Photovoltaic Devices

Photo-induced electron transfer between semiconducting conjugated polymers and SWNTs has attracted significant attention in recent years. Electroluminescence is a phenomenon in which a material emits light in response to an applied electric field. Studies of the electroluminescent properties of SWNT-polymer composites have also been carried out [206, 476]. Poly(3-hexyl-thiophene) (P3HT), with a bandgap of 1.8–2.1 eV has been the most widely used polymer for such applications, because of its high mobility and environmental stability [206, 333, 476]. Electroluminescence has been reported mainly from s-SWNT devices, with an emission peak in the NIR assigned to a radiative decay over the first interband transition of the π bands at the K point [300]. Electroluminescence was also observed from biased m-SWNTs [112, 282], MWNTs [112] and graphene [112]. Reference [112] assigned such light emission to phonon-assisted radiative decay from π^* states at the M point to the Fermi level at the K point.

Graphene has a work function of 4.5 eV, similar to ITO. This, combined with its promise as flexible and cheap transparent conductor, makes it an ideal candidate as organic light-emitting diode (OLED) anode. Graphene-based transparent conductor film (GTCFs) anodes enable out-coupling efficiency comparable to ITO [470]. Chemically derived graphene was also implemented as transparent cathode in a metal-free and solution-processed light-emitting electrochemical cell [290].

A photovoltaic (PV) device converts light to electricity [68]. V_{OC} is the maximum open circuit voltage, while I_{SC} is the maximum short circuit current. The fill

factor (FF) is defined as: $FF = (V_{max} \times I_{max})/(V_{OC} \times I_{SC})$, where I_{max} and V_{max} are maximum current and voltage. The energy conversion efficiency is $\eta = P_{max}/P_{inc}$, where $P_{max} = V_{OC} \times I_{SC} \times FF$ and P_{inc} is the incident power. The fraction of absorbed photons converted to current defines the internal photocurrent efficiency (IPCE).

SWNTs and graphene have been proposed as promising materials in organic [35, 460] and dye sensitized solar cells (DSSCs) [434]. Indeed, both SWNTs and graphene can fulfill multiple functions in photovoltaic devices: (1) transparent conductor window, (2) photoactive material, (3) channel for charge transport, (4) catalyst [40]. SWNTs and GTCFs are used as window electrodes both in organic and DSSC devices [40]. Organic solar cells based on SWNTs-polymer composites have also been demonstrated, due to the excellent electron transfer with poly(p-phenylene vinylene) (PPV) [2], poly(2-methoxy-5-(2-ethylhexyloxy)-1,4-phenylenevinylene)(MEHPPV) [205], P3HT [260, 347], poly(3-ocylthiophene-2,5-diyl) (P3OT) [205, 240] as the host.

Photoinduced electron transfer in bulk heterojunctions of MEH-PPV/C_{60} and β-carotene/C_{60} was reported more than 20 years ago [366], with fullerenes used as acceptors. Combining both these ideas, using C_{60} as electron acceptor and the high mobility of SWNTs, C_{60}-SWNT-P3HT composites have been reported with up to ~390 mV open circuit voltage and 2.7 mA/cm^{-2} short circuit current density [260]. Chemically modified graphene dispersions were also used in bulk heterojunction PV devices, as electron-acceptors with poly(3-hexylthiophene) and poly(3-octylthiophene) as donors, achieving $\eta \sim 1.4\%$ [269]. Reference [485] claims that $\eta > 12\%$ should be possible with graphene as photoactive material.

SWNTs and graphene can cover an even larger number of functions in DSSCs. Indeed, other than as TC windows at the photoanode [459], SWNTs and graphene can be incorporated into the nanostructured TiO_2 photoanode, through which the photoelectrons generated from dye molecules are transported to the anodes [146]. A recombination reaction (i.e. reverse charge transfer from TiO_2 to the dye or redox couple) reduces the overall cell efficiency [314, 410, 483]. One way to promote charge transfer, reducing recombination, is to incorporate a conductive network into TiO_2. In this context, SWNTs and graphene show potential not only because of their extremely high carrier mobility, but also because of their unique one and two dimensional structures.

Reference [52] used a SWNT network as scaffolds of dye-sensitized TiO_2 nanoparticles to promote charge transport in mesoscopic semiconductor films. The authors demonstrated that, although the SWNT network in the film has no noticeable influence on the charge injection process from the excited Ru(II) trisbipyridyl complex into TiO_2 particles, it plays an important role in improving the charge separation, as the rate of back electron transfer between the oxidized sensitizer (Ru(III)) and the injected electrons becomes slower in the presence of the SWNTs scaffold [52]. Reference [483] used graphene as TiO_2 bridge, achieving faster electron transport and lower recombination, leading to $\eta \sim 6.97\%$, higher than conventional nanocrystalline TiO_2 photoanodes [481, 483].

Another option in DSSCs is to use SWNTs and graphene at the counter electrode (CE). Regeneration of dye molecules is accomplished by capturing electrons from a liquid electrolyte (Iodide/Iodine solution), sandwiched on the CE, which catalyzes the reduction of tri-iodide [328]. Another important function of the counter electrode is the back-transfer of the electrons arriving from the external circuit to the redox system [328]. The most important requirements for the counter electrode material are a high exchange current density and a low charge-transfer resistance [9]. Currently, DSSC cathodes are made of Platinum (Pt) layers deposited on transparent glass, in turn, coated by a TC such as ITO [145]. ITO suffers many limitation listed above, while Pt is rare and expensive. Furthermore Pt tends to degrade over time when in contact with an iodide/iodine liquid electrolyte, reducing the overall efficiency of DSSCs [232]. Strong efforts have been directed towards the replacement of such elements with low-cost and more versatile materials. The use of SWNTs and graphene at the CE of DSSCs is attractive for several reasons, such as high specific surface area, good catalytic properties, electronic conductivity, corrosion resistance towards iodine, high reactivity, abundance, and low cost. Thus, SWNTs and graphene films and/or composites are good candidates as CE material in DSSCs [173, 417, 434].

Reference [434] demonstrated that ozone-treated SWNTs films increase their catalytic activity due to the introduction of defects. Graphene has also great potential. Semi-transparent graphene thin films on FTO were reported with high electrocatalytic activity toward Iodide/Iodine redox couple [202]. An hybrid poly(3,4-ethylenedioxythiophene (PEDOT):poly-(styrenesulfonate) (PSS)/GO composite was used as counter electrode, getting $\eta = 4.5\%$, comparable to 6.3%, for a Pt counter electrode tested under the same conditions [173], but achieved with a cheaper material.

9.10.3 Saturable Absorbers (SAs)

9.10.3.1 Nanotube Based SAs

A material's response to an electric field can be described in terms of polarization, defined as the dipole moment per unit volume. The relationship between polarization and electric field is [45]:

$$P = \varepsilon_0 \chi E \tag{9.9}$$

where χ is the dielectric susceptibility [45]. For very high electric fields Eq. (9.9) is no longer sufficient to describe the behavior of some materials. In this case polarization can be expressed as a power series in the electric field [45]

$$P = \varepsilon_0(\chi_1 E + \chi_2 E^2 + \chi_3 E^3 + ...) \tag{9.10}$$

where χ_1 is the linear susceptibility and χ_2 and χ_3 are the second- and third-order nonlinear susceptibilities. These are responsible for phenomena such as

difference frequency generations, optical parametric oscillation, self-focusing, saturable absorption, two-photon absorption etc. [45].

Strong nonlinear optical effects have been demonstrated in SWNTs [76, 286, 357, 359, 363, 427]. The very high density of states at the van Hove singularities allows strong optical absorption if the frequency of the incident electromagnetic field matches their energy spacing. As strong absorption occurs, the excited energy levels fill up and the material becomes transparent to higher power irradiation. This saturable absorption, to a first approximation, can be described as [45]:

$$\alpha(I) = \frac{\alpha_0}{1 + I(t)/I_{sat}} + \alpha_{ns}, \tag{9.11}$$

where α_0 is the linear optical absorption; $I(t)$ is the laser intensity; I_{sat} is the saturation intensity, defined by Eq. (9.11) as the intensity necessary to reduce the absorption coefficient to half of the initial value; α_{ns} is the nonsaturable absorption component [45]. The dynamic response of nonlinear absorption is specified by the recovery time (τ_A), defined as the time necessary to reduce the carriers by a factor of $1/e$, and shows how fast is the relaxation to the ground state, after excitation [211]. The modulation depth is defined as the maximum possible absorption change between low power and high power irradiation [211].

Reference [76] firstly measured saturable absorption in SWNTs at 1.55 μm by pump-probe spectroscopy, showing a sub-picosecond relaxation of excited carriers. They reported $\chi_3 \sim 10^{-10}$ esu (1 esu = $1.11 \times 10^{-9} m^2/V^2$ [45]), due to the non-resonant condition. A much higher χ_3 value of 10^{-7} esu, was achieved under resonant condition in Ref. [427], with a recovery time of about 600 fs. Saturable absorption can be further enhanced if SWNT are highly oriented along the light polarization direction, because of the anisotropy of their interaction with light [357].

SWNTs have a number of benefits compared to other SA materials, such as organic dyes, color filter glasses [367], dye-doped solids [139] and semiconductors [213, 215]. Since the SWNT absorption depends on the diameter, this can be fine tuned across the visible and infrared spectral range. This could allow a number of ultrafast optoelectronic applications in medicine, sensing, telecommunication and materials processing. SWNT based SAs have a high laser damage threshold, excellent environmental stability and are much easier and cheaper to assemble [357, 371].

As an example, for telecommunications at 1.55 μm, the SWNTs should have a maximum absorption around this wavelength. In laser ablation grown SWNT, diameter control can be achieved by varying the temperature in the laser oven, as shown in Fig. 9.23. Figure 9.24 plots the Raman spectra from SWNTs with absorption peak centered at 1.55 μm. From the radial breathing modes, a diameter distribution of 1–1.3 nm can be deduced [116, 429]. Therefore, the SWNTs grown at 1,000°C in Fig. 9.23 are more suitable for 1.55 μm operation than the other SWNTs presented in Fig. 9.25.

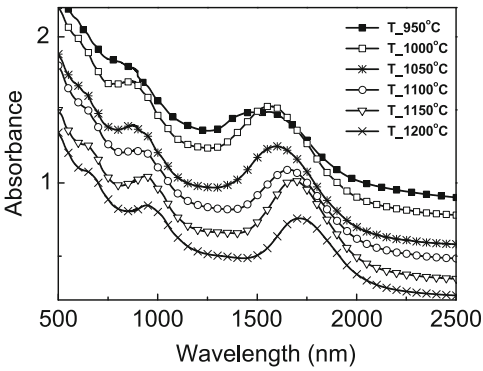

Fig. 9.23 Tuning LA-SWNT diameter by growth parameters; the absorbance reflects the change in SWNT diameter with the growth temperature

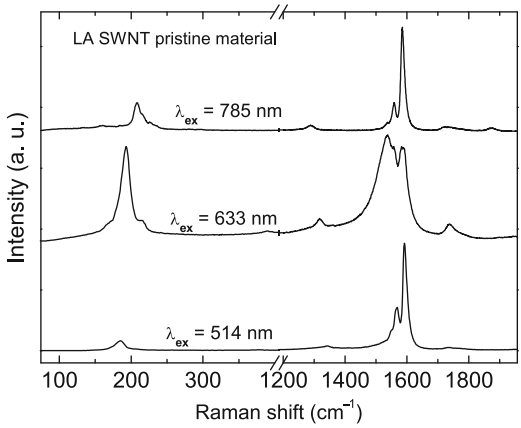

Fig. 9.24 Raman spectra of LA-SWNTs grown at 1,000°C (See Fig. 9.23)

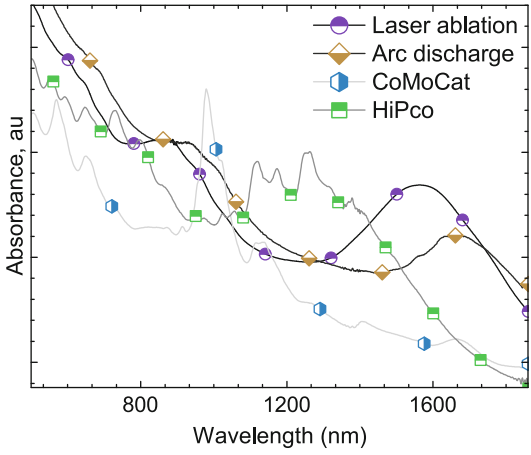

Fig. 9.25 Absorption spectra of SWNTs produced by different growth methods. The nanotubes are dispersed in D_2O with SDBS

In addition to strong optical absorption at the wavelength of interest, an ideal SWNT-polymer SAs should have a large modulation depth, small non-saturable loss [357] and ultra-fast recovery time [451]. The modulation depth is generally tuned by changing the concentration of dispersed SWNTs in the polymer matrix. It can also be increased by aligning tubes in the polymer matrix [357], as discussed in Section 9.8.1.1. The non-saturable losses can be minimized by preparing composites free from defects (e.g. cracks, voids etc.) or SWNT aggregates, using host polymers that are transparent at the device operation wavelength. However, bundles could be beneficial in SWNT-based SAs, since they allow to achieve a shorter recovery time. However bundle-sizes must be smaller than the device operation wavelength to avoid non-saturable losses due to scattering [39, 357]. It is thus important to properly characterize both SWNT solutions and composites, as discussed in Sections 9.7 and 9.9.

In earlier implementations of SWNTs as SAs, SWNTs were spray-coated on quartz substrates [381] or used in dispersion [181]. Direct synthesis of highly purified SWNT thin films on fibre-ends was also proposed [477]. However, high losses were reported due to the residual presence of large aggregates as well as catalyst particles [379, 477], or due the formation of bubbles when SWNT dispersions were used [181, 379, 477]. In addition, the device fabrication methods were time consuming and had low throughput [479]. The best way to overcome such disadvantages is to disperse SWNTs in a polymer matrix [96, 181, 358, 360, 363, 370, 371, 380, 428, 477].

9.11 Nanotube Composites as Mode Lockers for Ultrafast Lasers

The most successful application of SWNT-based SAs demonstrated thus far is as mode-lockers for ultrashort pulse lasers and noise suppression filters. The use of SAs as a mode-lockers to generate ultrashort pulses was first proposed shortly after the invention of laser itself [97, 393]. Various optical materials, such as organic dyes, color filter glasses [367], dye-doped solids [139] and semiconductors [213, 215] have so far been used for this purpose. However, it was challenging to achieve stable mode-locking operation with these conventional SAs [213, 215, 325]. The advances in molecular beam epitaxial (MBE) growth of semiconductor quantum wells (SQW) at the end of the 80s resulted in production of new semiconductor heterostructures with SA properties useful for photonics applications [215, 451]. Because of the SQW normally growth on high reflectivity mirrors (e.g. semiconductor Bragg mirrors), these structures are widely known as Semiconductor Saturable Absorber Mirrors(SESAMs) [215]. SESAMs typically are complex multi quantum well heterostructures, which are usually grown by expensive molecular beam epitaxy, and often undergo heavy-ion implantation to create defects, in order to reduce the recovery time [214, 277]. Moreover, they can only cover a narrow wavelength operation range [325]. On the other hand, SWNTs are cheap to produce, and different parameters can be well-controlled, such as modulation depth and operation

wavelength range, as discussed above. SWNT composites are also mechanically robust and environmentally stable. SAs based on SWNTs have thus the potential to compete with traditional SESAMs [29, 96, 129, 160, 209, 210, 358, 360, 363, 370, 372, 413, 415, 416, 453–455, 479].

To date, SWNT-based SAs have been successfully used as mode-lockers in fibre lasers [160, 208–210, 220, 358, 360, 363, 370, 372, 380, 413, 415, 416, 453–455], waveguide lasers [29, 96], solid-state lasers [125, 376], and semiconductor lasers [396], at 0.8 [219], 1 [210], 1.1 [208], 1.3 [401], 1.55 [160, 413, 416, 453–455, 478], 1.6 [415, 478] and 2 μm [394]. Wavelength-tunable lasers using SWNTs, were demonstrated in Ref. [454] and later in Refs. [115, 219, 377, 378]. So far, the shortest reported pulse duration is 68 fs [376]. A repetition rate of 17.2 GHz was demonstrated [396]. The maximum output power reported to date is 1.6 W [416].

A large range of host polymers, e.g. polycarbonate (PC) [29, 372, 454], polyvinyl alcohol (PVA) [208–210, 413, 415, 416, 453, 455], Carboxymethyl cellulose, Polyimide (PI), Polydimethylsiloxane (PDMS), Polymethyl methacrylate (PMMA), poly(3-hexylthiophene) (P3HT) and poly(9,9-dioctyfluoreny1-2,7-diyl) (PFO) have been used [160]. Different SWNT growth technologies, e.g. laser ablation (LA), CoMoCAT, HiPCO, arc discharge (AD), chemical vapor deposition (CVD), catalytic CO disproportionation reaction [160], producing different mean diameter and diameter distribution, have been employed for mode-locking at different wavelengths.

Since ∼1.55 μm is the most attractive wavelength for telecommunications, significant effort has been devoted to optimize SWNT-polymer SAs for mode-locking of Erbium-doped fiber lasers at this wavelength [160, 372, 413, 416, 453–455]. ∼123 fs pulses were reported with a repetition rate of ∼18 MHz [413]. Mode-locking in an active waveguide laser was reported, with transform-limited 1.6 ps [96], and 320 fs pulses [29].

To realize various functions, different configurations of SAs using SWNTs were proposed, such as evanescent field interaction in a tapered fibre [395], in a D-shaped optical fibre [398, 399], and with vertically aligned SWNTs [397]. Incorporating SWNT polymer composites into the evanescent field of the fibre taper [220] and polymer fiber [442] was also proposed. Thus far, the most common way to integrate SWNTs-devices into fiber lasers is to sandwich a SWNT polymer composite film between two fiber connectors, offering ease of integration into various lightwave systems with the flexibility of polymer photonics [160, 360, 363, 370, 372, 378, 413, 416, 453–455]. Figure 9.26a is a photograph of a FC/PC fibre patchcord with a SWNT-PVA film incorporated into it. A typical mode-locked fibre laser setup is schematized in Fig. 9.26b. The laser cavity is constructed using a mode-locker, a coupler, a fibre polarization controller (PC), an isolator (ISO), an Erbium-doped fiber (EDF), and a wavelength division multiplexer (WDM) [160]. The optical isolator ensures unidirectional light propagation. To improve the output pulse stability, a polarization controller is used, consisting of 2 spools of single-mode fiber acting as retarders. The total retardation induced by the polarization controller is a function of the fiber geometry in the spool [3]. One port of the coupler is used for a feedback

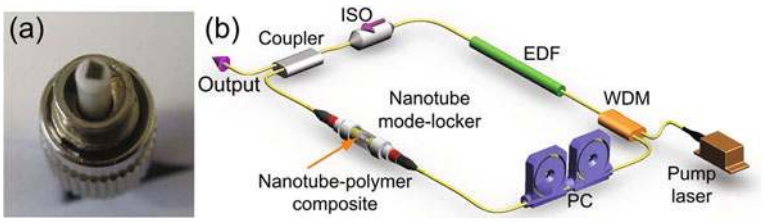

Fig. 9.26 (**a**) Fiber connector with SWNT-PVA film; (**b**) EDF laser with SWNT-mode-locker

into the cavity, while the other serves to study the cavity repetition rate, autocorrelation trace, pulse spectrum and output power [160]. The EDF is pumped by a diode laser at 960 nm to provide gain for lasing [160]. This results in the excitation of the Er^{3+} to its high-energy states, followed by a non-radiative recombination to lower-energy excited states. The subsequent radiative recombination from these levels to ground state gives an emission around ~1.5 μm [3]. The laser feedback is created using the optical fibre coupler to obtain gain [360]. The laser beam returns to the EDFA through a wavelength division multiplexer, which combines light at 1,529 and 960 nm in a single fibre. Thus, the stored pumping energy of the low-energy excited state is used to amplify the signal through stimulated emission. When the gain exceeds the loss induced by the intracavity components, the laser generation starts.

The mechanism of pulse formation can be understood as follows [211]. The SA works as a loss modulator when a short pulse circulates in the cavity (Fig. 9.27a). The peak intensity saturates the absorber more than the low intensity pulse wings. This produces an amplitude loss modulation with a frequency proportional to the cavity round trip time. The pulse circulation in the cavity gives enough gain to overcome the losses induced by the absorber. As a result, the net gain window has duration equal to the absorber recovery time [211]. The initial pulse formation can start from noise fluctuations in the laser cavity, when a high intensity spike significantly decreases its losses passing through the SA. It should be noted that it is possible to achieve pulses significantly shorter than the SA recovery time, see Fig. 9.27b [199]. In this case, soliton pulses form in the cavity as a balance between negative group velocity dispersion and self-phase-modulation [199]. Thus, the SA

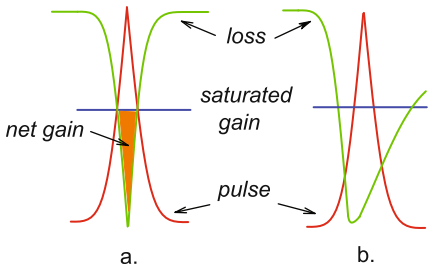

Fig. 9.27 Mode-locking mechanisms: (**a**) saturable absorber, (**b**) soliton mode-locking [360]

acts as a loss mechanism for starting the pulse formation and later on stabilizes the pulses [199].

To achieve pulse generation from the continuous-wave (CW) regime, a pig-tailed SWNT-PVA mode-locker can be placed in the cavity (Fig. 9.26b) [160]. This gives stable mode-locking with a fundamental repetition rate f_r. This can be estimated as $f_r = c/(nL)$, where c the velocity of light in vacuum, n the average refractive index of the cavity ($n \approx 1.5$ in the case of a common single mode-fiber based cavity), and L is the cavity length. Figure 9.28a plots the output pulse spectra of wavelength-tunable pulses mode-locked by SWNTs [454]. Typical soliton side-bands were observed for the laser cavity without the intracavity filter. These can usually be attributed to perturbation of pulses propagating in the cavity, caused by paths with different dispersions as well as output coupling loss [3]. Soliton pulses lose part of their energy passing through different passive cavity components (e.g. output coupler), but then regain it in EDF during the cavity round trip. The

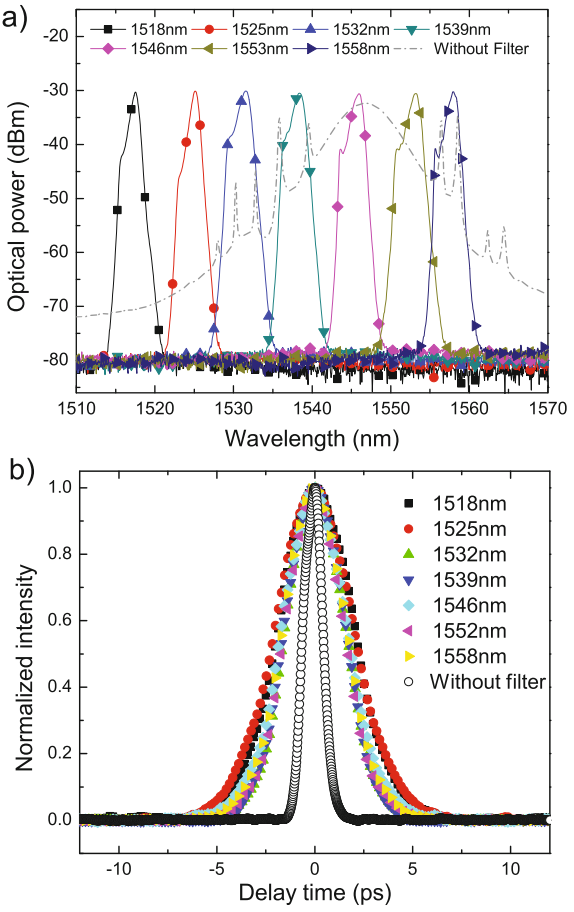

Fig. 9.28 Wavelength-tunable pulses mode-locked by nanotubes. (**a**) output optical pulse spectra, (**b**) output autocorrelation traces [454]

soliton adjusts to these perturbations by forming dispersive waves, which appear as sidebands [3]. The pulse width can be measured using second harmonic generation (SHG) auto-correlation [435]. The pulses in Fig. 9.28b are fitted with a sech^2 autocorrelation function, with a full width at half maximum (FWHM) of ~ 3.68 ps. To get the pulse width, the autocorrelation width needs to be divided by the decorrelation factor for sech^2 (1.54) [435], giving an average pulse duration of $\sim$2.39 ps.

9.12 Graphene for Ultrafast Photonics

Various graphene based photonic and optoelectronic devices, from solar cells [269, 459] and light-emitting devices to touch screens [290, 470] and photo-detectors [473], have already been demonstrated.

In graphene, interband excitation by ultrafast optical pulses produces a non-equilibrium carrier population in the valence and conduction bands, Fig. 9.29a. Time-resolved experiments give two typical relaxation timescales: a faster one $\leq$100 fs, usually associated with carrier-carrier intraband collisions and phonon emission, and a slower one, on a ps timescale, which corresponds to interband recombination and cooling of hot phonons [40, 49, 91, 411]. In addition, the linear dispersion of the Dirac electrons [40, 160, 311, 411] in graphene implies that for any excitation, there is always an electron-hole pair in resonance. Thus graphene is an ideal ultrafast wideband saturable absorber for ultrafast pulse generation. After the first demonstration of ultrafast pulse generation using graphene [160], a variety of ultrafast lasers mode-locked by graphene have been reported [40, 160, 288, 344, 400, 411, 414, 492]. Reference [411] explained the fundamentals of the photo-excited carrier dynamics in graphene saturable absorbers (GSAs), in good agreement with experimental results.

Different fabrication strategies, e.g. liquid phase exfoliation [160, 161, 288, 344, 411, 414], CVD [491], reduced GO [400], carbon segregation from silicon carbide [445], and micro-mechanical cleavage [40, 67], have been used to fabricate GSAs. A widely used method involves wet chemistry processing of graphene-polymer composites, as discussed in the previous sections.

Saturable absorbers using functionalized graphene (e.g. graphene oxide) have also been demonstrated for mode-locking [40]. Mode-locking of fiber [40, 160, 161, 288, 344, 400, 411, 414, 491] and solid-state [412, 424] lasers have been demonstrated with GSAs. Reference [344] reported sub-200 fs pulse generation using a GSA-based stretched-pulse cavity design. High output power (>1 W) has also been reported [412].

Unlike nanotubes, GSAs are intrinsically ultrawideband (Fig. 9.29b) [40, 160, 161, 411, 414]. GSAs have successfully been used to mode-lock lasers at 1 [424], and 1.5 μm [40, 160, 161, 344, 411, 414]. Recently, we demonstrated a widely tunable fiber laser mode-locked with a GSA (Fig. 9.29c) [40, 414]. It can produce picosecond pulses (Fig. 9.29d) in a tuning range of 1,525–1,559 nm (Fig. 9.29c), only limited by the filter used inside the cavity [40, 414]. In addition

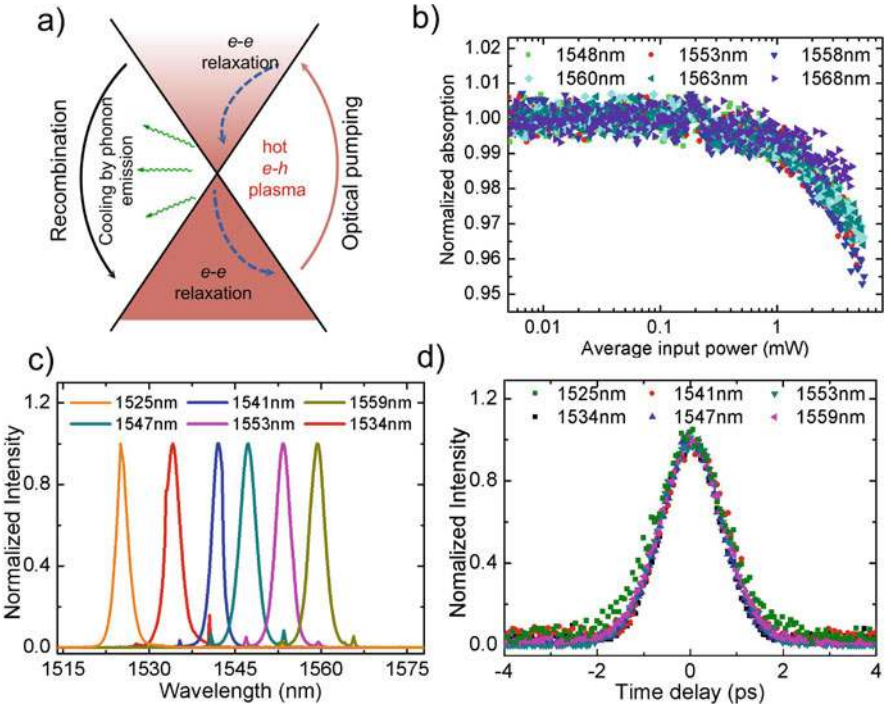

Fig. 9.29 Graphene based saturable absorbers: (**a**) Schematic of photo-excited electron kinetics in graphene, with possible relaxation mechanisms for the non-equilibrium electron population, (**b**) wideband saturable absorption of graphene, (**c**) output spectrum and (**d**) pulse duration measurements of wide-band tunable pulses mode-locked with graphene [411, 414]

to mode-locking, GSAs have also been used in Q-switching, for both wavelength-tunable [345] and dual-wavelength [274] lasers. These demonstrations underscore the potential of graphene for wideband ultrafast lasers, in principle, covering ultraviolet to THz spectral range [40, 311, 411].

9.13 Conclusions

Both nanotube and graphene are very promising for near term optoelectronic applications. Research on SWNT based optoelectronics, in particular ultrafast pulse generation, has soared over the past few years. This is primarily because of their optoelectronic properties and ease of device fabrication. In this chapter, we presented an overview of their polymer composites, starting from solution processing of the raw nanotubes, their sorting, characterization and incorporation into polymers, device fabrication and testing. We have also discussed some of the main applications, with particular focus on saturable absorbers for ultrafast lasers. Graphene has

also emerged as a strong competitor of SWNTs in the field of photonics and optoelectronics. We thus concluded this chapter with a discussion on graphene based devices for ultra wideband photonic and optoelectronic applications.

Acknowledgments We thank D. Popa, F. Torrisi, F. Wang, W. B. Cho for useful discussions. TH acknowledges funding from King's College, Cambridge, FB from a Newton International Fellowship, PHT from NSF of China (No. 10874177). ACF from EPSRC (Grant Nos. GR/S97613/01 and EP/E500935/1) ERC NANOPOTS, Royal Society Brian Mercer Award for Innovation, The Cambridge Integrated Knowledge Centre in Advanced Manufacturing Technology for Photonics and Electronics, the EU grants GENIUS and RODIN.

References

1. Adams, S. R., Harootunian, A. T., Buechler, Y. J., Taylor, S. S. & Tsien, R. Y. Fluorescence ratio imaging of cyclic AMP in single cells. *Nature* **349**, 694–697 (1991).
2. Ago, H., Petritsch, K., Shaffer, M. S. P., Windle, A. H. & Friend, R. H. Composites of carbon nanotubes and conjugated polymers for photovoltaic devices. *Adv. Mater.* **11**, 1281–1285 (1999).
3. Agrawal, G. P. *Application of nonlinear fiber optics*. Academic, San Diego (2001).
4. Ajayan, P. M. & Banhart, F. Nanotubes: Strong bundles. *Nat. Mater.* **3**, 135–136 (2004).
5. Ajayan, P. M., Stephan, O., Colliex, C. & Trauth, D. Aligned carbon nanotube arrays formed by cutting a polymer resin-nanotube composite. *Science* **265**, 1212–1214 (1994).
6. Ajiki, H. & Ando, T. Aharonov-Bohm effect in carbon nanotubes. *Physica B* **201**, 349–352 (1994).
7. Allington, R. W., Brakke, M. K., Nelson, J. W., Aron, C. G. & Larkins, B. A. Optimum conditions for high-resolution gradient analysis. *Anal. Biochem.* **73**, 78–92 (1976).
8. Alvarez, L., Righi, A., Rols, S., Anglaret, E., Sauvajol, J. L., Munoz, E., Maser, W. K., Benito, A. M., Martinez, M. T. & de la Fuente, G. F. Diameter dependence of Raman intensities for single-wall carbon nanotubes. *Phys. Rev. B* **63**, 153401 (2001).
9. Anandan, S. Recent improvements and arising challenges in dye-sensitized solar cells. *Solar Energy Mater. Solar Cells* **91**, 843–846 (2007).
10. Ando, T. Excitons in carbon nanotubes. *J. Phys. Soc. Jpn.* **66**, 1066–1073 (1997).
11. Araujo, P. T., Doorn, S. K., Kilina, S., Tretiak, S., Einarsson, E., Maruyama, S., Chacham, H., Pimenta, M. A. & Jorio, A. Third and fourth optical transitions in semiconducting carbon nanotubes. *Phys. Rev. Lett.* **98**, 067401 (2007).
12. Arnold, M. S., Green, A. A., Hulvat, J. F., Stupp, S. I. & Hersam, M. C. Sorting carbon nanotubes by electronic structure using density differentiation. *Nat. Nanotech.* **1**, 60–65 (2006).
13. Arnold, M. S., Stupp, S. I. & Hersam, M. C. Enrichment of single-walled carbon nanotubes by diameter in density gradients. *Nano Lett.* **5**, 713–718 (2005).
14. Artukovic, E., Kaempgen, M., Hecht, D. S., Roth, S. & Gruner, G. Transparent and flexible carbon nanotube transistors. *Nano Lett.* **5**, 757–760 (2005).
15. Ausman, K. D., Piner, R., Lourie, O., Ruoff, R. S. & Korobov, M. Organic solvent dispersions of single-walled carbon nanotubes: Toward solutions of pristine nanotubes. *J. Phys. Chem. B* **104**, 8911–8915 (2000).
16. Bachilo, S. M., Balzano, L., Herrera, J. E., Pompeo, F., Resasco, D. E. & Weisman, R. B. Narrow (n,m)-distribution of single-walled carbon nanotubes grown using a solid supported catalyst. *J. Am. Chem. Soc.* **125**, 11186–11187 (2003).
17. Bachilo, S. M., Strano, M. S., Kittrell, C., Hauge, R. H., Smalley, R. E. & Weisman, R. B. Structure-assigned optical spectra of single-walled carbon nanotubes. *Science* **298**, 2361–2366 (2002).

18. Bae, S., Kim, H., Lee, Y., Xu, X., Park, J.-S., Zheng, Y., Balakrishnan, J., Lei, T., Ri Kim, H., Song, Y. I., Kim, Y.-J., Kim, K. S., Ozyilmaz, B., Ahn, J.-H., Hong, B. H. & Iijima, S. Roll-to- roll production of 30-inch graphene films for transparent electrodes. *Nat. Nano* **5**, 574–578 (2010).
19. Bahr, J. L., Mickelson, E. T., Bronikowski, M. J., Smalley, R. E. & Tour, J. M. Dissolution of small diameter single-wall carbon nanotubes in organic solvents? *Chem. Commun.* 193–194 (2001).
20. Bahr, J. L., Yang, J., Kosynkin, D. V., Bronikowski, M. J., Smalley, R. E. & Tour, J. M. Functionalization of carbon nanotubes by electrochemical reduction of aryl diazonium salts: A bucky paper electrode. *J. Am. Chem. Soc.* **123**, 6536–6542 (2001).
21. Bandow, S., Asaka, S., Saito, Y., Rao, A. M., Grigorian, L., Richter, E. & Eklund, P. C. Effect of the growth temperature on the diameter distribution and chirality of single-wall carbon nanotubes. *Phys. Rev. Lett.* **80**, 3779 (1998).
22. Bandyopadhyaya, R., Nativ-Roth, E., Regev, O. & Yerushalmi-Rozen, R. Stabilization of individual carbon nanotubes in aqueous solutions. *Nano Lett.* **2**, 25–28 (2002).
23. Banerjee, S., Hemraj-Benny, T. & Wong, S. S. Covalent surface chemistry of single-walled carbon nanotubes. *Adv. Mater.* **17**, 17–29 (2005).
24. Banerjee, S., Kahn, M. G. C. & Wong, S. S. Rational chemical strategies for carbon nanotube functionalization. *Chem. Eur. J.* **9**, 1898–1908 (2003).
25. Baranov, A. V., Bekhterev, A. N., Bobovich, Y. S. & Petrov, V. I. Interpretation of some singularities in raman spectra of graphite and glass carbon. *Opt Spektrosk.* **62**, 1036–1042 (1987).
26. Basko, D. M., Piscanec, S. & Ferrari, A. C. Electron-electron interactions and doping dependence of the two-phonon Raman intensity in graphene. *Phys. Rev. B* **80**, 165413 (2009).
27. Becker, K., Lupton, J. M., Muller, J., Rogach, A. L., Talapin, D. V., Weller, H. & Feldmann, J. Electrical control of Förster energy transfer. *Nat. Mater.* **5**, 777–781 (2006).
28. Beecher, P., Servati, P., Rozhin, A., Colli, A., Scardaci, V., Pisana, S., Hasan, T., Flewitt, A. J., Robertson, J., Hsieh, G. W., Li, F. M., Nathan, A., Ferrari, A. C. & Milne, W. I. Ink-jet printing of carbon nanotube thin film transistors. *J. Appl. Phys.* **102**, 043710 (2007).
29. Beecher, S. J., Thomson, R. R., Psaila, N. D., Sun, Z., Hasan, T., Rozhin, A. G., Ferrari, A. C. & Kar, A. K. 320 fs pulse generation from an ultrafast laser inscribed waveguide laser mode-locked by a nanotube saturable absorber. *Appl. Phys. Lett.* **97**, 111114 (2010).
30. Behrens, M. In Abdelhalden's Handbuch der Biologischen Arbeitsmethoden. Abt. 5, Teil 10, Part 2, pp. 1363–1392. Urban and Schwarzenberg, Berlin (1938).
31. Berber, S., Kwon, Y.-K. & Tománek, D. Unusually high thermal conductivity of carbon nanotubes. *Phys. Rev. Lett.* **84**, 4613–4616 (2000).
32. Bergin, S. D., Nicolosi, V., Streich, P. V., Giordani, S., Sun, Z., Windle, A. H., Ryan, P., Niraj, N. P. P., Wang, Z.-T., Carpenter, L., Blau, W. J., Boland, J. J., Hamilton, J. P. & Coleman, J. N. Towards solutions of single-walled carbon nanotubes in common solvents. *Adv. Mater.* **20**, 1876 (2008).
33. Bergin, S. D., Sun, Z., Streich, P., Hamilton, J. & Coleman, J. N. New solvents for nanotubes: Approaching the dispersibility of surfactants. *J. Phys. Chem. C* **114**, 231–237 (2010).
34. Bharathan, J. & Yang, Y. Polymer electroluminescent devices processed by inkjet printing: I. Polymer light-emitting logo. *Appl. Phys. Lett.* **72**, 2660–2662 (1998).
35. Bhattacharyya, S., Kymakis, E. & Amaratunga, G. A. J. Photovoltaic properties of dye functionalized single-wall carbon nanotube/conjugated polymer devices. *Chem. Mater.* **16**, 4819–4823 (2004).
36. Biju, V., Itoh, T., Baba, Y. & Ishikawa, M. Quenching of photoluminescence in conjugates of quantum dots and single-walled carbon nanotube. *J. Phys. Chem. B* **110**, 26068–26074 (2006).
37. Blake, P., Brimicombe, P. D., Nair, R. R., Booth, T. J., Jiang, D., Schedin, F., Ponomarenko, L. A., Morozov, S. V., Gleeson, H. F., Hill, E. W., Geim, A. K. & Novoselov, K. S. Graphene-based liquid crystal device. *Nano Lett.* **8**, 1704–1708 (2008).

38. Bo, X. Z., Lee, C. Y., Strano, M. S., Goldfinger, M., Nuckolls, C. & Blanchet, G. B. Carbon nanotubes-semiconductor networks for organic electronics: The pickup stick transistor. *Appl. Phys. Lett.* **86**, 182102 (2005).
39. Bohren, C. F. & Huffman, D. R. *Absorption and scattering of light by small particles*. Wiley, New York 1998.
40. Bonaccorso, F., Sun, Z., Hasan, T. & Ferrari, A. C. Graphene photonics and optoelectronics. *Nat. Photonics* **4**, 611–622 (2010).
41. Bonaccorso, F., Hasan, T., Tan, P. H., Sciascia, C., Privitera, G., Di Marco, G., Gucciardi, P. G. & Ferrari, A. C. Density gradient ultracentrifugation of nanotubes: Interplay of bundling and surfactants encapsulation. *J. Phys. Chem. C* **114**, 17267–17285 (2010).
42. Born, M. & Oppenheimer, R. Zur Quantentheorie der Molekeln. *Ann. Phys.* **84**, 457 (1927).
43. Born, M. & Huang, K. *Dynamical theory of crystal lattices*. Clarendon Press, Oxford (1954).
44. Botti, S., Ciardi, R., De Dominicis, L., Asilyan, L. S., Fantoni, R. & Marolo, T. DFWM measurements of third-order susceptibility of single-wall carbon nanotubes grown without catalyst. *Chem. Phys. Lett.* **378**, 117–121 (2003).
45. Boyd, R. W. *Nonlinear optics*. Academic, San Diego (2003).
46. Brakke, M. K. Zonal separations by density-gradient centrifugation. *Arch. Biochem.* **45**, 275–290 (1953).
47. Brakke, M. K. Photometric scanning of centrifuged density gradient columns. *Arch. Biochem.* **5**, 271–283 (1963).
48. Brakke, M. K. Density gradient centrifugation and its application to plant viruses. *Advan. Virus Res.* **7**, 193–224 (1960).
49. Breusing, M., Ropers, C. & Elsaesser, T. Ultrafast carrier dynamics in graphite. *Phys. Rev. Lett.* **102**, 086809 (2009).
50. Bronikowski, M. J., Willis, P. A., Colbert, D. T., Smith, K. A. & Smalley, R. E. Gas-phase production of carbon single-walled nanotubes from carbon monoxide via the HiPco process: A parametric study. *J. Vacuum Sci. Technol. A* **19**, 1800–1805 (2001).
51. Brown, S. D. M., Jorio, A., Corio, P., Dresselhaus, M. S., Dresselhaus, G., Saito, R. & Kneipp, K. Origin of the Breit-Wigner-Fano lineshape of the tangential G-band feature of metallic carbon nanotubes. *Phys. Rev. B* **63**, 155414 (2001).
52. Brown, P., Takechi, K. & Kamat, P. V. Single-walled carbon nanotube scaffolds for dyesensitized solar cells. *J. Phys. Chem. C* **112**, 4776–4782 (2008).
53. Bruesch, P. *Phonons: Theory and experiments I, lattice dynamics and models of interatomic forces.* Springer, Berlin, Heidelberg, New York (1982).
54. Butt, H., Graf, K. & Kappl, M. *Physics and chemistry of interfaces.* Wiley VCH, Berlin (2006).
55. Cacace, M. G., Landau, E. M. & Ramsden, J. J. The Hofmeister series: Salt and solvent effects on interfacial phenomena. *Quart. Rev. Bioph.* **3**, 241–277 (1997).
56. Calvert, P. Inkjet printing for materials and devices. *Chem. Mater.* **13**, 3299–3305 (2001).
57. Calzolari, A., Marzari, N., Souza, I. & Buongiorno Nardelli, M. Ab initio transport properties of nanostructures from maximally localized Wannier functions. *Phys. Rev. B* **69**, 035108 (2004).
58. Cançado, L. G., Jorio, A., Martins Ferreira, E. H., Stavale, F., Achete, C. A., Capaz, R. B., Moutinho, M. V. O., Lombardo, A., Kulmala, T. & Ferrari, A. C. Quantifying defects in grapheme via Raman spectroscopy at different excitation energies. arXiv:1105.0175 (2011).
59. Cancado, L. G., Pimenta, M. A., Neves, B. R. A., Dantas, M. S. S. & Jorio, A. *Phys. Rev. Lett*. **93**, 247401 (2004).
60. Capaz, R. B., Spataru, C. D., Ismail-Beigi, S. & Louie, S. G. Diameter and chirality dependence of exciton properties in carbon nanotubes. *Phys. Rev. B* **74**, 121401(R) (2006).
61. Casiraghi, C., Hartschuh, A., Qian, H., Piscanec, S., Georgi, C., Fasoli, A., Novoselov, K. S., Basko, D. M. & Ferrari, A. C. *Nano Lett.* **9**, 1433 (2009).
62. Casiraghi, C., Pisana, S., Novoselov, K. S., Geim, A. K. & Ferrari, A. C. *Appl. Phys. Lett.* 91, 233108 (2007).

63. Carlson, L. J., Maccagnano, S. E., Zheng, M., Silcox, J. & Krauss, T. D. Fluorescence efficiency of individual carbon nanotubes. *Nano Lett.* **7**, 3698–3703 (2007).
64. Cathcart, H., Quinn, S., Nicolosi, V., Kelly, J. M., Blau, W. J. & Coleman, J. N. Spontaneous debundling of single-walled carbon nanotubes in DNA-based dispersions. *J. Phys. Chem. C* **111**, 66–74 (2007).
65. Chandrasekhar, R., Charles, S. W. & O'Grady, K. Cobalt ferrite fluids and their application to magnetic ink-jet printing. *J. Imaging Technol.* **13**, 55–59 (1987).
66. Chang, E., Bussi, G., Ruini, A. & Molinari, E. Excitons in carbon nanotubes: An Ab Initio symmetry-based approach. *Phys. Rev. Lett.* **92**, 196401 (2004).
67. Chang, Y. M., Kim, H., Lee, J. H. & Song, Y.-W. Multilayered graphene efficiently formed by mechanical exfoliation for nonlinear saturable absorbers in fiber mode-locked lasers. *Appl. Phys. Lett.* **97**, 211102–3 (2010).
68. Chapin, D. M., Fuller, C. S. & Pearson, G. L. A new silicon p-n junction photocell for converting solar radiation into electrical power. *J. Appl. Phys.* **25**, 676–677 (1954).
69. Charlier, J.-C., Lambin, Ph. & Ebbesen, T. W. Electronic properties of carbon nanotubes with polygonized cross sections. *Phys. Rev. B* **54**, R8377–R8380 (1996).
70. Collins, K. & Washabaugh, M. The Hofmeister effect and the behaviour of water at interfaces. *Q. Rev. Biophys.* **18**, 323–422 (1985).
71. Cote, L. J., Kim, F. & Huang, J. Langmuir-Blodgett assembly of graphite oxide single layers. *J. Am. Chem. Soc.* **131**, 1043–1049 (2008).
72. Chen, G. Z., Shaffer, M. S. P., Coleby, D., Dixon, G., Zhou, W., Fray, D. J. & Windle, A. H. Carbon nanotube and polypyrrole composites: Coating and doping. *Adv. Mater.* **12**, 522–526 (2000).
73. Chen, H.-Y. & Lee, W. Suppression of field screening in nematic liquid crystals by carbon nanotubes. *Appl. Phys. Lett.* **88**, 222105 (2006).
74. Chen, H.-Y., Lee, W. & Clark, N. A. Faster electro-optical response characteristics of a carbonnanotube-nematic suspension. *Appl. Phys. Lett.* **90**, 033510-3 (2007).
75. Chen, J., Rao, A. M., Lyuksyutov, S., Itkis, M. E., Hamon, M. A., Hu, H., Cohn, R. W., Eklund, P. C., Colbert, D. T., Smalley, R. E. & Haddon, R. C. Dissolution of full-length single-walled carbon nanotubes. *J. Phys. Chem. B* **105**, 2525–2528 (2001).
76. Chen, Y.-C., Raravikar, N. R., Schadler, L. S., Ajayan, P. M., Zhao, Y.-P., Lu, T.-M., Wang, G.-C. & Zhang, X.-C. Ultrafast optical switching properties of single-wall carbon nanotube polymer composites at 1.55 um. *Appl. Phys. Lett.* **81**, 975–977 (2002).
77. Cheng, H. M., Li, F., Sun, X., Brown, S. D. M., Pimenta, M. A., Marucci, A., Dresselhaus, G. & Dresselhaus, M. S. Bulk morphology and diameter distribution of single-walled carbon nanotubes synthesized by catalytic decomposition of hydrocarbons. *Chem. Phys. Lett.* **289**, 602–610 (1998).
78. Cheng, W. D., Wu, D. S., Zhang, H., Li, X. D., Lan, Y. Z., Chen, D. G. & Wang, H. X. Enhancements of third-order nonlinear optical response in the triplet excited state of finite open single-walled carbon nanotubes. *J. Chem. Phys.* **119**, 13100–13105 (2003).
79. Choi, J. H. Solvatochromism in single-walled carbon nanotubes. *Appl. Phys. Lett.* **90**, 223114 (2007).
80. Cohen, R. & Claverie, J. M. Sedimentation of generalized systems of interacting particles. II. Active enzyme centrifugation – theory and extensions of its validity range. *Biopolymers* **14**, 1701–1716 (1975).
81. Coleman, J. N., Khan, U., Blau, W. J. & Gun'ko, Y. K. Small but strong: A review of the mechanical properties of carbon nanotube-polymer composites. *Carbon* **44**, 1624–1652 (2006).
82. Coleman, J. N., Khan, U. & Gun'ko, Y. K. Mechanical reinforcement of polymers using carbon nanotubes. *Adv. Mater.* **18**, 689–706 (2006).
83. Coleman, J. N. Liquid-phase exfoliation of nanotubes and graphene. *Adv. Funct. Mater.* **19**, 3680–3695 (2009).
84. Crawford, L. V. & Waring, M. J. Supercoiling of polyoma virus DNA measured by its interaction with ethium bromide. *J. Mol. Biol.* **25**, 23–30 (1967).

85. Creeth, J. H. & Pain, R. H. The determination of molecular weights of biological macromolecules by ultracentrifuge methods. *Prog. Biophys. Mol. Biol.* **17**, 217–287 (1967).
86. Crochet, J., Clemens, M. & Hertel, T. Quantum yield heterogeneities of aqueous single-wall carbon nanotube suspensions. *J. Am. Chem. Soc.* **129**, 8058–8059 (2007).
87. Dai, H. Carbon nanotubes: Synthesis, integration, and properties. *Acc. Chem. Res.* **35**, 1035–1044 (2002).
88. Dalton, A. B., Collins, S., Muñoz, E., Razal, J. M., Ebron, V. H., Ferraris, J. P., Coleman, J. N., Kim, B. G. & Baughman, R. H. Super-tough carbon-nanotube fibres. *Nature* **423**, 703 (2003).
89. Das, A., Chakraborty, B., Piscanec, S., Pisana, S., Sood, A. K. & Ferrari, A. C. Phonon renormalization in doped bilayer graphene. *Phys. Rev. B* **79**, 155417 (2009).
90. Das, A., Pisana, S., Chakraborty, B., Piscanec, S., Saha, S. K., Waghmare, U. V., Novoselov, K. S., Krishnamurthy, H. R., Geim, A. K., Ferrari, A. C. & Sood, A. K. *Nat. Nanotechnol.* **3**, 210 (2008).
91. Dawlaty, J. M., Shivaraman, S., Strait, J., George, P., Chandrashekhar, M., Rana, F., Spencer, M. G., Veksler, D. & Chen, Y. Measurement of the optical absorption spectra of epitaxial graphene from terahertz to visible. *Appl. Phys. Lett.* **93**, 131905 (2008).
92. De, S., Lyons, P. E., Sorel, S., Doherty, E. M., King, P. J., Blau, W. J., Nirmalraj, P. N., Boland, J. J., Scardaci, V., Joimel, J. & Coleman, J. N. Transparent, flexible, and highly conductive thin films based on polymer-nanotube composites. *ACS Nano* **3**, 714–720 (2009).
93. De Dominicis, L., Botti, S., Asilyan, L. S., Ciardi, R., Fantoni, R., Terranova, M. L., Fiori, A., Orlanducci, S. & Appolloni, R. Second- and third- harmonic generation in single-walled carbon nanotubes at nanosecond time scale. *Appl. Phys. Lett.* **85**, 1418–1420 (2004).
94. De, S., King, P. J., Lotya, M., O'Neill, A., Doherty, E. M., Hernandez, Y., Duesberg, G. S. & Coleman, J. N. Flexible, transparent, conducting films of randomly stacked graphene from surfactant-stabilized, oxide-free graphene dispersions. *Small* **6**, 458–464 (2010).
95. De, S., Higgins, T. M., Lyons, P. E., Doherty, E. M., Nirmalraj, P. N., Blau, W. J., Boland, J. J. & Coleman, J. N. Silver nanowire networks as flexible, transparent, conducting films: Extremely high DC to optical conductivity ratios. *ACS Nano* **3**, 1767–1774 (2009).
96. Della Valle, G., Osellame, R., Galzerano, G., Chiodo, N., Cerullo, G., Laporta, P., O., S., Morgner, U., Rozhin, A. G., Scardaci, V. & Ferrari, A. C. Passive mode locking by carbon nanotubes in a femtosecond laser written waveguide laser. *Appl. Phys. Lett.* **89**, 231115 (2006).
97. DeMaria, A. J., Stetser, D. A. & Heynau, H. Self mode-locking of lasers with saturable absorbers. *Appl. Phys. Lett.* **8**, 174–176 (1966).
98. Denneulin, A., Bras, J., Blayo, A., Khelifi, B., Roussel-Dherbey, F. & Neuman, C. The influence of carbon nanotubes in inkjet printing of conductive polymer suspensions. *Nanotechnology* **20**, 385701 (2009).
99. Dettlaff-Weglikowska, U., Kaempgen, M., Hornbostel, B., Skakalova, V., Wang, J., Liang, J. & Roth, S. Conducting and transparent SWNT/polymer composites. *Phys. Stat. Sol. (b)* **243**, 3440–3444 (2006).
100. Dieckmann, G. R., Dalton, A. B., Johnson, P. A., Razal, J., Chen, J., Giordano, G. M., Muñoz, E., Musselman, I. H., Baughman, R. H. & Draper, R. K. Controlled assembly of carbon nanotubes by designed amphiphilic peptide helices. *J. Am. Chem. Soc.* **125**, 1770–1777 (2003).
101. Dierking, I., Scalia, G. & Morales, P. Liquid crystal–carbon nanotube dispersions. *J. Appl. Phys.* **97**, 044309 (2005).
102. Dierking, I., Scalia, G., Morales, P. & LeClere, D. Aligning and reorienting carbon nanotubes with nematic liquid crystals. *Adv. Mater.* **16**, 865–869 (2004).
103. Dobardžić, E., Maultzsch, J., Milošević, I., Thomsen, C. & Damjanović, M. The radial breathing mode frequency in double-walled carbon nanotubes: An analytical approximation. *Phys. Stat. Sol. (b)* **237**, R7 (2003).

104. Doorn, S. K., Strano, M. S., O'Connell, M. J., Haroz, E. H., Rialon, K. L., Hauge, R. H. & Smalley, R. E. Capillary electrophoresis separations of bundled and individual carbon nanotubes. *J. Phys. Chem. B* **107**, 6063–6069 (2003).
105. Dyke, C. A. & Tour, J. M. Solvent-free functionalization of carbon nanotubes. *J. Am. Chem. Soc.* **125**, 1156–1157 (2003).
106. Dyke, C. A. & Tour, J. M. Covalent functionalization of single-walled carbon nanotubes for materials applications. *J. Phys. Chem. A* **108**, 11151–11159 (2004).
107. Dyke, C. A. & Tour, J. M. Overcoming the insolubility of carbon nanotubes through high degrees of sidewall functionalization. *Chem. Eur. J.* **10**, 812–817 (2004).
108. Eda, G. & Chhowalla, M. Chemically derived graphene oxide: Towards large-area thin-film electronics and optoelectronics. *Adv. Mater.* **22**, 2392–2415 (2010).
109. Eivindvik, K. & Sjogren, C. E. Physicochemical properties of iodixanol. *Acta Radiologica* **36**, 32–38 (1995).
110. Elias, D. C., Nair, R. R., Mohiuddin, T. M. G., Morozov, S. V., Blake, P., Halsall, M. P., Ferrari, A. C., Boukhvalov, D. W., Katsnelson, M. I., Geim, A. K. & Novoselov, K. S. Control of graphene's properties by reversible hydrogenation: Evidence for graphane. *Science* **323**, 610 (2009).
111. Eschrig, H. Unified perturbation treatment for phonons in metallic covalent and ionic crystals. *Phys. Stat. Sol. (b)* **56**, 197 (1973).
112. Essig, S., Marquardt, C. W., Vijayaraghavan, A., Ganzhorn, M., Dehm, S., Hennrich, F., Ou, F., Green, A. A., Sciascia, C., Bonaccorso, F., Bohnen, K.-P., v Lonhneysen, H., Kappes, M. M., Ajayan, P. M., Hersam, M. C., Ferrari, A. C. & Krupke, R. Phonon-assisted electroluminescence from metallic carbon nanotubes and graphene. *Nano lett*. **10**, 1589–1594 (2010).
113. Fagan, J. A., Becker, M. L., Chun, J., Nie, P., Bauer, B. J., Simpson, J. R., Hight-Walker, A. & Hobbie, E. K. Centrifugal length separation of carbon nanotubes. *Langmuir* **24**, 13880–13389 (2008).
114. Fairhurst, C. E., Fuller, S., Gray, J., Holmes, M. C. & Tiddy, G. J. T. In *Lyotropic surfactant liquid crystals*, Vol. 3. High molecular mass liquid crystals (Eds.: Demus, D., Goodby, J., Gray, G. W., Spiess, H. W., and Vill, V.), New York, Wiley-VCH (1998).
115. Fang, Q., Kieu, K. & Peyghambarian, N. An all-fiber 2-um wavelength-tunable mode-locked laser. *IEEE Photonics Technol. Lett.* **22**, 1656–1658 (2010).
116. Fantini, C., Jorio, A., Souza, M., Strano, M. S., Dresselhaus, M. S. & Pimenta, M. A. Optical transition energies for carbon nanotubes from resonant Raman spectroscopy: Environment and temperature effects. *Phys. Rev. Lett.* **93**, 147406 (2004).
117. Feng, W., Bai, X. D., Lian, Y. Q., Liang, J., Wang, X. G. & Yoshino, K. Well-aligned polyaniline/carbon-nanotube composite films grown by in-situ aniline polymerization. *Carbon* **41**, 1551–1557 (2003).
118. Ferrari, A. C. Raman spectroscopy of graphene and graphite: Disorder, electron-phonon coupling, doping and nonadiabatic effects. *Solid State Comm.* **143**, 47 (2007).
119. Ferrari, A. C., Robertson, J. *Raman spectroscopy in carbons: From nanotubes to diamond.* Philos. Trans. R. Soc. A, **362,** 2267–2565 (2004)
120. Ferrari, A. C. & Robertson, J. Interpretation of Raman spectra of disordered and amorphous carbon. *Phys. Rev. B* **61**, 14095–14107 (2000).
121. Ferrari, A. C. & Robertson, J. Resonant Raman spectroscopy of disordered, amorphous, and diamondlike carbon. *Phys. Rev. B* **64**, 075414 (2001).
122. Ferrari, A. C., Meyer, J. C., Scardaci, V., Casiraghi, C., Lazzeri, M., Mauri, F., Piscanec, S., Jiang, D., Novoselov, K. S., Roth, S. & Geim, A. K. Raman spectrum of graphene and graphene layers. *Phys. Rev. Lett.* **97**, 187401 (2006).
123. Ferrer-Anglada, N., Kaempgen, M., Skakalova, V., Dettlaf-Weglikowska, U. & Roth, S. Synthesis and characterization of carbon nanotube-conducting polymer thin films. *Diamond Relat. Mater.* **13**, 256–260 (2004).
124. Finnie, P., Homma, Y. & Lefebvre, J. Band-gap shift transition in the photoluminescence of single-walled carbon nanotubes. *Phys. Rev. Lett.* **94**, 247401 (2005).

125. Fong, K. H., Kikuchi, K., Goh, C. H., Set, S. Y., Grange, R., Haiml, M., Schlatter, A. & Keller, U. Solid-state Er:Yb:glass laser mode-locked by using single-wall carbon nanotube thin film. *Opt. Lett.* **32**, 38–40 (2007).
126. Ford, T., Graham, J. & Rickwood, D. Iodixanol-a non ionic isosmotic centrifugation medium for the formation of self-generated gradients. *Anal. Biochem.* **220**, 360–366 (1994).
127. Förster, T. Transfer mechanisms of electronic excitation. *Discuss. Faraday Soc.* **27**, 7–17 (1959).
128. Fox, N. A., Youh, M. J., Steeds, J. W. & Wang, W. N. Patterned diamond particle films. *J. Appl. Phys.* **87**, 8187–8191 (2000).
129. Freifelder, D. Molecular weights of coliphages and coliphages DNA. Molecular weights of DNA from bacteriophages T4, T5, and general problem of determination of M. *J. Mol. Bio.* **54**, 567–577 (1970).
130. Gambetta, A., Galzerano, G., Rozhin, A. G., Ferrari, A. C., Ramponi, R., Laporta, P. & Marangoni, M. Sub-100 fs two-color pump-probe spectroscopy of single wall carbon nanotubes with a 100 MHz Er-fiber laser system. *Opt. Express* **16**, 11727–11734 (2008).
131. Gamerith, S., Klug, A., Scheiber, H., Scherf, U., Moderegger, E., & List, E. J. W. Direct ink-jet printing of Ag-Cu nanoparticle and Ag-Precursor based electrodes for OFET applications. *Adv. Funct. Mater.* **17**, 3111–3118 (2007).
132. Gans, B.-J. de, Duineveld, P. C. & Schubert, U. S. Inkjet printing of polymers: State of the art and future developments. *Adv. Mater.* **16**, 203–213 (2004).
133. Garber, R. C. & Yoder, O. C. Isolation of DNA from filamentous fungi and separation into nuclear, mitochondrial, ribosomal, and plasmid components. *Anal. Biochem.* **135**, 416–422 (1983).
134. Garcia-Vidal, F. J. & Pitarke, J. M. Optical absorption and energy-loss spectra of aligned carbon nanotubes. *Eur. Phys. J. B* **22**, 257–265 (2001).
135. Geim, A. K. & Novoselov, K. S. The rise of graphene. *Nat. Mater.* **6**, 183–191 (2007).
136. Geng, H. Z., Kim, K. K., So, K. P., Lee, Y. S., Chang, Y. & Lee, Y. H. Effect of acid treatment on carbon nanotube-based flexible transparent conducting films. *J. Am. Chem. Soc.* **129**, 7758–7759 (2007).
137. Ghatee, M. H. & Pakdel, L. Surface tension regularity of non-polar, polar, and weak electrolyte liquid hydrocarbons. *Fluid Phase Equilib.* **234**, 101–107 (2005).
138. Giordani, S., Bergin, S. D., Nicolosi, V., Lebedkin, S., Kappes, M. M., Blau, W. J. & Coleman, J. N. Debundling of single-walled nanotubes by dilution: Observation of large populations of individual nanotubes in amide solvent dispersions. *J. Phys. Chem. B* **110**, 15708–15718 (2006).
139. Giorgetti, E., Margheri, G., Sottini, S., Casalboni, M., Senesi, R., Scarselli, M. & Pizzoferrato, R. Dye-doped zirconia-based Ormosil planar waveguides: Optical properties and surface morphology. *J. Non-Cryst. Solids* **255**, 193–198 (1999).
140. Girifalco, L. A., Hodak, M. & Lee, R. S. Carbon nanotubes, buckyballs, ropes, and a universal graphitic potential. *Phys. Rev. B* **62**, 13104–13110 (2000).
141. Girifalco, L. A. & Lad, R. A. Energy of cohesion, compressibility, and the potential energy functions of the graphite system. *J. Chem. Phys.* **25**, 693–697 (1956).
142. Gracia-Espino, E., Sala, G., Pino, F., Halonen, N., Luomahaara, J., Maklin, J., Toth, G., Kordas, K., Jantunen, H., Terrones, M., Helisto, P., Seppa, H., Ajayan, P. M. & Vajtai, R. Electrical transport and field-effect transistors using inkjet-printed SWCNT films having different functional side groups. *ACS Nano* **4**, 3318–3324 (2010).
143. Graf, D., Molitor, F., Ensslin, K., Stampfer, C., Jungen, A., Hierold, C. & Wirtz, L. Spatially resolved Raman spectroscopy of single- and few-layer graphene. *Nano Lett.* **7**, 238 (2007).
144. Graham, J. M. *Biological centrifugation.* BIOS Scientific Publisher Limited, Oxford (2001).
145. Granqvist, C. G. Transparent conductors as solar energy materials: A panoramic review. *Sol. Energ. Mat. Sol. C.* **91**, 1529–1598 (2007).
146. Gratzel, M. Dye-sensitized solar cells. *J. Photochem. Photobiol. C* **4**, 145–153 (2003).
147. Green, A. A. & Hersam, M. C. Processing and properties of highly enriched double-wall carbon nanotubes. *Nat. Nanotechnol.* **4**, 64–70 (2009).

148. Green, A. A. & Hersam, M. C. Solution phase production of graphene with controlled thickness via density differentiation. *Nano Lett.* **9**, 4031–4036 (2009).
149. Gruner, G. Carbon nanotube films for transparent and plastic electronics. *J. Mater. Chem.* **16**, 3533–3539 (2006).
150. Guo, Y., Minami, N., Kazaoui, S., Peng, J., Yoshida, M. & Miyashita, T. Multi-layer LB films of single-wall carbon nanotubes. *Physica B* **323**, 235–236 (2002).
151. Hagen, A. & Hertel, T. Quantitative analysis of optical spectra from individual single-wall carbon nanotubes. *Nano Lett.* **3**, 383–388 (2003).
152. Hagen, A., Steiner, M., Raschke, M. B., Lienau, C., Hertel, T., Qian, H. H., Meixner, A. J. & Hartschuh, A. Exponential decay lifetimes of excitons in individual single-walled carbon nanotubes. *Phys. Rev. Lett.* **95**, 197401 (2005).
153. Hamberg, I. & Granqvist, C. G. Evaporated Sn-doped In2O3 films: Basic optical properties and applications to energy-efficient windows. *J. Appl. Phys.* **60**, R123–R160 (1986).
154. Han, J.-I. Stability of externally deformed ITO films. In *Flexible and flat panel dispolays* (Ed.: Crawford, G. P.). Sussex, England (2005).
155. Hansen, C. M. *Hansen solubility parameters: A user's handbook.* CRC Press Inc., Boca Raton, FL (2007).
156. Harris, P. J. F. Carbon nanotube composites. *Int. Mat. Rev.* **49**, 31–43 (2004).
157. Hasan, T., Tan, P. H., Bonaccorso, F., Rozhin, A., Scardaci, V., Milne, W. I. & Ferrari, A. C. Polymer-assisted isolation of singlewall carbon nanotubes in organic solvents for optical-quality nanotube-polymer composites. *J. Phys. Chem. C* **112**, 20227–20232 (2008).
158. Hasan, T., Scardaci, V., Tan, P. H., Rozhin, A. G., Milne, W. I. & Ferrari, A. C. Stabilization and 'de-bundling' of single-wall carbon nanotube dispersions in N-Methyl-2-Pyrrolidone (NMP) by polyvinylpyrrolidone (PVP). *J. Phys. Chem. C* **111**, 12594–12602 (2007).
159. Hasan, T., Scardaci, V., Tan, P. H., Rozhin, A. G., Milne, W. I. & Ferrari, A. C. Dispersibility and stability improvement of unfunctionalized nanotubes in amide solvents by polymer wrapping. *Physica E* **40**, 2414–2418 (2008).
160. Hasan, T., Sun, Z., Wang, F., Bonaccorso, F., Tan, P. H., Rozhin, A. G. & Ferrari, A. C. Nanotube-polymer composites for ultrafast photonics. *Adv. Mater.* **21**, 3874–3899 (2009).
161. Hasan, T., Torrisi, F., Sun, Z., Popa, D., Nicolosi, V., Privitera, G., Bonaccorso, F. & Ferrari, A. C. Solution-phase exfoliation of graphite for ultrafast photonics. *Physica Status Solidi (b)* **247**, 2953–2957 (2010).
162. Haschemeyer, R. H. & Bowers, W. F. Exponential analysis of concentration or concentration difference data for discrete molecular weight distributions in sedimentation equilibrium. *Biochemistry* **9**, 435–445 (1970).
163. Hearst, J. E. & Vinograd, J. A Three-Component Theory of Sedimentation Equilibrium in a Density Gradient. *J. Natl. Acad. Sci. USA* **47**, 999–1004 (1961).
164. Hecht, D, Hu, L. & Gruner, G. Conductivity scaling with bundle length and diameter in single walled carbon nanotube networks. *Appl. Phys. Lett.* **89**, 133112 (2006).
165. Henrard, L., Hernández, E., Bernier, P. & Rubio, A. Van der Waals interaction in nanotube bundles: Consequences on vibrational modes. *Phys. Rev. B* **60**, R8521 (1999).
166. Hernandez, Y., Nicolosi, V., Lotya, M., Blighe, F. M., Sun, Z., De, S., McGovern, I. T., Holland, B., Byrne, M., Gun'Ko, Y. K., Boland, J. J., Niraj, P., Duesberg, G., Krishnamurthy, S., Goodhue, R., Hutchison, J., Scardaci, V., Ferrari, A. C. & Coleman, J. N. High-yield production of graphene by liquid-phase exfoliation of graphite. *Nat. Nano* **3**, 563–568 (2008).
167. Hersam, M. Progress towards monodisperse single-walled carbon nanotubes. *Nat. Nanotech.* **3**, 387 (2008).
168. Hertel, T., Fasel, R. & Moos, G. Charge-carrier dynamics in single-wall carbon nanotube bundles: A time-domain study. *Appl. Phys. A* **75**, 449–465 (2002).
169. Hertel, T. & Moos, G. Electron-phonon interaction in single-wall carbon nanotubes: A time-domain study. *Phys. Rev. Lett.* **84**, 5002–5005 (2000).

170. Hertel, T., Perebeinos, V., Crochet, J., Katharina, A., Kappes, M. & Phaedon, A. Intersubband decay of 1-D exciton resonances in carbon nanotubes. *Nano Lett.* **8**, 87–91 (2008).
171. Hertel, T., Walkup, R. E. & Avouris, Ph. Deformation of carbon nanotubes by surface van der Waals forces. *Phys. Rev. B* **58**, 13870–13873 (1998).
172. Hirsch, A. Functionalization of single-walled carbon nanotubes. *Angew. Chem. Int. Ed.* **41**, 1853–1859 (2002).
173. Hong, W., Xu, Y., Lu, G., Li, C. & Shi, G. Transparent graphene/PEDOT-PSS composite films as counter electrodes of dye-sensitized solar cells. *Electrochem. Commun.* **10**, 1555–1558 (2008).
174. Hsieh, G. W., Beecher, P., Li, F. M., Servati, P., Colli, A., Fasoli, A., Chu, D., Nathan, A., Ong, B., Robertson, J., Ferrari, A. C. & Milne, W. I. Formation of composite organic thin film transistors with nanotubes and nanowires. *Physica E* **40**, 2406–2413 (2008).
175. Htoon, H., O'Connell, M. J., Doorn, S. K. & Klimov, V. I. Single carbon nanotubes probed by photoluminescence excitation spectroscopy: The role of phonon-assisted transitions. *Phys. Rev. Lett.* **94**, 127403 (2005).
176. Huang, C.-Y., Hu, C.-Y., Pan, H.-C. & Lo, K.-Y. Electrooptical responses of carbon nanotube-doped liquid crystal devices. *Jpn. J. Appl. Phys.* **44**, 8077–8081 (2005).
177. Hwang, J., Gommans, H. H., Ugawa, A., Tashiro, H., Haggenmueller, R., Winey, K. I., Fisher, J. E., Tanner, D. B. & Rinzler, A. G. Polarized spectroscopy of aligned single-wall carbon nanotubes. *Phys. Rev. B* **62**, 13310–13313 (2000).
178. Ichida, M., Hamanaka, Y., Kataura, H., Achiba, Y. & Nakamura, A. Ultrafast relaxation dynamics of photoexcited carriers in metallic and semiconducting single-walled carbon nanotubes. *J. Phys. Soc. Jpn.* **73**, 3479–3483 (2004).
179. Ichida, M., Mizuno, S., Kataura, H., Achiba, Y. & Nakamura, A. Anisotropic optical properties of mechanically aligned single-walled carbon nanotubes in polymer. *Appl. Phys. A* **78**, 1117–1120 (2004).
180. Ifft, J. B. & Vinograd, J. The Buoyant behavior of Bovine serum mercaptalbumin in salt solutions at equilibrium in the ultracentrifuge. II. Net hydration, ion binding, and solvated molecular weight in various salt solutions. *J. Phys. Chem.* **70**, 2814–2822 (1966).
181. Il'ichev, N. N., Garnov, S. V. & Obraztsova, E. D. Single-wall carbon nanotube suspension as a passive Q-switch for self mode-locking of solid state lasers. *AIP Conf. Proc. Electron. Prop. Novel Nanostruct.* **786**, 611–615 (2005).
182. Islam, M. F., Milkie, D. E., Kane, C. L., Yodh, A. G. & Mikkawa, J. M. Direct measurement of the polarized optical absorption cross section of single-wall carbon nanotubes. *Phys. Rev. Lett.* **93**, 037404 (2004).
183. Islam, M. F., Rojas, E., Bergey, D. M., Johnson, A. T. & Yodh, A. G. High weight fraction surfactant solubilization of single-wall carbon nanotubes in water. *Nano Lett.* **3**, 269–273 (2003).
184. Jiang, J., Dong, J. M., Wan, X. G. & Xing, D. Y. A new kind of nonlinear optical material: The fullerene tube. *J. Phys. B* **31**, 3079–3086 (1998).
185. Jiang, J., Saito, R., Gruneis, A., Dresselhaus, G. & Dresselhaus, M. S. Optical absorption matrix elements in single-wall carbon nanotubes. *Carbon* **42**, 3169–3176 (2004).
186. Jishi, R. A., Venkataraman, L., Dresselhaus, M. S. & Dresselhaus, G. Phonon modes in carbon nanotubes. *Chem. Phys. Lett.* **209**, 77 (1993)
187. Jorio, A., Fantini, C., Pimenta, M. A., Heller, D. A., Strano, M. S., Dresselhaus, M. S., Oyama, Y., Jiang, J. & Saito, R. Carbon nanotube population analysis from Raman and photoluminescence intensities. *Appl. Phys. Lett.* **88**, 023109 (2006).
188. Jorio, A., Saito, R., Hafner, J. H., Lieber, C. M., Hunter, M., McClure, T., Dresselhaus, G. & Dresselhaus, M. S. Structural (n,m) determination of isolated single-wall carbon nanotubes by resonant Raman scattering. *Phys. Rev. Lett.* **86**, 1118–1121 (2001).
189. Jorio, A., Fantini, C., Dantas, M. S. S., Pimenta, M. A., Souza, A. G., Samsonidze, G. G., Brar, V. W., Dresselhaus, G., Dresselhaus, M. S., Swan, A. K., Ünlü, M. S., Goldberg,

B. B. & Saito, R. Linewidth of the Raman features of individual single-wall carbon nanotubes. *Phys. Rev. B* **66**, 115411 (2002).
190. Jorio, A., Souza, A. G., Dresselhaus, G., Dresselhaus, M. S., Swan, A. K., Unlu, M. S., Goldberg, B. B., Pimenta, M. A., Hafner, J. H., Lieber, C. M. & Saito, R. G-band resonant Raman study of 62 isolated single-wall carbon nanotubes. *Phys. Rev. B* **65**, 155412 (2002).
191. Jost, O., Gorbunov, A. A., Pompe, W., Pichler, T., Friedlein, R., Knupfer, M., Reibold, M., Bauer, H. D., Dunsch, L., Golden, M. S. & Fink, J. Diameter grouping in bulk samples of single-walled carbon nanotubes from optical absorption spectroscopy. *Appl. Phys. Lett.* **75**, 2217–2219 (1999).
192. Journet, C., Maser, W. K., Bernier, P., Loiseau, A., Lamy de la Chapelle, M., Lefrant, S., Deniard, P., Lee, R. & Fischer, J. E. Large-scale production of single-walled carbon nanotubes by the electric-arc technique. *Nature* **388**, 756–758 (1997).
193. Kaempgen, M., Dettlaff, U. & Roth, S. Characterization of carbon nanotubes by optical spectra. *Synth. Met.* **135–136**, 755–756 (2003).
194. Kagan, C. R., Murray, C. B., Nirmal, M. & Bawendi, M. G. Electronic energy transfer in CdSe quantum dot solids. *Phys. Rev. Lett.* **76**, 1517–1520 (1996).
195. Kamaraju, N., Kumar, S., Sood, A. K., Guha, S., Krishnamurthy, S. & Rao, C. N. R. Large nonlinear absorption and refraction coefficients of carbon nanotubes estimated from femtosecond z-scan measurements. *Appl. Phys. Lett.* **91**, 251103 (2007).
196. Kamyshny, A., Ben-Moshe, M., Aviezer, S. & Magdassi, S. Ink-jet printing of metallic nanoparticles and microemulsions. *Macromol. Rapid Commun.* **26**, 281–288 (2005).
197. Kane, C. L. & Mele, E. J. Ratio problem in single carbon nanotube fluorescence spectroscopy. *Phys. Rev. Lett.* **90**, 207401 (2003).
198. Kang, Y. & Taton, T. A. Micelle-encapsulated carbon nanotubes: A route to nanotube composites. *J. Am. Chem. Soc.* **125**, 5650–5651 (2003).
199. Kartner, F. H., Brovelli, L. R., Kopf, D., Kamp, M., Calasso, I. & Keller, U. Control of solid-state laser dynamics by semiconductor devices. *Opt. Eng.* **34**, 2024–2036 (1995).
200. Kataura, H., Kumazawa, Y., Maniwa, Y., Ohtsuka, Y., Sen, R., Suzuki, S. & Achiba, Y. Diameter control of single-walled carbon nanotubes. *Carbon* **38**, 1691–1697 (2000).
201. Kataura, H., Kumazawa, Y., Maniwa, Y., Umezu, I., Suzuki, S., Ohtsuka, Y. & Achiba, Y. Optical properties of single-wall carbon nanotubes. *Synth. Met.* **103**, 2555–2558 (1999).
202. Kavan, L., Ho Yum, J. & Gratzel, M. Optically transparent cathode for dye-sensitized solar cells based on graphene nanoplatelets. *ACS Nano*, **5**, 165–172 (2011).
203. Kawase, T., Shimoda, T., Newsome, C., Sirringhaus, H. & Friend, R. H. Inkjet printing of polymer thin film transistors. *Thin Solid Films* **438–439**, 279–287 (2003).
204. Kawase, T., Sirringhaus, H., Friend, R. H. & Shimoda, T. Inkjet printed via-hole interconnections and resistors for all-polymer transistor circuits. *Adv. Mater.* **13**, 1601–1605 (2001).
205. Kazaoui, S., Minami, N., Nalini, B., Kim, Y. & Hara, K. Near-infrared photoconductive and photovoltaic devices using single-wall carbon nanotubes in conductive polymer films. *J. Appl. Phys.* **98**, 084314 (2005).
206. Kazaoui, S., Minami, N., Nalini, B., Kim, Y., Takada, N. & Hara, K. Near-infrared electroluminescent devices using single-wall carbon nanotubes thin flms. *Appl. Phys. Lett.* **87**, 211914 (2005).
207. Kazaoui, S., Minami, N., Yamawaki, H., Aoki, K., Kataura, H. & Achiba, Y. Pressure dependence of the optical absorption spectra of single-walled carbon nanotube films. *Phys. Rev. B* **62**, 1643 (2000).
208. Kelleher, E. J. R., Travers, J. C., Sun, Z., Ferrari, A. C., Golant, K. M., Popov, S. V. & Taylor, J. R. Bismuth fiber integrated laser mode-locked by carbon nanotubes. *Laser Phys. Lett.* **7**, 790–794 (2010).
209. Kelleher, E. J. R., Travers, J. C., Ippen, E. P., Sun, Z., Ferrari, A. C., Popov, S. V. & Taylor, J. R. Generation and direct measurement of giant chirp in a passively mode-locked laser. *Opt. Lett.* **34**, 3526–3528 (2009).

210. Kelleher, E. J. R., Travers, J. C., Sun, Z., Rozhin, A. G., Ferrari, A. C., Popov, S. V. & Taylor, J. R. Nanosecond-pulse fiber lasers mode-locked with nanotubes. *Appl. Phys. Lett.* **95**, 111108 (2009).
211. Keller, U. Recent developments in compact ultrafast lasers. *Nature* **424**, 831–838 (2003).
212. Keller, U. In *Ultrafast solid-state lasers,* Vol. 46 (Ed.: Wolf, E.), Elsevier, 2004.
213. Keller, U., Miller, D. A. B., Boyd, G. D., Chiu, T. H., Ferguson, J. F. & Asom, M. T. Solidstate low-loss intracavity saturable absorber for Nd:YLF lasers: An antiresonant semiconductor Fabry – Perot saturable absorber. *Opt. Lett.* **17**, 505–507 (1992).
214. Keller, U. & Tropper, A. C. Passively modelocked surface-emitting semiconductor lasers. *Phys. Rep.* **429**, 67–120 (2006).
215. Keller, U., Weingarten, K. J., Kartner, F. X., Kopf, D., Braun, B., Jung, I. D., Fluck, R., Hönninger, C., Matuschek, N. & Aus der Au, J. Semiconductor Saturable Absorber Mirrors (SESAM's) for Femtosecond to Nanosecond pulse generation in solid-state lasers. *IEEE J. Sel. Top. Quant. Electron.* **2**, 435–453 (1996).
216. Kennedy, J. W., Vardeny, Z. V., Collins, S., Baughman, R. H., Zhao, H. & Mazumdar, S. Electroabsorption spectroscopy of single walled nanotubes. *arXiv:cond-mat/0505071v1* (2005).
217. Kohn, W. Image of the Fermi surface in the vibration spectrum of a metal. *Phys. Rev. Lett* **2**, 393 (1959).
218. Khoo, I. C., Ding, J., Zhang, Y., Chen, K. & Diaz, A. Supra-nonlinear photorefractive response of single-walled carbon nanotube- and C60-doped nematic liquid crystal. *Appl. Phys. Lett.* **82**, 3587–3589 (2003).
219. Khudyakov, D. V., Lobach, A. S. & Nadtochenko, V. A. Passive mode locking in a Ti:sapphire laser using a single-walled carbon nanotube saturable absorber at a wavelength of 810 nm. *Opt. Lett.* **35**, 2675–2677 (2010).
220. Kieu, K. & Mansuripur, M. Femtosecond laser pulse generation with a fiber taper embedded in carbon nanotube/polymer composite. *Opt. Lett.* **32**, 2242–2244 (2007).
221. Kilbride, B. E., Coleman, J. N., Fraysse, J., Fournet, P., Cadek, M., Drury, A., Hutzler, S., Roth, S. & Blau, W. J. Experimental observation of scaling laws for alternating current and direct current conductivity in polymer-carbon nanotube composite thin films. *J. Appl. Phys.* **92**, 4024–4030 (2002).
222. Kim, D. S., Nepal, D. & Geckeler, K. E. Individualization of single-walled carbon nanotubes: Is the solvent important? *Small* **1**, 1117–1124 (2005).
223. Kim, K. S., Zhao, Y., Jang, H., Lee, S. Y., Kim, J. M., Kim, K. S., Ahn, J. H., Kim, P., Choi, J. Y. & Hong, B. H. Large-scale pattern growth of graphene films for stretchable transparent electrodes. *Nature* **457**, 706–710 (2009).
224. Kim, Y., Minami, N. & Kazaoui, S. Highly polarized absorption and photoluminescence of stretch-aligned single-wall carbon nanotubes dispersed in gelatin films. *Appl. Phys. Lett.* **86**, 073103 (2005).
225. Kim, Y., Minami, N., Zhu, W., Kazaoui, S., Azumi, R. & Matsumoto, M. Langmuir-Blodgett films of single-wall carbon nanotubes: Layer-by-layer deposition and in-plane orientation of tubes. *Jpn. J. Appl. Phys.* **42**, 7629–7634 (2003).
226. Kiowski, O., Lebedkin, S., Hennrich, F. & Kappes, M. M. Single-walled carbon nanotubes show stable emission and simple photoluminescence spectra with weak excitation sidebands at cryogenic temperatures. *Phys. Rev. B* **76**, 075422 (2007).
227. Kiowski, O., Lebedkin, S., Hennrich, F., Malik, S., Rösner, H., Arnold, K., Sürgers, C. & Kappes, M. M. Photoluminescence microscopy of carbon nanotubes grown by chemical vapor deposition: Influence of external dielectric screening on optical transition energies. *Phys. Rev. B* **75**, 075421 (2007).
228. Kirschner, M. W. & Schachman, H. K. Conformational changes in proteins as measured by difference sedimentation studies. II. Effect of stereospecific ligands on the catalytic subunit of aspartate transcarbamylase. *Biochemistry* **10**, 1919–1926 (1971).

229. Kis, A., Csanyi, G., Salvetat, J. P., Lee, T.-N., Couteau, E., Kulik, A. J., Benoit, W., Brugger, J. & Forro, L. Reinforcement of single-walled carbon nanotube bundles by intertube bridging. *Nat. Mater.* **3**, 153–157 (2004).
230. Kono, J., Ostojic, G. N., Zaric, S., Strano, M. S., Moore, V. C., Shaver, J., Hauge, R. H. & Smalley, R. E. Ultra-fast optical spectroscopy of micelle-suspended single-walled carbon nanotubes. *Appl. Phys. A* **78**, 1093–1098 (2004).
231. Koo, H. S., Chen, M., Pan, P. C., Chou, L. T., Wu, F. M., Chang, S. J. & Kawai, T. Fabrication and chromatic characteristics of the greenish LCD colour-filter layer with nano-particle ink using inkjet printing technique. *Displays* **27**, 124–129 (2006).
232. Koo, B.-K., Lee, D.-Y., Kim, H.-J., Lee, W.-J., Song, J.-S. & Kim, H.-J. Seasoning effect of dye-sensitized solar cells with different counter electrodes. *J. Electroceram.* **17**, 79–82 (2006).
233. Kordas, K., Mustonen, T., Toth, G., Jantunen, H., Lajunen, M., Soldano, C., Talapatra, S., Kar, S., Vajtai, R. & Ajayan, Pulickel M. Inkjet printing of electrically conductive patterns of carbon nanotubes. *Small* **2**, 1021–1025 (2006).
234. Kravets, V. G., Grigorenko, A. N., Nair, R. R., Blake, P., Anissimova, S., Novoselov, K. S. & Geim, A. K. Spectroscopic ellipsometry of graphene and an exciton-shifted van Hove peak in absorption. *Phys. Rev. B* **81**, 155413 (2010).
235. Krupke, R., Hennrich, F., von Lohneysen, H. & Kappes, M. M. Separation of metallic from semiconducting single-walled carbon nanotubes. *Science* **301**, 344–347 (2003).
236. Krupke, R., Hennrich, F., Hampe, O. & Kappes, M. M. Near-infrared absorbance of single-walled carbon nanotubes dispersed in dimethylformamide. *J. Phys. Chem. B* **107**, 5667–5669 (2003).
237. Kumar, S., Dang, T. D., Arnold, F. E., Bhattacharyya, A. R., Min, B. G., Zhang, X., Vaia, R. A., Park, C., Adams, W. W., Hauge, R. H., Smalley, R. E., Ramesh, R. & Willis, P. A. Synthesis, structure, and properties of PBO/SWNT composites. *Macromolecules* **35**, 9039–9043 (2002).
238. Kurti, J., Kresse, G. & Kuzmany, H. First-principles calculations of the radial breathing mode of single-wall carbon nanotubes. *Phys. Rev. B* **58**, R8869–R8872 (1998).
239. Kwon, Y.-K., Saito, S. & Tomanek, D. Effect of intertube coupling on the electronic structure of carbon nanotube ropes. *Phys. Rev. B* **58**, R13314–R13317 (1998).
240. Kymakis, E., Alexandrou, I. & Amaratunga, G. A. J. High open-circuit voltage photovoltaic devices from carbon-nanotube-polymer composites. *J. Appl. Phys.* **93**, 1764–1768 (2003).
241. Kymakis, E. & Amaratunga, G. A. J. Single-wall carbon nanotube/conjugated polymer photovoltaic devices. *Appl. Phys. Lett.* **80**, 112–114 (2002).
242. Labban, A. S. & Marcus, Y. Solvatochromic parameters of ethanolamines. *J. Chem. Soc. Faraday Trans.* **93**, 77–79 (1997).
243. Lagerwall, J. P. F., Scalia, G., Haluska, M., Dettlaff-Weglikowska, U., Giesselmann, F. & Roth, S. Simultaneous alignment and dispersion of carbon nanotubes with lyotropic liquid crystals. *Phys. Stat. Sol. (b)* **243**, 3046–3049 (2006).
244. Lagerwall, J. P. F., Scalia, G., Haluska, M., Dettlaff-Weglikowska, U., Roth, S. & Giesselmann, F. Nanotube alignment using lyotropic liquid crystals. *Adv. Mater.* **19**, 359–364 (2007).
245. Landi, B. J., Ruf, H. J., Worman, J. J. & Raffaelle, R. P. Effects of alkyl amide solvents on the dispersion of single-wall carbon nanotubes. *J. Phys. Chem. B* **108**, 17089–17095 (2004).
246. Lauret, J. S., Voisin, C., Cassabois, G., Delalande, C., Roussignol, P., Jost, O. & Capes, L. Ultrafast carrier dynamics in single-wall carbon nanotubes. *Phys. Rev. Lett.* **90**, 057404 (2003).
247. Lazzeri, M., Piscanec, S., Mauri, F., Ferrari, A. C. & Robertson, J. Phonon linewidths and electron-phonon coupling in graphite and nanotubes. *Phys. Rev. B* **73**, 155426 (2006).
248. Lebedkin, S., Hennrich, F., Kiowski, O. & Kappes, M. M. Photophysics of carbon nanotubes in organic polymer-toluene dispersions: Emission and excitation satellites and relaxation pathways. *Phys. Rev. B* **77**, 165429 (2008).

249. Lebedkin, S., Schweiss, P., Renker, B., Malik, S., Hennrich, F., Neumaier, M., Stoermer, C. & Kappes, M. M. Single-wall carbon nanotubes with diameters approaching 6 nm obtained by laser vaporization. *Carbon* **40**, 417–423 (2002).
250. Lee, J. Y., Connor, S. T., Cui, Y. & Peumans, P. Solution-processed metal nanowire mesh transparent electrodes. *Nano Lett.* **8**, 689–692 (2008).
251. Lee, W. & Chiu, C.-S. Observation of self-diffraction by gratings in nematic liquid crystals doped with carbon nanotubes. *Opt. Lett.* **26**, 521–523 (2001).
252. Lee, W., Gau, J.-S. & Chen, H.-Y. Electro-optical properties of planar nematic cells impregnated with carbon nanosolids. *Appl. Phys. B* **81**, 171–175 (2005).
253. Lee, W., Wang, C.-Y. & Shih, Y.-C. Effects of carbon nanosolids on the electro-optical properties of a twisted nematic liquid-crystal host. *Appl. Phys. Lett.* **85**, 513–515 (2004).
254. Lee, Y.-S., Buongiorno Nardelli, M. & Marzari, N. Band structure and quantum conductance of nanostructures from maximally localized wannier functions: The case of functionalized carbon nanotubes. *Phys. Rev. Lett.* **95**, 076804 (2005).
255. Lefebvre, J. & Finnie, P. Polarized photoluminescence excitation spectroscopy of single-walled carbon nanotubes. *Phys. Rev. Lett.* **98**, 167406 (2007).
256. Lefebvre, J., Fraser, J. M., Finnie, P. & Homma, Y. Photoluminescence from an individual single-walled carbon nanotube. *Phys. Rev. B* **69**, 075403 (2004).
257. Lefebvre, J., Fraser, J. M., Homma, Y. & Finnie, P. Photoluminescence from single walled carbon nanotubes: A comparison between suspended and micelle-encapsulated nanotubes. *Appl. Phys. A* **78**, 1107–1110 (2004).
258. Lefebvre, J., Homma, Y. & Finnie, P. Bright band gap photoluminescence from unprocessed single-walled carbon nanotubes. *Phys. Rev. Lett.* **90**, 217401 (2003).
259. Heller, D. A., Mayrhofer, R. M., Baik, S., Grinkova, Y. V., Usrey, M. L. & Strano, M. S. Concomitant Length and Diameter Separation of Single-Walled Carbon Nanotubes. *J. Am. Chem. Soc.* **126**, 14567–14573 (2004).
260. Li, C., Chen, Y., Wang, Y., I., Z., Chhowalla, M. & Mitra, S. A fullerene-single wall carbon nanotube complex for polymer bulk heterojunction photovoltaic cells. *J. Mater. Chem.* **17**, 2406–2411 (2007).
261. Li, F., Cheng, H. M., Bai, S., Su, G. & Dresselhaus, M. S. Tensile strength of single-walled carbon nanotubes directly measured from their macroscopic ropes. *Appl. Phys. Lett.* **77**, 3161–3163 (2000).
262. Li, Y.-L., Kinloch, I. A. & Windle, A. H. Direct spinning of carbon nanotube fibers from chemical vapor deposition synthesis. *Science* **304**, 276–278 (2004).
263. Li, Z. M., Tang, Z. K., Liu, H. J., Wang, N., Chan, C. T., Saito, R., Okada, S., Li, G. D., Chen, J. S., Nagasawa, N. & Tsuda, S. Polarized absorption spectra of single-walled 4 angstrom carbon nanotubes aligned in channels of an AlPO4-5 single crystal. *Phys. Rev. Lett.* **8712**, 127401 (2001).
264. Li, X. L., Zhang, G. Y., Bai, X. D., Sun, X. M., Wang, X. R., Wang, E. & Dai, H. J. Highly conducting graphene sheets and Langmuir-Blodgett films. *Nat. Nano* **3**, 538–542 (2008).
265. Lin, M. F. Optical spectra of single-wall carbon nanotube bundles. *Phys. Rev. B* **62**, 13153–13159 (2000).
266. Lin, M. F. & Chuu, D. S. π plasmons in carbon nanotube bundles. *Phys. Rev. B* **57**, 10183–10187 (1998).
267. Liu, P. Modifications of carbon nanotubes with polymers. *Eur. Polym. J.* **41**, 2693–2703 (2005).
268. Liu, X., Si, J., Chang, B., Xu, G., Yang, Q., Pan, Z., Xie, S., Ye, P., Fan, J. & Wan, M. Thirdorder optical nonlinearity of the carbon nanotubes. *Appl. Phys. Lett.* **74**, 164–166 (1999).
269. Liu, Z., Liu, Q., Huang, Y., Ma, Y., Yin, S., Zhang, X., Sun, W. & Chen, Y. Organic photovoltaic devices based on a novel acceptor material: Graphene. *Adv. Mater.* **20**, 3924–3930 (2008).
270. Lopez, M. J., Rubio, A., Alonso, J. A., Qin, L. C. & Iijima, S. Novel polygonized single-wall carbon nanotube bundles. *Phys. Rev. Lett.* **86**, 3056 (2001).

271. Lotya, M., Hernandez, Y., King, P. J., Smith, R. J., Nicolosi, V., Karlsson, L. S., Blighe, F. M., De, S., Wang, Z., McGovern, I. T., Duesberg, G. S. & Coleman, J. N. Liquid phase production of graphene by exfoliation of graphite in surfactant/water solutions. *J. Am. Chem. Soc.* **131**, 3611–3620 (2009).
272. Lu, J., Nagase, S., Zhang, X. W., Wang, D., Ni, M., Maeda, Y., Wakahara, T., Nakahodo, T., Tsuchiya, T., Akasaka, T., Gao, Z. X., Yu, D. P., Ye, H. Q., Mei, W. N. & Zhou, Y. S. Selective interaction of large or charge-transfer aromatic molecules with metallic single-wall carbon nanotubes: Critical role of the molecular size and orientation. *J. Am. Chem. Soc.* **128**, 5114–5118 (2006).
273. Lu, J. P. Elastic properties of carbon nanotubes and nanoropes. *Phys. Rev. Lett.* **79**, 1297 (1997).
274. Luo, Z., Zhou, M., Weng, J., Huang, G., Xu, H., Ye, C. & Cai, Z. Graphene-based passively Q-switched dual-wavelength erbium-doped fiber laser. *Opt. Lett.* **35**, 3709–3711 (2010).
275. Lyklema, J. The surface tension of pure liquids: Thermodynamic components and corresponding states. *Colloids Surf. A* **156**, 413–421 (1999).
276. Lynch, M. D. & Patrick, D. L. Organizing carbon nanotubes with liquid crystals. *Nano Lett.* **2**, 1197–1201 (2002).
277. Ma, H, Jen, A. K.-H. & Dalton, A. R. Polymer-based optical waveguides: Materials, processing and devices. *Adv. Mater.* **14**, 1339–1365 (2002).
278. Maeda, A., Matsumoto, S., Kishda, H., Takenobu, T., Iwasa, Y., Shraishi, M., Ata, M. & Okamoto, H. Large optical nonlinearity of semiconducting single-walled carbon nanotubes under resonant excitations. *Phys. Rev. Lett.* **94**, 047404 (2005).
279. Maeda, Y., Kimura, S.-i., Hirashima, Y., Kanda, M., Lian, Y., Wakahara, T., Akasaka, T., Hasegawa, T., Tokumoto, H., Shimizu, T., Kataura, H., Miyauchi, Y., Maruyama, S., Kobayashi, K. & Nagase, S. Dispersion of single-walled carbon nanotube bundles in nonaqueous solution. *J. Phys. Chem. B* **108**, 18395–18397 (2004).
280. Mahan, G. D. Oscillations of a thin hollow cylinder: Carbon nanotubes. *Phys. Rev. B* **65**, 235402 (2002).
281. Mamedov, A. A., Kotov, N. A., Prato, M., Guldi, D. M., Wicksted, J. P. & Hirsch, A. Molecular design of strong single-wall carbon nanotube/polyelectrolyte multilayer composites. *Nat. Mater.* **1**, 190–194 (2002).
282. Mann, D., Kato, Y. K., Kinkhabwala, A., Pop, E., Cao, J., Wang, X., Zhang, L., Wang, Q., Guo, J. & Dai, H. Electrically driven thermal light emission from individual single-walled carbon nanotubes *Nat. Nano.* **2**, 32–38 (2007).
283. Manzoni, C., Gambetta, A., Menna, E., Meneghetti, M., Lanzani, G. & Cerullo, G. Intersubband exciton relaxation dynamics in single-walled carbon nanotubes. *Phys. Rev. Lett.* **94**, 207401 (2005).
284. Marago, O. M., Bonaccorso, F., Saija, R., Privitera, G., Gucciardi, P. G., Iati, M. A., Calogero, G., Jones, P. H., Borghese, F., Denti, P., Nicolosi, V. & Ferrari, A. C. Brownian motion of graphene. *ACS Nano* **4**, 7515–7523 (2010).
285. Marcus, Y. The properties of organic liquids that are relevant to their use as solvating solvents. *Chem. Soc. Rev.* **22**, 409–416 (1993).
286. Margulis, V. A. Theoretical estimations of third-order optical nonlinearities for semiconductor carbon nanotubes. *J. Phys. Condens. Mat.* **11**, 3065 (1999).
287. Margulis, V. A. & Sizikova, T. A. Theoretical study of third-order nonlinear optical response of semiconductor carbon nanotubes. *Physica B* **245**, 173–189 (1998).
288. Martinez, A., Fuse, K., Xu, B. & Yamashita, S. Optical deposition of graphene and carbon nanotubes in a fiber ferrule for passive mode-locked lasing. *Opt. Express* **18**, 23054–23061 (2010).
289. Kozinsky, B. & Marzari, N. Static dielectric properties of carbon nanotubes from firstprinciples. *Phys. Rev. Lett.* **96**, 166801-4 (2006).
290. Matyba, P., Yamaguchi, H., Eda, G., Chhowalla, M., Edman, L. & Robinson, N. D. Graphene and mobile ions: The key to all-plastic, solution-processed light-emitting devices. *ACS Nano* **4**, 637–642 (2010).

291. Maultzsch, J., Reich, S., Schlecht, U. & Thomsen, C. High-energy phonon branches of an individual metallic carbon nanotube. *Phys. Rev. Lett.* **91**, 087402 (2003).
292. Maultzsch, J., Reich, S., Thomsen, C., Requardt, H. & Ordejón, P. Phonon dispersion of graphite. *Phys. Rev. Lett.* **92**, 075501 (2004).
293. Maultzsch, J., Pomraenke, R., Reich, S., Chang, E., Prezzi, D., Ruini, A., Molinari, E., Strano, M. S., Thomsen, C. & Lienau, C. Exciton binding energies in carbon nanotubes from two-photon photoluminescence. *Phys. Rev. B* **72**, 241402(R) (2005).
294. Maultzsch, J., Telg, H., Reich, S. & Thomsen, C. Radial breathing mode of single-walled carbon nanotubes: Optical transition energies and chiral-index assignment. *Phys. Rev. B* **72**, 205438 (2005).
295. Mazer, N. A., Carey, M. C., Kwasnick, R. F. & Benedeck, G. B. Quasielastic light scattering studies of aqueous biliary lipid systems. Size, shape, and thermodynamics of bile salt micelles. *Biochemistry* **18**, 3064–3075 (1979).
296. McDonald, T. J., Engtrakul, C., Jones, M., Rumbles, G. & Heben, M. J. Kinetics of PL quenching during single-walled carbon nanotube rebundling and diameter-dependent surfactant interactions. *J. Phys. Chem. B* **110**, 25339 (2006).
297. Meyer, J. C., Paillet, M., Michel, T., Moreac, A., Neumann, A., Duesberg, G. S., Roth, S. & Sauvajol, J. L. Raman modes of index-identified freestanding single-walled carbon nanotubes. *Phys. Rev. Lett.* **95**, 217401 (2005).
298. Milnera, M., Kürti, J., Hulman, M. & Kuzmany, H. Periodic resonance excitation and intertube interaction from quasicontinuous distributed helicities in single-wall carbon nanotubes. *Phys. Rev. Lett.* **84**, 1324 (2000).
299. Minami, N., Kim, Y., Miyashita, K., Kazaoui, S. & Nalini, B. Cellulose derivatives as excellent dispersants for single-wall carbon nanotubes as demonstrated by absorption and photoluminescence spectroscopy. *Appl. Phys. Lett.* **88**, 093123 (2006).
300. Misewich, J. A., Martel, R., Avouris, Ph., Tsang, J. C., Heinze, S. & Tersoff, J. Electrically induced optical emission from a carbon nanotube FET. *Science* **300**, 783–786 (2003).
301. Miyajima, K. Correlation between the hydrophobic nature of monosaccharides and cholates, and their hydrophobic indices. *J. Chem. Soc. Faraday Trans.* **84**, 2537–2544 (1988).
302. Miyauchi, Y., Chiashi, S., Murakami, Y., Hayashida, Y. & Maruyama, S. Fluorescence spectroscopy of single-walled carbon nanotubes synthesized from alcohol. *Chem. Phys. Lett.* **387**, 198–203 (2004).
303. Miyauchi, Y. & Maruyama, S. Identification of an excitonic phonon sideband by photoluminescence spectroscopy of single-walled carbon-13 nanotubes. *Phys. Rev. B* **74**, 035415 (2006).
304. Miyauchi, Y., Oba, M. & Maruyama, S. Cross-polarized optical absorption of single-walled nanotubes by polarized photoluminescence excitation spectroscopy. *Phys. Rev. B* **74**, 205440 (2006).
305. Miyauchi, Y., Saito, R., Sato, K., Ohno, Y., Iwasaki, S., Mizutani, T., Jiang, J. & Maruyama, S. Dependence of exciton transition energy of single-walled carbon nanotubes on surrounding dielectric materials. *Chem. Phys. Lett.* **442**, 394–399 (2007).
306. Mohiuddin, T. M. G., Lombardo, A., Nair, R. R., Bonetti, A., Savini, G., Jalil, R., Bonini, N., Basko, D. M., Galiotis, C., Marzari, N., Novoselov, K. S., Geim, A. K. & Ferrari, A. C. *Phys. Rev. B* **79**, 205433 (2009).
307. Moniruzzaman, M. & Winey, K. I. Polymer nanocomposites containing carbon nanotubes. *Macromolecules* **39**, 5194–5205 (2006).
308. Moore, V. C., Strano, M. S., Haroz, E. H., Hauge, R. H. & Smalley, R. E. Individually suspended single-walled carbon nanotubes in various surfactants. *Nano Lett.* **3**, 1379–1382 (2003).
309. Murakami, Y., Einarsson, E., Edamura, T. & Maruyama, S. Polarization dependence of the optical absorption of single-walled carbon nanotubes. *Phys. Rev. Lett.* **94**, 087402 (2005).
310. Nakazawa, M., Nakahara, S., Hirooka, T., Yoshida, M., Kaino, T. & Komatsu, K. Polymer saturable absorber materials in the 1.5 mm band using poly-methyl-methacrylate and

polystyrene with single-wall carbon nanotubes and their application to a femtosecond laser. *Opt. Lett.* **31**, 915–917 (2006).
311. Nair, R. R., Blake, P., Grigorenko, A. N., Novoselov, K. S., Booth, T. J., Stauber, T., Peres, N. M. R. & Geim, A. K. Fine structure constant defines visual transparency of graphene. *Science* **320**, 1308 (2008).
312. Nemanich, R. J. & Solin, S. A. First- and second-order Raman scattering from finite-size crystals of graphite. *Phys. Rev. B* **20**, 392 (1979).
313. Newell, J. O. & Schachman, H. K. Amino acid substitution which stabilize aspirate transcarbamoylase in the R state disrupt both homotropic and heterotropic effects. *Biophys. Chem.* **37**, 183–196 (1960).
314. Ng, Y. H., Lightcap, I. V., Goodwin, K., Matsumura, M. & Kamat, P. V. To what extent do graphene Scaffolds improve the photovoltaic and photocatalytic response of TiO2 nanostructured films? *J. Phys. Chem. Lett.* **1**, 2222–2227 (2010).
315. Nguyen, B. T., Gautrot, J. E., Nguyen, M. T. & Zhu, X. X. Nitrocellulose-stabilized silver nanoparticles as low conversion temperature precursors useful for inkjet printed electronics. *J. Mater. Chem.* **17**, 1725–1730 (2007).
316. Niyogi, S., Boukhalfa, S., Chikkannanavar, S. B., Mcdonald, T. J., Heben, M. J. & Doorn, S. K. Selective aggregation of single-walled carbon nanotubes via salt addition. *J. Am. Chem. Soc.* **129**, 1898 (2007).
317. Niyogi, S., Hamon, M. A., Hu, H., Zhao, B., Bhowmik, P., Sen, R., Itkis, M. E. & Haddon, R. C. Chemistry of single-walled carbon nanotubes. *Acc. Chem. Res.* **35**, 1105 (2002).
318. Noh, Y. Y., Zhao, N., Caironi, M. & Sirringhaus, H. Downscaling of self-aligned, all-printed polymer thin-film transistors. *Nat. Nanotech.* **2**, 784–789 (2007).
319. O'Connell, M. J., Bachilo, S. M., Huffman, C. B., Moore, V. C., Strano, M. S., Haroz, E. H., Rialon, K. L., Boul, P. J., Noon, W. H., Kittrell, C., Ma, J., Hauge, R. H., Weisman, R. B. & Smalley, R. E. Band gap fluorescence from individual single-walled carbon nanotubes. *Science* **297**, 593–596 (2002).
320. O'Connell, M. J., Boul, P., Ericson, L. M., Huffman, C., Wang, Y., Haroz, E., Kuper, C., Tour, J., Ausman, K. D. & Smalley, R. E. Reversible water-solubilization of single-walled carbon nanotubes by polymer wrapping. *Chem. Phys. Lett.* **342**, 265–271 (2001).
321. O'Connell, M. J., Sivaram, S. & Doorn, S. K. Near-infrared resonance Raman excitation profile studies of single-walled carbon nanotube intertube interactions: A direct comparison of bundled and individually dispersed HiPco nanotubes. *Phys. Rev. B* **69**, 235415 (2004).
322. O'Flaherty, S. A., Murphy, R., Hold, S. V., Cadek, M., Coleman, J. N. & Blau, W. J. Material investigation and optical limiting properties of carbon nanotube and nanoparticle dispersions. *J. Phys. Chem. B* **107**, 958–964 (2003).
323. Okazaki, T., Saito, T., Matsuura, K., Ohshima, S., Yumura, M., Oyama, Y., Saito, R. & Iijima, S. Photoluminescence and population analysis of single-walled carbon nanotubes produced by CVD and pulsed-laser vaporization methods. *Chem. Phys. Lett.* **420**, 286–290 (2006).
324. Okazaki, T., Saito, T., Matsuura, K., Ohshima, S., Yumura, M. & Iijima, S. Photoluminescence mapping of "As-Grown" single-walled carbon nanotubes: A comparison with Micelle-encapsulated nanotube solutions. *Nano Lett.* **5**, 2618–2623 (2005).
325. Okhotnikov, O., Grudinin, A. & Pessa, M. Ultra-fast fibre laser systems based on SESAM technology: New horizons and applications. *New J. Phys.* **6**, 177 (2004).
326. Okimoto, H., Takenobu, T., Yanagi, K., Miyata, Y., Shimotani, H., Kataura, H. & Iwasa, Y. Tunable carbon nanotube thin-film transistors produced exclusively via inkjet printing. *Adv. Mater.* **22**, 3981–3986 (2010).
327. Olek, M., Ostrander, J., Jurga, S., Möhwald, H., Kotov, N., Kempa, K. & Giersig, M. Layerby-layer assembled composites from multiwall carbon nanotubes with different morphologies. *Nano Lett.* **4**, 1889–1895 (2004).
328. O'Regan, B. & Gratzel, M. A low-cost, high-efficiency solar cell based on dye-sensitized colloidal TiO2 films. *Nature*, **353**, 737–740 (1991).

329. Ostojic, G. N., Zaric, S., Kono, J., Strano, M. S., Moore, V. C., Hauge, R. H. & Smalley, R. E. Interband recombination dynamics in resonantly excited single-walled carbon nanotubes. *Phys. Rev. Lett.* **92**, 117402 (2004).
330. Oyama, Y., Saito, R., Sato, K., Jiang, J., Samsonidze, G. G., Gruneis, A., Miyauchi, Y., Maruyama, S., Jorio, A., Dresselhaus, G. & Dresselhaus, M. S. Photoluminescence intensity of single-wall carbon nanotubes. *Carbon* **44**, 873–879 (2006).
331. Park, C., Ounaies, Z., Watson, K. A., Crooks, R. E., Smith, J., Lowther, S. E., Connell, J. W., Siochi, E. J., Harrison, J. S. & Clair, T. L. S. Dispersion of single wall carbon nanotubes by in situ polymerization under sonication. *Chem. Phys. Lett.* **364**, 303–308 (2002).
332. Park, S. & Ruoff, R. S. Chemical methods for the production of graphenes. *Nat. Nano* **4**, 217–224 (2009).
333. Pasquier, A.-Du, Unalan, H. E., Kanwal, A., Miller, S. & Chhowalla, M. Conducting and transparent single-wall carbon nanotube electrodes for polymer-fullerene solar cells. *Appl. Phys. Lett.* **87**, 203511-3 (2005).
334. Perebeinos, V. & Avouris, P. Exciton ionization, Franz-Keldysh, and Stark effects in carbon nanotubes. *Nano Lett.* **7**, 609–613 (2007).
335. Perebeinos, V., Tersoff, J. & Avouris, P. Scaling of excitons in carbon nanotubes. *Phys. Rev. Lett.* **92**, 257402 (2004).
336. Peumans, P., Uchida, S. & Forrest, S. R. Efficient bulk heterojunction photovoltaic cells using small-molecular-weight organic thin films. *Nature* **425**, 158–162 (2003).
337. Pickels, E. G. & Smadel, J. E. Ultracentrifugation studies on the elementary bodies of vaccine virues: I. General methods and determination of particle size *J. Exp. Med.* **68**, 583–606 (1938).
338. Pimenta, M. A., Marucci, A., Empedocles, S. A., Bawendi, M. G., Hanlon, E. B., Rao, A. M., Eklund, P. C., Smalley, R. E., Dresselhaus, G. & Dresselhaus, M. S. Raman modes of metallic carbon nanotubes. *Phys. Rev. B* **58**, 16016 (1998).
339. Pisana, S., Lazzeri, M., Casiraghi, C., Novoselov, K. S., Geim, A. K., Ferrari, A. C. & Mauri, F. Breakdown of the adiabatic Born-Oppenheimer approximation in graphene. *Nat. Mater.* **6**, 198 (2007).
340. Piscanec, S., Lazzeri, M., Mauri, F., Ferrari, A. C. & Robertson, J. Kohn anomalies and electron-phonon interactions in graphite. *Phys. Rev. Lett.* **93**, 185503 (2004).
341. Piscanec, S., Lazzeri, M., Robertson, J., Ferrari, A. C. & Mauri, F. Optical phonons in carbon nanotubes: Kohn anomalies, Peierls distortions, and dynamic effects. *Phys. Rev. B* **75**, 035427 (2007).
342. Plentz, F., Ribeiro, H. B., Jorio, A., Strano, M. S. & Pimenta, M. A. Direct experimental evidence of exciton-phonon bound states in carbon nanotubes. *Phys. Rev. Lett.* **95**, 247401 (2005).
343. Pocsik, I., Hundhausen, M., Koos, M. & Ley, L. Origin of the D peak in the Raman spectrum of microcrystalline graphite. *J. Non-cryst. Solids* **230**, 1083–1086 (1998).
344. Popa, D., Sun, Z., Torrisi, F., Hasan, T., Wang, F. & Ferrari, A. C. Sub 200 fs pulse generation from a graphene mode-locked fiber laser. *Appl. Phys. Lett.* **97**, 203106-3 (2010).
345. Popa, D., Sun, Z., Hasan, T., Torrisi, F., Wang, F. & Ferrari, A. C. Graphene Q-switched, tunable fiber laser. *Appl. Phys. Lett.* **98**, 073106-3 (2011).
346. Popov, V. N., Van Doren, V. E. & Balkanski, M. Lattice dynamics of single-walled carbon nanotubes. *Phys. Rev. B* **59**, 8355–8358 (1999).
347. Pradhan, B., Batabyal, S. K. & Pal, A. J. Functionalized carbon nanotubes in donor/acceptortype photovoltaic devices. *Appl. Phys. Lett.* **88**, 093106 (2006).
348. Priya, B. R. & Byrne, H. J. Investigation of sodium dodecyl benzene sulfonate assisted dispersion and debundling of single-wall carbon nanotubes. *J. Phys. Chem. C* **112**, 332–337 (2008).
349. Qu, L., Lin, Y., Hill, D. E., Zhou, B., Wang, W., Sun, X., Kitaygorodskiy, A., Suarez, M., Connell, J. W., Allard, L. F. & Sun, Y.-P. Polyimide-functionalized carbon nanotubes: Synthesis and dispersion in nanocomposite films. *Macromolecules* **37**, 6055–6060 (2004).

350. Rao, A. M., Richter, E., Bandow, S., Chase, B., Eklund, P. C., Williams, K. A., Fang, S., Subbaswamy, K. R., Menon, M., Thess, A., Smalley, R. E., Dresselhaus, G. & Dresselhaus, M. S. Diameter-selective Raman scattering from vibrational modes in carbon nanotubes. *Science* **275**, 187–191 (1997).
351. Reich, S., Dworzac, M., Hoffmann, A., Thomsen, C. & Strano, M. S. Excited-state carrier lifetime in single-walled carbon nanotubes. *Phys. Rev. B* **71**, 033402 (2005).
352. Reich, S., Thomsen, C. & Ordejón, P. Electronic band structure of isolated and bundled carbon nanotubes. *Phys. Rev. B* **65**, 155411 (2002).
353. Reich, S., Thomsen, C. & Robertson, J. Exciton resonances Quench the photoluminescence of zigzag carbon nanotubes. *Phys. Rev. Lett.* **95**, 077402-4 (2005).
354. Riddik, J. A., Bunger, W. B. & Sakano, T. K. *Organic solvents, physical properties and methods of purification.* Wiley, New York (1986).
355. Rinzler, A. G., Liu, J., Dai, H., Nikolaev, P., Huffman, C. B., Rodríguez-Macías, F. J., Boul, P. J., Lu, A. H., Heymann, D., Colbert, D. T., Lee, R. S., Fischer, J. E., Rao, A. M., Eklund, P. C. & Smalley, R. E. Large-scale purification of single-wall carbon nanotubes: Process, product, and characterization. *Appl. Phys. A* **67**, 29 (1998).
356. Roda, A., Hofmann, A. F. & Mysels, K. J. The influence of bile salt structure on selfassociation in aqueous solutions. *J. Bio. Chem.* **258**, 6362 (1983).
357. Rozhin, A. G., Sakakibara, Y., Kataura, H., Matsuzaki, S., Ishida, K., Achiba, Y. & Tokumoto, M. Anisotropic saturable absorption of single-wall carbon nanotubes aligned in polyvinyl alcohol. *Chem. Phys. Lett.* **405**, 288–293 (2005).
358. Rozhin, A. G., Sakakibara, Y., Namiki, S., Tokumoto, M. & Kataura, H. Sub-200-fs pulsed erbium-doped fiber laser using a carbon nanotube-polyvinylalcohol mode locker. *Appl. Phys. Lett.* **88**, 051118 (2006).
359. Rozhin, A. G., Sakakibara, Y., Tokumoto, M., Kataura, H. & Achiba, Y. Near-infrared nonlinear optical properties of single-wall carbon nanotubes embedded in polymer film. *Thin Solid Films* **464–465**, 368–372 (2004).
360. Rozhin, A. G., Scardaci, V., Wang, F., Hennrich, F., White, I. H., Milne, W. I. & Ferrari, A. C. Generation of ultra-fast laser pulses using nanotube mode-lockers. *Phys. Stat. Sol. (b)* **243**, 3551 (2006).
361. Sackett, D. L. & Lippoldt, R. E. Thermodynamics of reversible monomer-dimer association of tubulin. *Biochemistry* **30**, 3511–3517 (1991).
362. Sakakibara, Y., Kintaka, K., Rozhin, A. G., ltatani, T., Soe, W. M., ltatani, H., Tokumoto, M. & Kataura, H. Optically uniform carbon nanotube-polyimide nanocomposite: Application to 165 fs mode-locked fiber laser and waveguide, presented at *31st European Conference on Optical Communication*, Glasgow, Scotland (2005).
363. Sakakibara, Y., Rozhin, A. G., Kataura, H., Achiba, Y. & Tokumoto, H. Carbon nanotube-poly(vinylalcohol) nanocomposite film devices: Applications for femtosecond fiber laser mode lockers and optical amplifier noise suppressors. *Jpn. J. Appl. Phys.* **44**, 1621–1625 (2005).
364. Salvetat, J.-P., Briggs, G. A. D., Bonard, J.-M., Bacsa, R. i. R., Kulik, A. J., Stöckli, T., Burnham, N. A. & Forró, L. Elastic and shear moduli of single-walled carbon nanotube ropes. *Phys. Rev. Lett.* **82**, 944 (1999).
365. Sánchez-Portal, D., Artacho, E., Soler, J. M., Rubio, A. & Ordejón, P. Ab initio structural, elastic, and vibrational properties of carbon nanotubes. *Phys. Rev. B* **59**, 12678–12688 (1999).
366. Sariciftci, N. S., Smilowitz, L., Heeger, A. J. & Wudl, F. Photoinduced electron transfer from a conducting polymer to buckminsterfullerene. *Science* **258**, 1474–1476 (1992).
367. Sarukura, N., Ishida, Y., Yanagawa, T. & Nakano, H. All solid-state cw passively modelocked Ti:sapphire laser using a colored glass filter. *Appl. Phys. Lett.* **57**, 229–230 (1990).
368. Sasaki, Y., Igura, T., Miyassu, Y. I., Lee, S., Nagadome, S., Takiguchi, H. & Sugihara, G. The adsorption behavior of four bile salt species on graphite in water – Evaluation of effective hydrophobicity of bile acids. *Colloids Surf. B* **5**, 241–247 (1995).

369. Scalia, G., Lagerwall, J. P. F., Schymura, S., Haluska, M., Giesselmann, F. & Roth, S. Carbon nanotubes in liquid crystals as versatile functional materials. *Phys. Stat. Sol. (b)* **244**, 4212–4217 (2007).
370. Scardaci, V., Rozhin, A. G., Hennrich, F., Milne, W. I. & Ferrari, A. C. Carbon nanotube-polymer composites for photonic devices. *Physica E* **37**, 115 (2007).
371. Scardaci, V., Rozhin, A. G., Tan, P. H., Wang, F., White, I. H., Milne, W. I. & Ferrari, A. C. Carbon nanotubes for ultrafast photonics. *Phys. Stat. Sol. (b)* **244**, 4303–4307 (2007).
372. Scardaci, V., Sun, Z., Wang, F., Rozhin, A. G., Hasan, T., Hennrich, F., White, I. H., Milne, W. I. & Ferrari, A. C. Carbon nanotube-polycarbonate composites for ultrafast lasers. *Adv. Mater.* **20**, 4040 (2008).
373. Scardaci, V., Coull, R. & Coleman, J. N. Very thin transparent, conductive carbon nanotube films on flexible substrates *Appl. Phys. Lett.* **97**, 023114 (2010).
374. Schabel, M. C. & Martins, J. L. Energetics of interplanar binding in graphite. *Phys. Rev. B* **46**, 7185 (1992).
375. Schedin, F., Lidorikis, E., Lombardo, A., Kravets, V. G., Geim, A. K., Grigorenko, A. N., Novoselov K. S. & Ferrari A. C. Surface-enhanced Raman spectroscopy of graphene. *ACS Nano* **4**, 5617 (2010).
376. Schibli, T. R., Minoshima, K., Kataura, H., Itoga, E., Minami, N., Kazaoui, S., Miyashita, K., Tokumoto, M. & Sakakibara, Y. Ultrashort pulse-generation by saturable absorber mirrors based on polymer-embedded carbon nanotubes. *Opt. Express* **13**, 8025–8031 (2005).
377. Schmidt, A., Rivier, S., Cho, W. B., Yim, J. H., Choi, S. Y., Lee, S., Rotermund, F., Rytz, D., Steinmeyer, G., Petrov, V. & Griebner, U. Sub-100 fs single-walled carbon nanotube saturable absorber mode-locked Yb-laser operation near 1 μm. *Opt. Express* **17**, 20109–20116 (2009).
378. Senoo, Y., Nishizawa, N., Sakakibara, Y., Sumimura, K., Itoga, E., Kataura, H. & Itoh, K. Polarization-maintaining, high-energy, wavelength-tunable, Er-doped ultrashort pulse fiber laser using carbon-nanotube polyimide film. *Opt. Express* **17**, 20233–20241 (2009).
379. Set, S., Yaguchi, H., Jablonski, M., Tanaka, Y., Sakakibara, Y., Rozhin, A., Tokumoto, M., Kataura, H., Achiba, Y. & Kikuchi, K. A noise suppressing saturable absorber at 1550 nm based on carbon nanotube technology", presented at *Optical Fiber Communications Conference (OFC)*, Washington, DC (2003).
380. Set, S. Y., Yaguchi, H., Tanaka, Y. & Jablonski, M. Ultrafast fiber pulsed lasers incorporating carbon nanotubes. *IEEE J. Sel. Top. Quant. Electron.* **10**, 137–146 (2004).
381. Set, S. Y., Yaguchi, H., Tanaka, Y., Jablonski, M., Sakakibara, Y., Rozhin, A., Tokumoto, M., Kataura, H., Achiba, Y. & Kikuchi, K. Mode-locked fiber lasers based on a saturable absorber incorporating carbon nanotubes", presented at *Optical Fiber Communication Conference (OFC)*, Washington, DC (2003).
382. Shaffer, M. S. P. & Windle, A. H. Fabrication and characterization of carbon nanotube/poly(vinyl alcohol) composites. *Adv. Mater.* **11**, 937–941 (1999).
383. Sheik-Bahae, M., Said, A. A. & Van Stryland, E. W. High-sensitivity, single-beam n2 measurements. *Opt. Lett.* **14**, 955–957 (1989).
384. Shigeta, M., Komatsu, M. & Nakashima, N. Individual solubilization of single-walled carbon nanotubes using totally aromatic polyimide. *Chem. Phys. Lett.* **418**, 115–118 (2006).
385. Shimoda, H., Oh, S. J., Geng, H. Z., Walker, R. J., Zhang, X. B., McNeil, L. E. & Zhou, O. Self-assembly of carbon nanotubes. *Adv. Mater.* **14**, 899–901 (2002).
386. Shimoda, T., Morii, K., Seki, S. & Kiguchi, H. Inkjet printing of light-emitting polymer displays. *Mater. Res. Soc. Bull.* **28**, 821–827 (2003).
387. Shyu, F. L. & Lin, M. F. π plasmons in two-dimensional arrays of aligned carbon nanotubes. *Phys. Rev. B* **60**, 14434–14440 (1999).
388. Singh, M., Haverinen, H. M., Dhagat, P. & Jabbour, G. E. Inkjet printing–process and its applications. *Adv. Mater.* **22**, 673–685 (2010).
389. Sirringhaus, H., Kawase, T., Friend, R. H., Shimoda, T., Inbasekaran, M., Wu, W. & Woo, E. P. High-resolution inkjet printing of all-polymer transistor circuits. *Science* **290**, 2123–2126 (2000).

390. Smale, G. & Sasse, J. RNA isolation form cartilage using density gradient centrifugation in cesium trifluoroacetate: An RNA preparation technique effective in the presence of high proteoglycan content. *Anal. Biochem.* **203**, 352–356 (1992).
391. Small, D. M., Penkett, S. A. & Chapman, D. Studies on simple and mixed bile salt micelles by nuclear magnetic resonance spectroscopy. *Biochim. Biophys. Acta* **176**, 178–189 (1969).
392. Small, W. R. & Panhuis, M. In het Inkjet printing of transparent, electrically conducting single-walled carbon-nanotube composites. *Small* **3**, 1500–1503 (2007).
393. Smith, Peter W. Mode-locking of lasers. *Proc. IEEE* **58**, 1342–1357 (1970).
394. Solodyankin, M. A., Obraztsova, E. D., Lobach, A. S., Chernov, A. I., Tausenev, A. V., Konov, V. I. & Dianov, E. M. Mode-locked 1.93 μm thulium fiber laser with a carbon nanotube absorber. *Opt. Lett.* **33**, 1336–1338 (2008).
395. Song, Y.-W., Morimune, K., Set, S. Y. & Yamashita, S. Polarization insensitive all-fiber mode-lockers functioned by carbon nanotubes deposited onto tapered fibers. *Appl. Phys. Lett.* **90**, 021101 (2007).
396. Song, Y.-W. & Yamashita, S. Passively mode-locked lasers with 17.2-GHz fundamentalmode repetition rate pulsed by carbon nanotubes. *Opt. Lett.* **32**, 430–432 (2007).
397. Song, Y.-W., Yamashita, S., Einarsson, E. & Maruyama, S. All-fiber pulsed lasers passively mode locked by transferable vertically aligned carbon nanotube film. *Opt. Lett.* **32**, 1399–1401 (2007).
398. Song, Y.-W., Yamashita, S., Goh, C. S. & Set, S. Y. Carbon nanotube mode lockers with enhanced nonlinearity via evanescent field interaction in D-shaped fibers. *Opt. Lett.* **32**, 148–150 (2007).
399. Song, Y.-W., Yamashita, S. & Maruyama, S. Single-walled carbon nanotubes for high-energy optical pulse formation. *Appl. Phys. Lett.* **92**, 021115 (2008).
400. Song, Y.-W., Jang, S.-Y., Han, W.-S. & Bae, M.-K. Graphene mode-lockers for fiber lasers functioned with evanescent field interaction. *Appl. Phys. Lett.* **96**, 051122-3 (2010).
401. Song, Y. W., Set, S. Y., Yamashita, S., Goh, C. S. & Kotake, T. 1300-nm pulsed fiber lasers mode-locked by purified carbon nanotubes. *IEEE Photonics Technol. Lett.* **17**, 1623–1625 (2005).
402. Spataru, C. D., Ismail-Beigi, S., Benedict, L. X. & Louie, S. G. Excitonic effects and optical spectra of single-walled carbon nanotubes. *Phys. Rev. Lett.* **92**, 077402 (2004).
403. Star, A., Liu, Y., Grant, K., Ridvan, L., Stoddart, J. F., Steuerman, D. W., Diehl, M. R., Boukai, A. & Heath, J. R. Noncovalent side-wall functionalization of single-walled carbon nanotubes. *Macromolecules* **36**, 553–560 (2003).
404. Star, A. & Stoddart, J. F. Dispersion and solubilization of single-walled carbon nanotubes with a hyperbranched polymer. *Macromolecules* **35**, 7516–7520 (2002).
405. Star, A., Stoddart, J. F., Steuerman, D., Diehl, M., Boukai, A., Wong, E. W., Yang, X., Chung, S.-W., Choi, H. & Heath, J. R. Preparation and properties of polymer-wrapped single-walled carbon nanotubes. *Angew. Chem. Int. Ed.* **40**, 1721–1725 (2001).
406. Steuerman, D. W., Star, A., Narizzano, R., Choi, H., Ries, R. S., Nicolini, C., Stoddart, J. F. & Heath, J. R. Interactions between conjugated polymers and single-walled carbon nanotubes. *J. Phys. Chem. B* **106**, 3124–3130 (2002).
407. Stillemark, P., Boren, J., Andersson, M., Larsson, T., Rustaeus, S., Karlsson, K. A. & Olofsson, S. O. The assembly and secretion of apolipoprotein B-48-containing very low density lipoproteins in McA-RH7777 cells. *J. Biol. Chem.* **275**, 10506–10513 (2000).
408. Stutzmann, N., Friend, R. H. & Sirringhaus, H. Self-aligned, vertical-channel, polymer field-effect transistors. *Science* **299**, 1881–1884 (2003).
409. Sugihara, G., Shigematsu, D.-S., Nagadome, S., Lee, S., Sasaki, Y. & Igimi, H. Thermodynamic study on the langmuir adsorption of various bile salts including taurine and glycine conjugates onto graphite in water. *Langmuir* **16**, 1825–1833 (2000).
410. Sun, Y., Wu, Q. & Shi, G. Graphene based new energy materials. *Energy Environ. Sci.* doi:10.1039/C0EE00683A (2011).
411. Sun, Z., Hasan, T., Torrisi, F., Popa, D., Privitera, G., Wang, F., Bonaccorso, F., Basko, D. M. & Ferrari, A. C. Graphene mode-locked ultrafast laser. *ACS Nano* **4**, 803–810 (2010).

412. Sun, Z., Lin, X., Yu, H., Hasan, T., Torrisi, F., Zhang, L., Sun, L., Guo, L., Hou, W., Li, J. & Ferrari, A. C. High-power ultrafast solid-state laser using graphene based saturable absorber. In *The Conference on Lasers and Electro-Optics* (Baltimore, US), JWA79 (2010).
413. Sun, Z., Hasan, T., Wang, F., Rozhin, A., White, I. & Ferrari, A. Ultrafast stretched-pulse fiber laser mode-locked by carbon nanotubes. *Nano Res.* **3**, 404–411 (2010).
414. Sun, Z., Popa, D., Hasan, T., Torrisi, F., Wang, F., Kelleher, E. J. R., Travers, J. C., Nicolosi, V. & Ferrari, A. C. A Stable, wideband tunable, near transform-limited, graphene-mode-locked, ultrafast laser. *Nano Res.* **3**, 653–660 (2010).
415. Sun, Z., Rozhin, A. G., Wang, F., Scardaci, V., Milne, W. I., White, I. H., Hennrich & F. Ferrari, A. C. L-band ultrafast fiber laser mode locked by carbon nanotubes. *Appl. Phys. Lett.* **93**, 061114 (2008).
416. Sun, Z., Rozhin, A. G., Wang, F., Hasan, T., Popa, D., O'Neill, W. & Ferrari, A. C. A compact, high power, ultrafast laser mode-locked by carbon nanotubes. *Appl. Phys. Lett.* **95**, 253102 (2009).
417. Suzuki, K., Yamaguchi, M., Kumagai, M. & Yanagida, S. Application of carbon nanotubes to counter electrodes of dye-sensitized solar cells. *Chem. Lett.* **32**, 28–29 (2003).
418. Svedberg, T. & Pedersen, K. O. *The ultracentrifuge.* Clarendon Press, Oxford (1940).
419. Takenobu, T., Miura, N., Lu, S.-Y., Okimoto, H., Asano, T., Shiraishi, M. & Iwasa, Y. Ink-jet printing of carbon nanotube thin-film transistors on flexible plastic substrates. *Appl. Phys. Express* **2**, 025005 (2009).
420. Takahashi, T., Tsunoda, K., Yajima, H. & Ishii, T. Dispersion and purification of single-wall carbon nanotubes using carboxymethylcellulose. *Jpn. J. Appl. Phys.* **43**, 3636–3639 (2004).
421. Tan, P. H., Rozhin, A. G., Hasan, T., Hu, P., Scardaci, V., Milne, W. I. & Ferrari, A. C. Photoluminescence spectroscopy of carbon nanotube bundles: Evidence for exciton energy transfer. *Phys. Rev. Lett.* **99**, 137402 (2007).
422. Tan, P. H., Hasan, T., Bonaccorso, F., Scardaci, V., Rozhin, A. G., Milne, W. I. & Ferrari, A. C. Optical properties of nanotube bundles by photoluminescence excitation and absorption spectroscopy. *Physica E* **40**, 2352–2359 (2008).
423. Tan, Y. & Resasco, D. E. Dispersion of single-walled carbon nanotubes of narrow diameter distribution. *J. Phys. Chem. B* **109**, 14454–14460 (2005).
424. Tan, W. D., Su, C. Y., Knize, R. J., Xie, G. Q., Li, L. J. & Tang, D. Y. Mode locking of ceramic Nd:yttrium aluminum garnet with graphene as a saturable absorber. *Appl. Phys. Lett.* **96**, 031106 (2010).
425. Tang, Z., Zhuang, J. & Wang, X. Exfoliation of graphene from graphite and their self-assembly at the oil-water interface. *Langmuir* **26**, 9045–9049 (2010).
426. Tasis, D., Tagmatarchis, N., Georgakilas, V. & Prato, M. Soluble carbon nanotubes. *Chem. Eur. J.* **9**, 4000–4008 (2003).
427. Tatsuura, S., Furuki, M., Sato, Y., Iwasa, I., Tian, M. & Mitsu, H. Semiconductor carbon nanotubes as ultrafast switching materials for optical telecommunications. *Adv. Mater.* **15**, 534–537 (2003).
428. Tausenev, A. V., Obraztsova, E. D., Lobach, A. S., Chernov, A. I., Konov, V. I., Konyashchenko, A. V., Kryukov, P. G. & Dianov, E. M. Self-mode-Iocking in erbium-doped fibre lasers with saturable polymer film absorbers containing single-wall carbon nanotubes synthesised by the arc discharge method. *Quantum Electron.* **37**, 205–208 (2007).
429. Telg, H., Maultzsch, J., Reich, S., Hennrich, F. & Thomsen, C. Chirality distribution and transition energies of carbon nanotubes. *Phys. Rev. Lett.* **93**, 177401 (2004).
430. Tersoff, J. & Ruoff, R. S. Structural properties of a carbon-nanotube crystal. *Phys. Rev. Lett.* **73**, 676 (1994).
431. Thess, A., Lee, R., Nikolaev, P., Dai, H., Petit, P., Robert, J., Xu, C., Lee, Y. H., Kim, S. G., Rinzler, A. G., Colbert, D. T., Scuseria, G. E., Tománek, D., Fischer, J. E. & Smalley, R. E. Crystalline ropes of metallic carbon nanotubes. *Science* **273**, 483–487 (1996).
432. Thomsen, C. & Reich, S. Double resonant Raman scattering in graphite. *Phys. Rev. Lett.* **85**, 5214–5217 (2000).

433. Torrens, O. N., Milkie, D. E., Zheng, M. & Kikkawa, J. M. Photoluminescence from intertube carrier migration in single-walled carbon nanotube bundles. *Nano Lett.* **6**, 2864–2867 (2006).
434. Trancik, J. E., Barton, S. C. & Hone, J. Transparent and catalytic carbon nanotube films, *Nano Lett.* **8**, 982–987 (2008).
435. Trebino, R. *Frequency-resolved optical gating: The measurement of ultrashort laser pulses.* Kluwer Academic Publishers, Norwell, MA (2002).
436. Trickey, S. B., Müller-Plathe, F., Diercksen, G. H. F. & Boettger, J. C. Interplanar binding and lattice relaxation in a graphite dilayer. *Phys. Rev. B* **45**, 4460 (1992).
437. Trushkevych, O., Collings, N., Crossland, W. A., Wilkinson, T. D., Georgiou, A. & Milne, W. I. Projection of holograms from photorefractive optically addressed spatial light modulators. *J. Nonlinear Opt. Phys.* **16**, 307–316 (2007).
438. Trushkevych, O., Collings, N., Hasan, T., Scardaci, V., Ferrari, A. C., Wilkinson, T. D., Crossland, W. A., Milne, W. I., Geng, J., Johnson, B. F. G. & Macaulay, S. Characterization of carbon nanotube-thermotropic nematic liquid crystal composites. *J. Phys. D* **41**, 125106 (2008).
439. Tsyboulsky, D., Rocha, J. D. R., Bachilo, S. M., Cognet, L. & Weisman, R. B. Structuredependent fluorescence efficiencies of individual single-walled cardon nanotubes. *Nano Lett.* **7**, 3080–3085 (2007).
440. Tuinstra, F. & Koenig, J. L. Raman spectrum of graphite. *J. Chem. Phys.* **53**, 1126–1130 (1970).
441. Tu, X., Manohar, S., Jagota, A. & Zheng, M. DNA sequence motifs for structure-specific recognition and separation of carbon nanotubes. *Nature* **460**, 250–253 (2009).
442. Uchida, S., Martinez, A., Song, Y.-W., Ishigure, T. & Yamashita, S. Carbon nanotube-doped polymer optical fiber. *Opt. Lett.* **34**, 3077–3079 (2009).
443. Umeyama, T., Kadota, N., Tezuka, N., Matano, Y. & Imahori, H. Photoinduced energy transfer in composites of poly[(p-phenylene-1,2-vinylene)-co-(p-phenylene-1,1-vinylidene)] and single-walled carbon nanotubes. *Chem. Phys. Lett.* **444**, 263–267 (2007).
444. Van Stryland, E. W. & Sheik-Bahae, M. In *Z-scan* (Eds.: Kuzyk, M. G. and Dirk, C. W.), New York, Marcel Dekker Inc., 1998.
445. Yu, H., Chen, X., Zhang, H., Xu, X., Hu, X., Wang, Z., Wang, J., Zhuang, S. & Jiang, M. Large energy pulse generation modulated by Graphene epitaxially grown on silicon carbide. *ACS Nano* **4**, 7582–7586 (2010).
446. Vidano, R. P., Fischbach, D. B., Willis, L. J. & Loehr, T. M. Observation of Raman band shifting with excitation wavelength for carbons and graphites. *Solid State Commun.* **39**, 341–344 (1981).
447. Vieira, O. V., Laranjinha, J. A. N., Madeira, V. M. C. & Almeida, L. M. Rapid isolation of low density lipoproteins in a concentrated fraction free from water-soluble plasma antioxidants. *J. Lipid Res.* **37**, 2715–2721 (1996).
448. Vigolo, B., Penicaud, A., Coulon, C., Sauder, C., Pailler, R., Journet, C., Bernier, P. & Poulin, P. Macroscopic fibers and ribbons of oriented carbon nanotubes. *Science* **290**, 1331–1334 (2000).
449. Viswanathan, G., Chakrapani, N., Yang, H. C., Wei, B. Q., Chung, H. S., Cho, K. W., Ryu, C. Y. & Ajayan, P. M. Single-step in situ synthesis of polymer-grafted single-wall nanotube composites. *J. Am. Chem. Soc.* **125**, 9258–9259 (2003).
450. Vivien, L., Anglaret, E., Riehl, D., Hache, F., Bacou, F., Andrieux, M., Lafonta, F., Journet, C., Goze, C., Brunet, M. & Bernier, P. Optical limiting properties of singlewall carbon nanotubes. *Opt. Commun.* **174**, 271–275 (2000).
451. Wada, O. Femtosecond all-optical devices for ultrafast communication and signal processing. *New J. Phys.* **6**, 183 (2004).
452. Walsh, A. G., Vamivakas, A. N., Yin, Y., Ünlü, M. S., Goldberg, B. B., Swan, A. K. & Cronin, S. B. Screening of excitons in single, suspended carbon nanotubes. *Nano Lett.* **7**, 1485–1488 (2007).

453. Wang, F., Rozhin, A., Sun, Z., Scardaci, V., Penty, R., White, I. & Ferrari, A. C. Fabrication, characterization and mode locking application of single-walled carbon nanotube/polymer composite saturable absorbers. *Int. J. Mater. Form.* **1**, 107–112 (2008).
454. Wang, F., Rozhin, A. G., Scardaci, V., Sun, Z., Hennrich, F., White, I. H., Milne, W. I. & Ferrari, A. C. Wideband-tuneable, nanotube mode-locked, fibre laser. *Nat. Nanotechnol.* **3**, 738–742 (2008).
455. Wang, F., Rozhin, A. G., Sun, Z., Scardaci, V., White, I. H. & Ferrari, A. C. Soliton fiber laser mode-locked by a single-wall carbon nanotube-polymer composite. *Phys. Stat. Sol. (b)* **245**, 2319–2322 (2008).
456. Wang, F., Dukovic, G., Brus, L. E. & Heinz, T. F. The optical resonances in carbon nanotubes arise from excitons. *Science* **308**, 838–841 (2005).
457. Wang, F., Sfeir, M. Y., Huang, L., Huang, X. M. H., Wu, Y., Kim, J., Hone, J., O'Brien, S., Brus, L. E. & Heinz, T. F. Interactions between individual carbon nanotubes studied by Rayleigh scattering spectroscopy. *Phys. Rev. Lett.* **96**, 167401 (2006).
458. Wang, J. Z., Zheng, Z. H., Li, H. W., Huck, W. T. S. & Sirringhaus, H. Dewetting of conducting polymer inkjet droplets on patterned surfaces. *Nat Mater* **3**, 171–176 (2004).
459. Wang, X., Zhi, L. & Mullen, K. Transparent, conductive graphene electrodes for dye-sensitized solar cells. *Nano Lett.* **8**, 323–327 (2008).
460. Wang, X., Zhi, L., Tsao, N., Tomovic, Z., Li, J. & Müllen, K. Transparent carbon films as electrodes in organic solar cells. *Angew. Chem.* **47**, 2990 (2008).
461. Wei, L., Wang, B., Goh, T. H., Li, L. J., Yang, Y. H., Chan-Park, M. B. & Chen, Y. Selective enrichment of (6,5) and (8,3) single-walled carbon nanotubes via cosurfactant extraction from narrow (n,m) distribution samples. *J. Phys. Chem. B* **112**, 2771–2774 (2008).
462. Weisman, R. B. & Bachilo, S. M. Dependence of optical transition energies on structure for single-walled carbon nanotubes in aqueous suspension: An empirical Kataura plot. *Nano Lett.* **3**, 1235 (2003).
463. Weisman, R. B., Bachilo, S. M. & Tsyboulsky, D. Fluorescence spectroscopy of singlewalled carbon nanotubes in aqueous suspension. *Appl. Phys. A* **78**, 1111–1116 (2004).
464. Weiss, V., Thiruvengadathan, R. & Regev, O. Preparation and characterization of a carbon nanotube-lyotropic liquid crystal composite. *Langmuir* **22**, 854–856 (2006).
465. Wenseleers, W., Vlasov, I. I., Goovaerts, E., Obraztsova, E. D., Lobach, A. S. & Bouwen, A. Efficient isolation and solubilization of pristine single-walled nanotubes in bile salt micelles. *Adv. Funct. Mater.* **14**, 1105–1112 (2004).
466. White, B., Banerjee, S., O'Brien, S., Turro, N. J. & Herman, I. P. Zeta-potential measurements of surfactant-wrapped individual single-walled carbon nanotubes. *J. Phys. Chem. C* **111**, 13684–13690 (2007).
467. Williams, J. W., Van Holde, K. E., Baldwin, R. L. & Fujita, H. The theory of sedimentation analysis. *Chem Rev.* **58**, 715–806 (1958).
468. Wu, J., Walukiewicz, W., Shan, W., Bourret-Courchesne, E., Ager III, J. W., Yu, K. M., Haller, E. E., Kissell, K., Bachilo, S. M., Weisman, R. B. & Smalley, R. E. Structure-dependent hydrostatic deformation potentials of individual single-walled carbon nanotubes. *Phys. Rev. Lett.* **93**, 017404 (2004).
469. Wu, J., Becerril, H. A., Bao, Z., Liu, Z., Chen, Y. & Peumans, P. Organic solar cells with solution-processed graphene transparent electrodes. *Appl. Phys. Lett.* **92**, 263302-3 (2008).
470. Wu, J., Agrawal, M., Becerril, H. C. A., Bao, Z., Liu, Z., Chen, Y. & Peumans, P. Organic light-emitting diodes on solution-processed graphene transparent electrodes. *ACS Nano* **4**, 43–48 (2009).
471. Wu, Y., Li, Y., Ong, B. S., Liu, P., Gardner, S. & Chiang, B. High-performance organic thin-film transistors with solution-printed gold contacts. *Adv. Mater.* **17**, 184–187 (2005).
472. Wu, Z., Chen, Z., Du, X., Logan, J. M., Sippel, J., Nikolou, M., Kamaras, K., Reynolds, J. R., Tanner, D. B., Hebard, A. F. & Rinzler, A. G. Transparent, conductive carbon nanotube films. *Science* **305**, 1273–1276 (2004).
473. Xia, F., Mueller, T., Lin, Y.-M., Valdes-Garcia, A. & Avouris, P. Ultrafast graphene photodetector. *Nat. Nano* **4**, 839–843 (2009).

474. Xie, H., Ortiz-Acevedo, A., Zorbas, V., Baughman, R. H., Draper, R. K., Musselman, I. H., Dalton, A. B. & Dieckmann, G. R. Peptide cross-linking modulated stability and assembly of peptide-wrapped single-walled carbon nanotubes. *J. Mater. Chem.* **15**, 1734–1741 (2005).
475. Xie, Xiao-Lin, Mai, Yiu-Wing & Zhou, Xing-Ping. Dispersion and alignment of carbon nanotubes in polymer matrix: A review. *Mater. Sci. Eng. R* **49**, 89–112 (2005).
476. Xu, Z., Wu, Y., Hu, B., Ivanov, I. N. & Geohegan, D. B. Carbon nanotube effects on electroluminescence and photovoltaic response in conjugated polymers. *Appl. Phys. Lett.* **87**, 263118 (2005).
477. Yamashita, S., Inoue, Y., Maruyama, S., Murakami, Y., Yaguchi, H., Jablonski, M. & Set, S. Y. Saturable absorbers incorporating carbon nanotubes directly synthesized onto substrates and fibers and their application to mode-locked fiber lasers. *Opt. Lett.* **29**, 1581–1583 (2004).
478. Yamashita, S., Inoue, Y., Yaguchi, H., Jablonski, M. & Set, S. Y. S-,C-,L-Band picosecond fiber pulse sources using a broadband carbon-nanotube-based mode-locker. *Euro. Conf. on Opt. Comm*. (ECOC), (Stockholm, 2004). pp. No.Th.1.3.4.
479. Yamashita, S., Set, S. Y., Goh, C. S. & Kikuchi, K. Ultrafast saturable absorbers based on carbon nanotubes and their applications to passively mode-locked fiber lasers. *Electron. Comm. Jpn.* **90**, 17–24 (2007).
480. Yan, J., Zhang, Y. B., Kim, P. & Pinczuk, A. *Phys. Rev. Lett.* **98**, 166802 (2007).
481. Yan, X., Cui, X., Li, B. & Li, L.-S. Large, solution-processable graphene quantum dots as light absorbers for photovoltaics. *Nano Lett.*, **10**, 1869–1873 (2010).
482. Yanagi, K., Miyata, Y. & Kataura, H. Optical and conductive characteristics of metallic single-wall carbon nanotubes with three basic colors; Cyan, magenta, and yellow. *Appl. Phys. Express* **1**, 034003 (2008).
483. Yang, N., Zhai, J., Wang, D., Chen, Y. & Jiang, L. Two-dimensional graphene bridges enhanced photoinduced charge transport in dye-sensitized solar cells. *ACS Nano* **4**, 887–894 (2010).
484. Yaws, C. L. *Thermophysical properties of chemicals and hydrocarbons.* William Andrew Inc. Norwich, NY (2008).
485. Yong, V. & Tour, J. M. Theoretical efficiency of nanostructured graphene-based photovoltaics. *Small* **6**, 313–318 (2009).
486. Yu, A., Hu, H., Bekyarova, E., Itkis, M. E., Gao, J., Zhao, B. & Haddon, R. C. Incorporation of highly dispersed single-walled carbon nanotubes in a polyimide matrix. *Compos. Sci. Tech.* **66**, 1187 (2006).
487. Yu, P. & Cardona, M. *Fundamentals of semiconductors.* Springer, Berlin (2005).
488. Zacharia, R., Ulbricht, H. & Hertel, T. Interlayer cohesive energy of graphite from thermal desorption of polyaromatic hydrocarbons. *Phys. Rev. B* **69**, 155406 (2004).
489. Zhang, J., Kang, D. E., Xia, W., Okochi, M., Mori, H., Selkoe, D. J. & Koo, E. H. Subcellular distribution and turnover of presenilins in transfected cells. *J. Biolog. Chem.* **273**, 12436–12442 (1998).
490. Zhang, D., Ryu, K., Liu, X., Polikarpov, E., Ly, J., Tompson, M. E. & Zhou, C. Transparent, conductive, and flexible carbon nanotube films and their application in organic light-emitting diodes. *Nano Lett.* **6**, 1880–1886 (2006).
491. Zhang, H., Tang, D. Y., Zhao, L. M., Bao, Q. L. & Loh, K. P. Large energy mode locking of an erbium-doped fiber laser with atomic layer graphene. *Opt. Express* **17**, 17630–17635 (2009).
492. Zhao, H. & Mazumdar, S. Electron-electron interaction effects on the optical excitations of semiconducting single-walled carbon nanotubes. *Phys. Rev. Lett.* **93**, 157402 (2004).
493. Zhao, H. & Mazumdar, S. Elucidation of the electronic structure of semiconducting single-walled carbon nanotubes by electroabsorption spectroscopy. *Phys. Rev. Lett.* **98**, 166805 (2007).
494. Zhao, N., Chiesa, M., Sirringhaus, H., Li, Y., Wu, Y. & Ong, B. Self-aligned inkjet printing of highly conducting gold electrodes with submicron resolution. *J. Appl. Phys.* **101**, 064513-6 (2007).

495. Zheng, M., Jagota, A., Semke, E. D., Diner, B. A., Mclean, R. S., Lustig, S. R., Richardson, R. E. & Tassi, N. G. DNA-assisted dispersion and separation of carbon nanotubes. *Nat. Mater.* **2**, 338–342 (2003).
496. Zheng, M., Jagota, A., Strano, M. S., Santos, A. P., Barone, P., Chou, S. G., Diner, B. A., Dresselhaus, M. S., McLean, R. S., Onoa, G. B., Samsonidze, G. G., Semke, E. D., Usrey, M. & Walls, D. J. Structure-based carbon nanotube sorting by sequence-dependent DNA assembly. *Science* **302**, 1545–1548 (2003).
497. Zhou, Y., Hu, L. & Gruner, G. A method of printing carbon nanotube thin films. *Appl. Phys. Lett.* **88**, 123109 (2006).
498. Zorbas, V., Ortiz-Acevedo, A., Dalton, A. B., Yoshida, M. M., Dieckmann, G. R., Draper, R. K., Baughman, R. H., Jose-Yacama, M. & Musselman, I. H. Preparation and characterization of individual peptide-wrapped single-walled carbon nanotubes. *J. Am. Chem. Soc.* **126**, 7222–7227 (2004).